Summer 2011

A Methodology to Repair or Deorbit LEO Satellite Constellations

Goksel Gurgenburan
Old Dominion University

A METHODOLOGY TO REPAIR OR DEORBIT LEO SATELLITE CONSTELLATIONS

by

Goksel Gurgenburan
B.S. August 2005, Turkish Air Force Academy

A Thesis Submitted to the Faculty of
Old Dominion University in Partial Fulfillment of the
Requirement for the Degree of

MASTER OF SCIENCE

AEROSPACE ENGINEERING

OLD DOMINION UNIVERSITY
August 2011

Approved by:

_____
Robert L. Ash (Director)

_____
Brett Newman (Member)

_____
Colin P. Britcher (Member)

ABSTRACT

A METHODOLOGY TO REPAIR OR DEORBIT LEO SATELLITE CONSTELLATIONS

Goksel Gurgenburan
Old Dominion University, 2011
Director: Dr. Robert L. Ash

In this thesis, mitigation of space debris is addressed by examining an approach for repair or de-orbit of a specific population of non-functional Low Earth Orbit (LEO) satellites. Basic orbital mechanics propagation of the orbits was used as the process for computing a solution to the time and intercept position for the targeted satellites. Optimal orbital maneuvers to reach the target satellites from a pre-established orbit were also considered. In this way minimum ΔV budget, rendezvous time and mass budgets were managed. The Clohessy-Wiltshire Equations and two-impulsive rendezvous maneuvers were used to determine the orbital path of a chase satellite between two position vectors, along with the time of flight. A monopropellant propulsion system was assumed in order to estimate propellant mass requirements. This methodology can be applied to a variety of satellite constellations, as implemented using MatLab and Analytical Graphics, Inc. STK software. Several cases were investigated in the study. Simulations showed that the methodology can provide guidance for the rendezvous process, facilitating a minimum ΔV budget and minimum rendezvous time.

ACKNOWLEDGEMENTS

This thesis would not have been possible without the guidance and the support of several individuals who contributed their valuable assistance in the preparation and completion of this study in one way or another.

First, I would like to offer my sincerest gratitude to my advisor Dr. Robert L. Ash who has supported me throughout my thesis with his excellent guidance, patience and knowledge. I also want to thank to all my commanders in the Turkish Air Force and Dr. Oktay Baysal and Dr. Osman Akan, for giving me the opportunity to pursue a master of science degree at Old Dominion University.

I would like to thank my all colleagues with whom I shared the voyage from our country to here. These include First Lieutenants Gokhan Caliskan, Omer Demirok, Taner Gundogdu, Serdar Torun, Emrah Cinar, Atila Ozdemir, Ertac Olgun, Emrah Koksalmis. I have never felt the absence of their friendship and support for me.

Finally, I would like to offer thanks with all my heart to my spouse Gulsah Gurgenburan, my whole family: Gulderen Gurgenburan and Saime Sevim, Rahmi Gurgenburan, my sisters Verda Gurgenburan, Sahide Baz and her husband Oguz Baz, and my brother Rasit Sevim. Even though there were thousands of miles between us, they always succeeded to make me feel morally sound throughout my study with their endless support.

TABLE OF CONTENTS

Page

LIST OF TABLES

Table Page

LIST OF FIGURES

Figure Page

CHAPTER 1

INTRODUCTION

On October 4, 1957, Sputnik I, the Russian-made spacecraft was placed in Earth's orbit. It was the first man-made Earth satellite in history. In just a few decades satellite technology has advanced to the point where it has become a critical element in supporting international communications. The development and advancement of satellite technology has played an important and pivotal role in nearly every field of modern human life, including civil and military communication, navigation and observation, remote sensing, broadcasting, scientific experiments, mapping, providing weather information, and so on. The utility and security for all satellite applications depends on three space environment related factors: (1) secure access to an orbital slot for each satellite; (2) secure access to a radio-frequency allocation to allow communication with each satellite; and (3) security against space debris with the capability to damage or destroy the satellite. Reduction of the orbital debris threat to existing and future spacecraft is the focus of this thesis.

1.1 Problem Motivation and Description

1.1.1 Space Debris and Risks

Every space launch creates space debris, just as every operating terrestrial vehicle creates pollution on the Earth's surface and in its atmosphere. The development and utilization of space-derived infrastructure has huge advantages, but as the variety of space applications and the associated population of orbiting platforms grows, the potential for catastrophic collisions between orbiting objects increases simultaneously. Many countries have the capability of putting spacecraft into orbit, and, depending on the orbit and the orbital insertion methods, a variety of man-made objects have become "satellites" even though they serve no useful function in space. Furthermore, depending on the orbital characteristics and orbital lifetime of each object, much of the population of man-made orbiting material becomes space debris.

Space debris can be divided into two types: (1) natural space debris, consisting of small pieces of cometary and asteroidal material called meteoroids; and (2) artificial space debris (also known as space waste, orbital debris or space junk)

consisting of all objects in Earth's orbit that were created by humans and that no longer function as operational satellites. Man-made space debris consists of everything that belongs to satellite systems, such as spent rocket bodies and stages, solid propellant slag, dust and liquids from rocket motors, defunct or failed satellites (dead satellites), explosion and collision fragments and paint flakes.

Man-made space debris is divided into four main groups: spent rocket bodies (R/B's), mission related debris, break-up fragments, and non-functional spacecraft. These space debris populations have different size distributions, as shown in Figure 1.1[1].

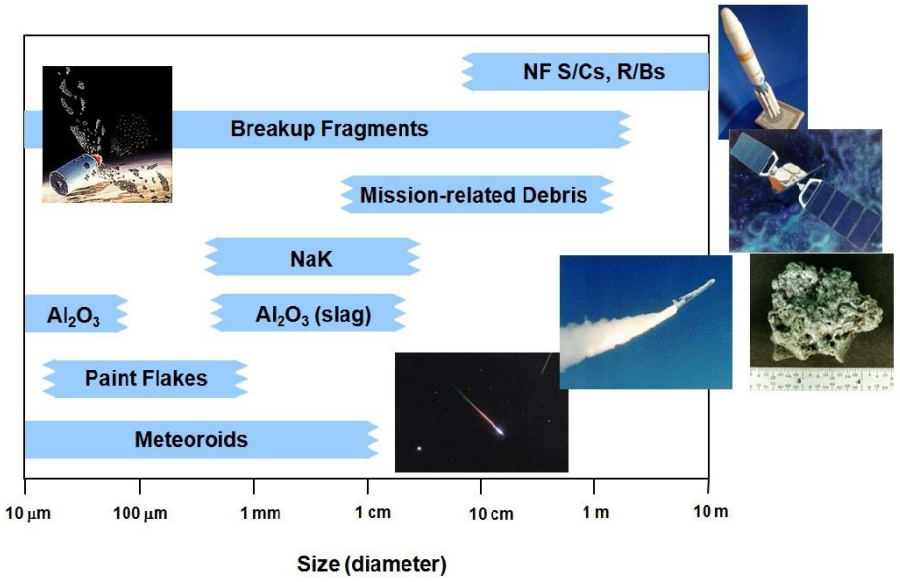

Figure 1.1 Size Ranges of Space Debris Types.

Spacecraft are particularly vulnerable to collisions with space debris. Beginning with the first launch into orbital space, the accumulating population of space debris has increased every year. Since the launch of Sputnik in 1957, over 36,761 man-made objects have been cataloged[2]; many have since re-entered the atmosphere. Currently, the Space Surveillance Network (SSN) tracks more than 22,000 man-made objects orbiting the Earth with characteristic dimensions of 10 centimeters or larger. About five percent of the tracked objects are functioning

payloads or satellites; eight percent are rocket bodies; and about 87 percent are fragmentation objects and inactive satellites[3]. However, the overwhelming majority of debris in Low Earth Orbit (LEO) is smaller than 10 centimeters and is too small to be verifiably tracked and cataloged[3]. There are tens of millions of objects with characteristic dimensions between 1 and 10 centimeters (i.e., larger than a marble), and perhaps trillions of pieces measuring less than one cm^3. Even tiny fragments of space debris can harm operational spacecraft due to the high relative velocities that can occur during in-orbit collisions.

1.1.2 Man-Made Orbital Object Population Growth

A computer-generated image comparison of man-made objects in Earth's orbit in 1956 (none, on the left) with January 2011, is displayed Figure 1.2[4].

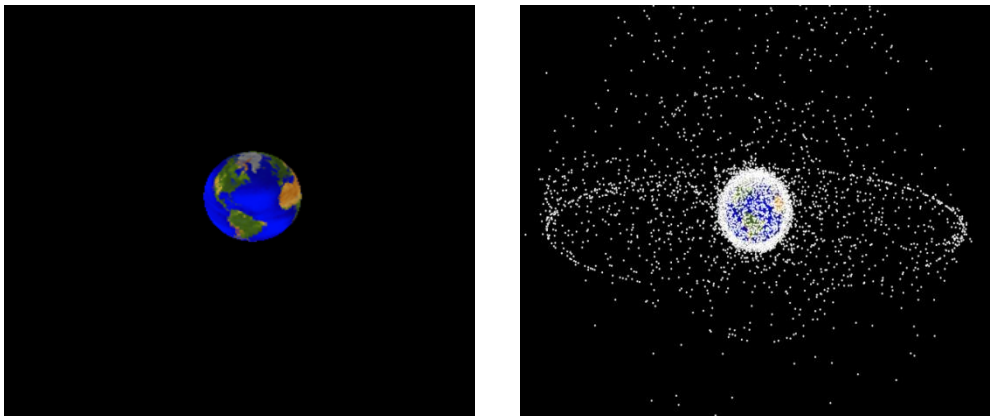

Figure 1.2 Comparison Space Debris between 1956 – 2011.

The orbital debris dots are scaled according to the image size of the graphic, in order to emphasize their locations and are therefore not scaled properly. However, these images provide a good visualization of regions of greatest orbital debris density.

The rate of increase in the population of orbiting space debris with time[5] is represented in Figure 1.3. Space debris is a growing problem and threat to the approximately one-thousand functional and operational satellites belonging to more than 40 countries at this time.

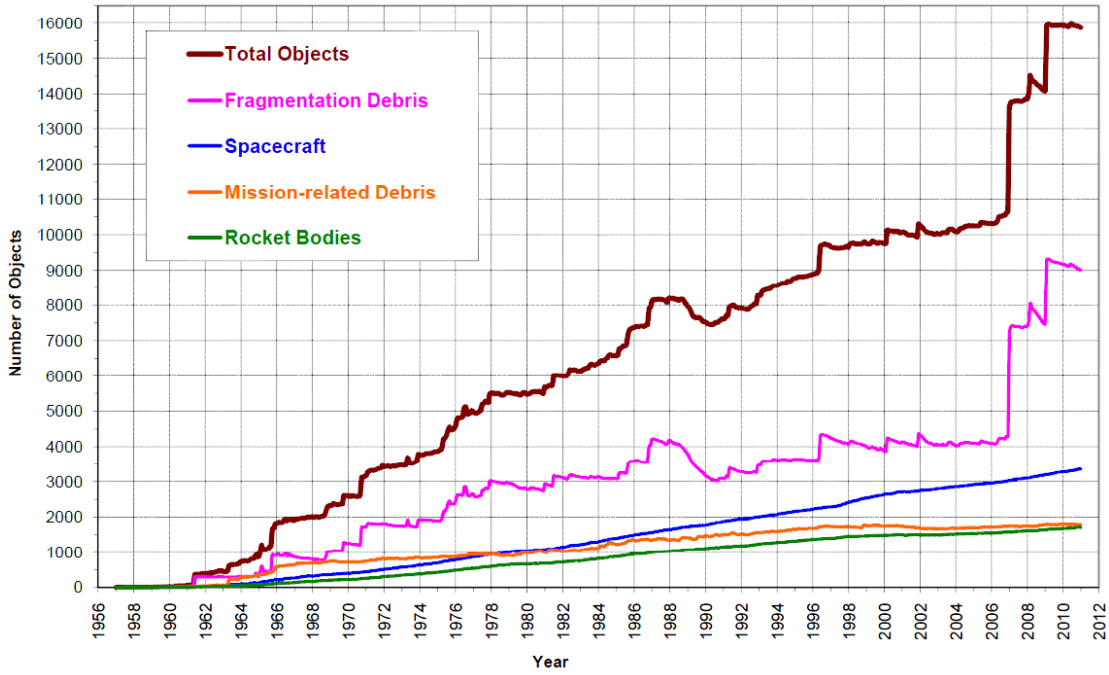

Figure 1.3 Monthly Number of Objects in Earth's Orbit by Object Type.

Space debris travels in a variety of orbits and is affected by various perturbation forces, including the effects of the Earth's atmosphere, gravitational perturbation effects, and solar radiation pressure. As orbital altitude increases, the influence of the atmosphere in accelerating orbital decay becomes small, and typically, large objects in orbits higher than approximately 600 km can remain in orbit for tens, hundreds, or even thousands of years[3]. Space debris has the potential to directly threaten space security since it increases risks associated with accessing and using space. On average, colliding objects in Low Earth Orbits (LEO) have relative velocities of about 10 kilometers per second (about 36,000 kilometers per hour). Thus, the impact from a 1 kilogram (10 centimeter diameter) object in LEO with this relative velocity is equivalent to that of a 35,000 kilogram truck moving at 190 kilometers per hour on earth. A collision with a debris fragment of this size could therefore result in the catastrophic break-up of a 1,000 kilogram spacecraft (a typical spacecraft bus weighs about 1,200 kilograms)[3]. All spacecraft routinely experience collisions with particles smaller than 1 millimeter in diameter, but with rare exceptions, such impacts do not have highly deleterious effects.

As mentioned above, space debris risks are escalating at present and future manned and unmanned space missions will have greater risk involved. Table 1.1 summarizes the significant known unintentional collisions between objects in space. The term “cataloged debris” generally refers to debris that is large enough to be detected and tracked from the ground[6].

Table 1.1 Unintentional Collision Chronology between Significant Space Objects.

YEAR	COLLISION DESCRIPTION
1991	Inactive Cosmos 1934 satellite hit by cataloged debris from Cosmos 296 satellite.
1996	Active French Cerise satellite hit by cataloged debris from Ariane rocket stage.
1997	Inactive NOAA 7 satellite hit by uncataloged debris large enough to change its orbit and create additional debris.
2002	Inactive Cosmos 539 satellite hit by uncataloged debris large enough to change its orbit and create additional debris.
2005	U.S. rocket body hit by cataloged debris from Chinese rocket stage.
2007	Active Meteosat 8 satellite hit by uncataloged debris large enough to change its orbit.
2007	Inactive NASA UARS satellite believed hit by uncataloged debris large enough to create additional debris.
2009	Active Iridium satellite hit by inactive Cosmos 2251.

After a collision, a debris cloud is created similar to that shown schematically in Figure 1.4[6]. There are two debris clouds in this case; one is associated with “Satellite 1” and the other is associated with “Satellite 2”. Figure 1.4 shows how the two clouds follow the orbits of the original satellites. As depicted, when the two orbits are perpendicular to each other, the space debris from the collision becomes a global problem threatening all satellites that pass through similar orbital altitudes.

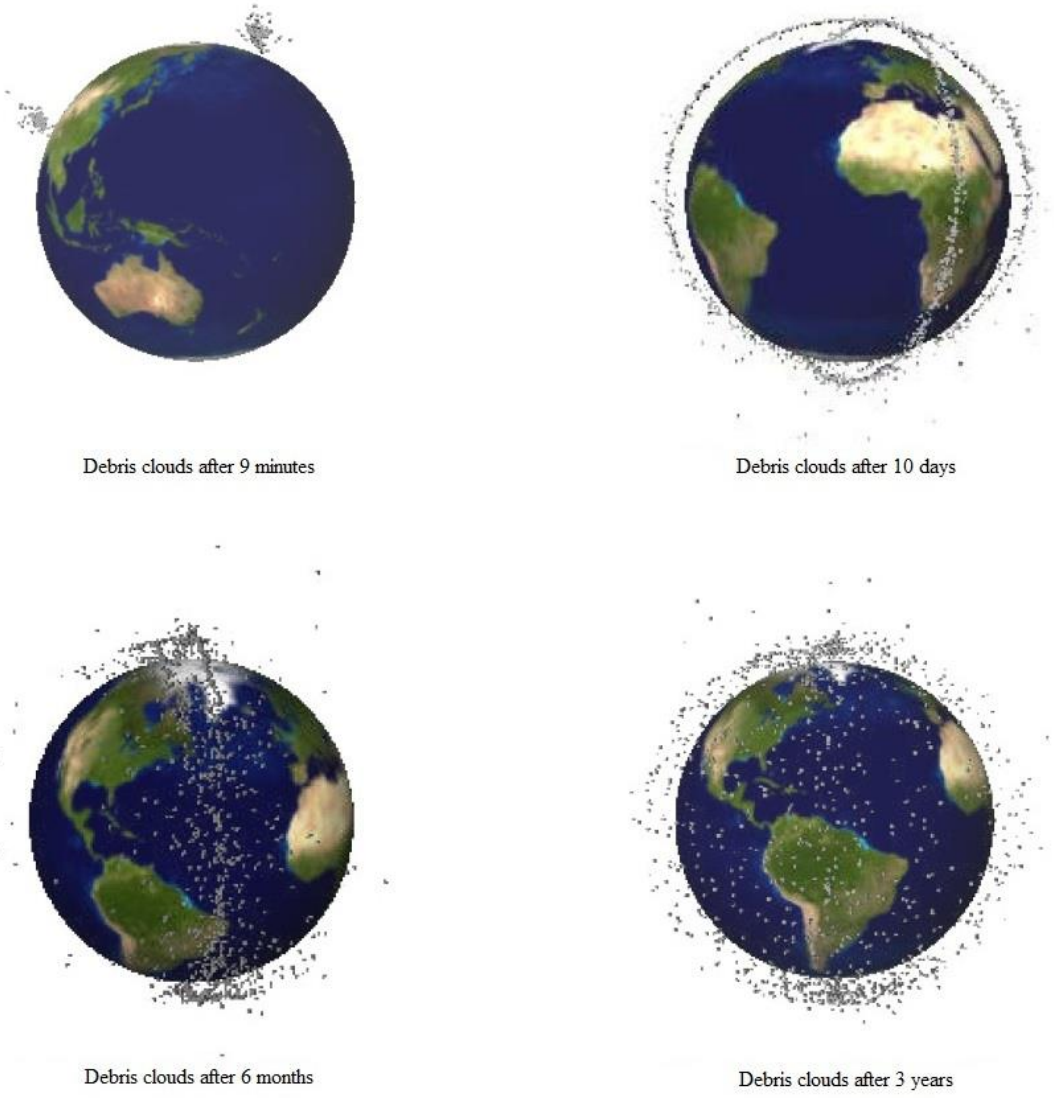

Figure 1.4 Debris Cloud History after the Collision of a Non-functioning Cosmos Satellite with a Functioning Iridium Communications Satellite[6].

Medium Earth Orbits (MEOs) between 2,000 km and about 36,000 km are emerging as a new focus in space debris studies, since those orbital altitudes contain the navigation satellite constellations; for example, the Global Positioning System (GPS) constellation, used to locate with high accuracy the position of a receiver on the ground, operates at a nominal altitude of 20,200 km. The vital role that this navigation system has achieved for air and terrestrial transportation traffic control makes these constellations and the orbital altitude correspondingly important. The

growing space debris problem will affect these important satellite constellations. One orbit spatial density (objects per unit volume) represents the effective number of spacecraft and other objects as a function of altitude. Spatial density with respect to altitude[7] for three different size thresholds includes: objects with diameters larger than 1 mm (top red line), 1 cm (middle green line) and 10 cm (bottom blue line) and is shown in Figure 1.5.

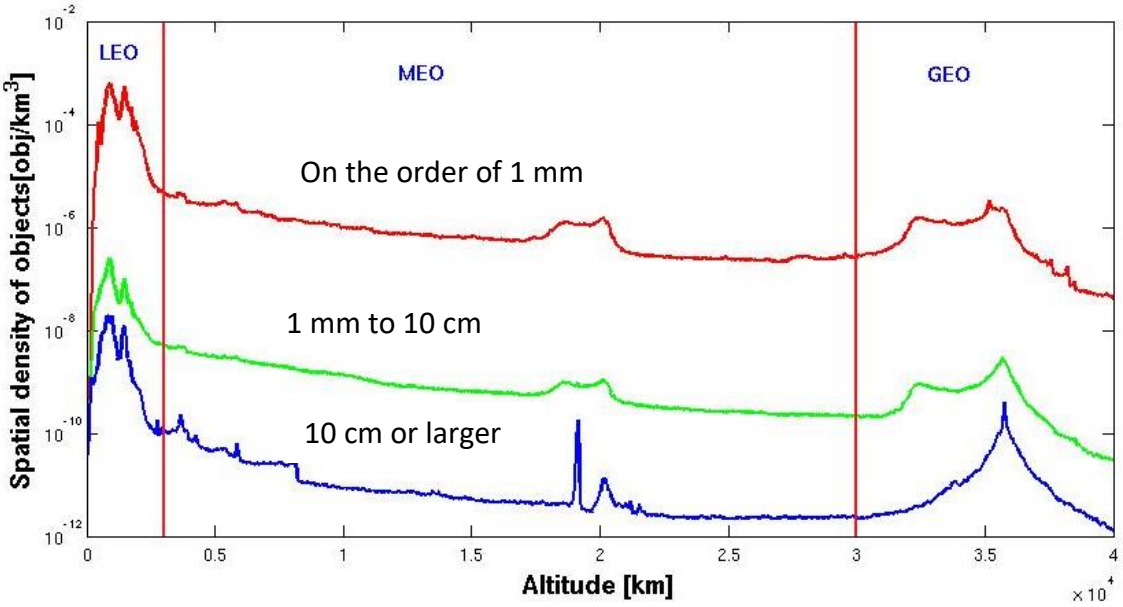

Figure 1.5 Spatial Density of Objects by Size as a Function of Altitude[7].

Obviously, the total space debris population above 2,000 km can threaten critical satellite constellations.

1.2 Turkey's Space Projects (GOKTURK)

The development and advancement of satellite technology and its capabilities provides more applications, not only for civil purposes such as television and radio broadcasting (TurkSat series), but also to support military objectives such as satellite based communication, intelligence, observation missions and so on. Hence, the Turkish Armed Forces has started the process of developing and deploying a very high resolution Electro-Optical (EO) Reconnaissance and Surveillance Satellite that

will serve both military and civilian purposes. After obtaining the necessary assessment and approval by the Turkish Armed Forces, the Under Secretariat of the Defense Industry, the project was named the *Gokturk Project* and was initiated in 2005. The Turkish Armed Forces assigned authority over the project to the Turkish Air Force who is responsible for determination of technical specifications for the satellite and its associated support systems. The Turkish Air Forces and Under Secretariat of the Defense Industry signed an agreement with Italian Telespazio and Thales Alenia Space Association on July 2009[8]. A rendition of the Gokturk satellite is shown in Figure 1.6[9].

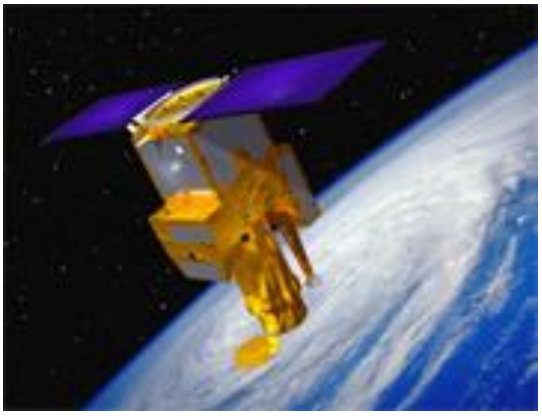

Figure 1.6 Gokturk Reconnaissance Satellite.

The Gokturk satellite has the following characteristics:[9]

- The orbital period will be approximately 100 minutes (it will complete 14 orbits per day) and it will make observations all over the world,
- An electro-optical camera system with 4-band multispectral (color) and panchromatic (black and white) images,
- A sun synchronous Low Earth Orbit (650-700 km) for proper target lighting, and
- The ability to operate in point, stereo, strip, and wide area observation modes.

The general technical properties for its ground station will be:[9]

- Satellite ground command and control systems,
- Reconfiguration of satellite position and tasking, mission loading and image downloading,
- Image processing, assessments, sensing, and
- Planning image requisitions, archive assessments and distribution of images.

The general and primary objectives of the Gokturk project will be to provide the necessary support for the Turkish Armed Forces. The satellite is expected to support additional functions associated with preventing terrorism while providing imaging and reconnaissance assistance to Turkey's allies. Gokturk is scheduled to enter orbit in 2014[9].

While Turkey is just starting its space program, it has a progressive and comprehensive plan for developing space technology. As a space-faring nation, Turkey will need to be involved in space programs related to space debris mitigation, supporting such countries as the United States (National Aeronautics and Space Administration), the European Union (European Space Agency, Agenzia Spaziale Italiana, German Aerospace Center), Japan (Japan Aerospace Exploration Agency) and the others members of the Inter-Agency Space Debris Coordination Committee (IADC).

1.3 Review of Previous Research on Debris Mitigation

In this section, previous research related to characterizing and remediating the space debris problem will be discussed. In addition, the possibility of orbital rendezvous and repair of inactive spacecraft will be explored, requiring a discussion of literature related to terminal rendezvous between two spacecraft and the associated development of spacecraft removal systems.

1.3.1 Space Debris Hazards and Mitigation

Space access and the sustainability of space-related missions are very important contemporary issues. Accelerating space technology developments continue, but those developments in space technology create additional constraints on

further expansion. One of those constraints is the associated space debris problem. In this section three space debris hazard and mitigation studies will be reviewed; one study summarized techniques for controlling the growing man-made debris population in Earth's orbits[10]; one study produced an orbital debris hazard and environment assessment for the satellite constellations[11] and one study is an examination of and estimations of orbit lifetimes of man-made objects[12].

Petro[10] has discussed man-made orbital debris control and mitigation, concluding that it can be approached as a problem of correction or prevention. Spacecraft shielding, efforts to retrieve derelict spacecraft and sweeper devices to remove small debris are corrective approaches for reducing the orbital debris population. Provisions for self-removal of spacecraft and rocket stages and the increased use of reusable space hardware are appropriate preventative approaches. Orbital debris studies of Petro's group have been examined by NASA Johnson Space Center, approaching the problem using four general debris control techniques: 1) active retrieval of large objects, 2) provisions for self-disposal incorporated in new spacecraft, 3) sweeper devices to remove small debris, and 4) increasing the use of reusable space hardware.

The approach for active retrieval of large objects is to collect non-functional or defunct satellites with an autonomous or remotely controlled dexterous vehicle. Petro's group handled the autonomous or remotely controlled dexterous vehicle employing two de-orbiting options[10] after the dexterous vehicle had grabbed the target satellite. In the first option, it executed the de-orbit maneuver while linked with the target satellite, then separated from the target satellite and reinserted itself into a different orbit, allowing the discarded object to re-enter the Earth's atmosphere. Alternatively, the target satellites can be collected and maintained together in a safe orbit for possible use as spare parts or raw materials. In the second option, the dexterous robot executed an autonomous or remotely controlled rendezvous with the target satellite then attached a separate de-orbit device to the target object. The attached device might be a de-orbit propulsion package or a passive drag device.

Designing for self-disposal in new spacecraft is a useful approach for reducing orbital debris as part of an integrated process. The integrated de-orbit device could be a propulsion package, a drag-augmentation system, or a combination of the two[10].

Launched spacecraft can have self-disposal devices incorporated as bus elements and representing a small fraction of the total spacecraft mass. Three cases were examined in terms of the mass penalty produced by the propulsive de-orbiting device, assuming specific impulse values of 250, 350, and 450 seconds and those results are shown in Figure 1.7[10].

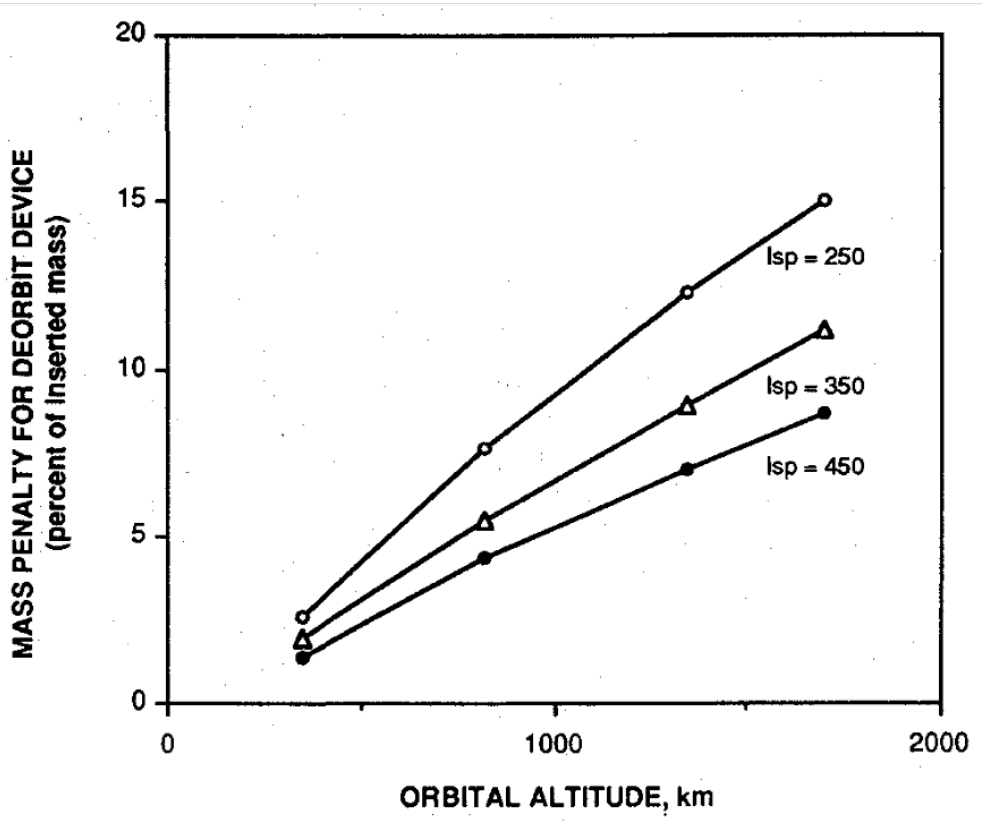

Figure 1.7 Mass Penalty (in percent) for Propulsive De-orbit (Circular Orbit).

The mass fraction penalty increases with altitude, but the slope becomes relatively flat above 10,000 km. For circular orbits above 25,000 km, an escape from Earth's orbit is less costly than a de-orbit maneuver[10].

The use of sweeper devices to remove small objects is a concept for clearing small size orbital debris. Large foam-filled balloons or large panels like the vanes of a windmill can be used as "sweepers". However, these devices are effective only when they can sweep huge areas and launch, deployment, and maintenance of these very

large systems would require an extremely large investment. Currently, these devices are not considered to be feasible and need more research and development.

Reusable space hardware is considered the best solution for orbital space debris mitigation. Single use satellites could be replaced by multipurpose space platforms that can be repaired and upgraded periodically. Reusable orbital maneuvering vehicles and orbital transfer vehicles could replace the expendable upper stages that litter the orbital environment[10].

Petro[10] showed that drag devices can be competitive with propulsion systems as a means of self-disposal for satellites and upper stages. The fact that the drag devices do not require active control makes them very attractive. Above 700 km, propulsive systems may be the only practical option, but above 25,000 km, a smaller ΔV is required to simply boost defunct satellites out of Earth's orbit rather than to de-orbit them.

Spencer et al.[11] examined two categories of environmental impacts for satellite constellations: (1) the effects of satellite constellations on the space debris environment and (2) the effects of the environment on the satellite constellations. They developed a methodology to assess the risk posed to and by a large satellite constellation. In their computer simulation study, they assumed that a satellite constellation included 800 satellites that were designed for a 10-year useful life, starting in 2001. The constellation was to be distributed in 20 orbital planes with 40 satellites per plane. The orbits were circular and sun-synchronous at 700 km altitude. The ascending nodes of adjacent planes were spaced every 18 degrees around the equator[11]. They used several computer models and they categorized their results into three risk components: 1) long-term hazard assessment, 2) short-term hazard assessment, and 3) intersatellite collision hazard assessment.

In Spencer et al.'s[11] long-term assessments, they estimated the collision probabilities for satellites and components. Based on the results of the study, the number of impacts from debris impacts greater than 1 mm over a 10-year mission lifespan was divided into upper and lower bound collision estimates for various satellite element categories and is displayed in Figure 1.8[11].

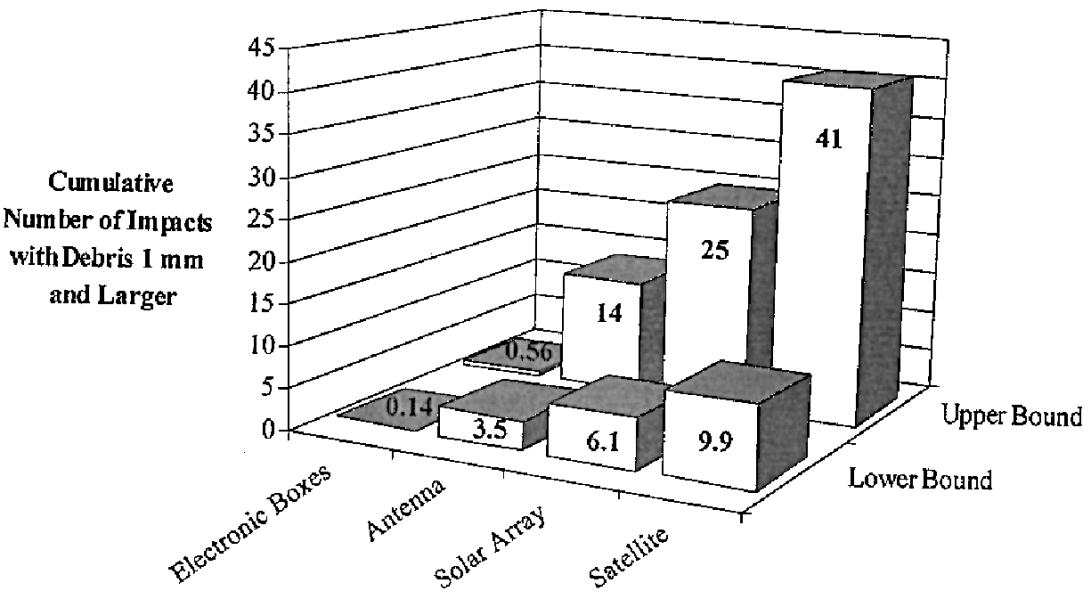

Figure 1.8 Average Number of Impacts on Representative Spacecraft over 10-Year Mission.

From the long term assessments, they found that this large constellation could expect a large number of impacts with smaller size debris. They suggested that manufacturers design these satellites incorporating shielded wires, cables, and other vulnerable parts in order to protect them from probable impacts with millimeter-sized debris during their operational lives. The functionality of the satellites can be assured by proper hardening via shielding and redundancy[11].

Spencer et al.'s[11] short term study examined collisions and breakup events near an operational satellite and the cascading effects of these collisions and breakup events for the nearest satellite. The authors assumed two types of collision and breakup events. One case assumed that a collision occurred at the same altitude (700 km) as the constellation satellite orbit and the other assumed that a collision occurred at a lower altitude (663 km). For both breakup altitudes, the collision probabilities for 1 mm and larger fragments was plotted during the 24 hours after breakup and is shown in Figure 1.9.

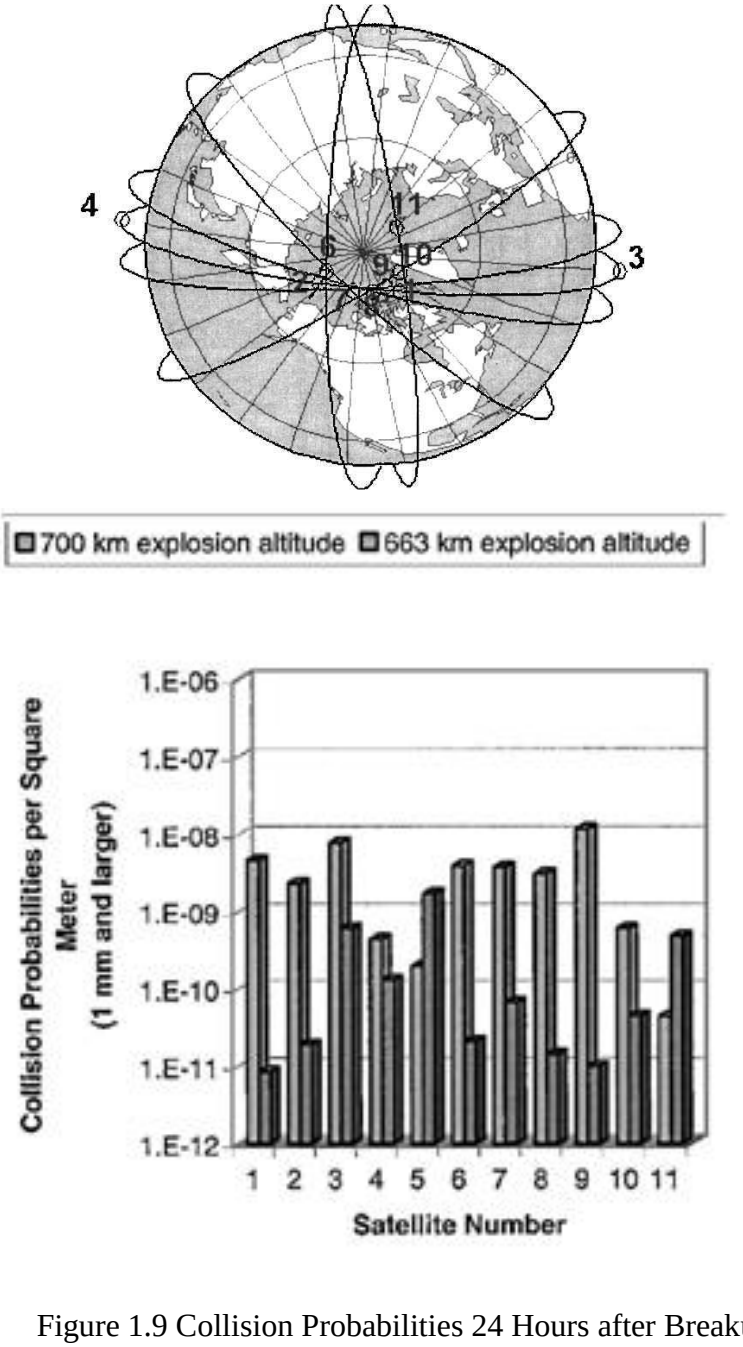

Figure 1.9 Collision Probabilities 24 Hours after Breakup.

The numbers refer to arbitrary satellite numbers in Figure 1.9. Spencer et al.[11] found from their IMPACT explosion models[11] that the impact probabilities for impacts from debris with dimensions of 1 mm and larger increased by a factor of 60.

Spencer et al.'s[11] intersatellite collision hazard assessment utilized three satellite collision time frames: 1) Normal operations, 2) Uncontrolled de-orbit operations and 3) Controlled de-orbit operations. They made simulations employing

all three scenarios and the results of their simulation showed that during the controlled de-orbit of a satellite using low-thrust propulsion, the time duration of the de-orbit process could vary between 8 months and 5 years, depending on the phase of the solar cycle. The time to descend through the constellation was estimated to be up to two years. Additional considerations such as variations in orbital spacing (altitude, inclination, and eccentricity) could be utilized to further reduce collision opportunities and decrease the collision risk[11].

From the Spencer et al.[11] comprehensive satellite constellation space debris assessment it is apparent that these events are an important consideration for constellation satellite design and orbit management.

Finkelman and Oltrogge[12] have examined the practical implications of the 25-year Low Earth Orbit post-mission lifetime guideline. Satellite orbit lifetimes vary with orbit characteristics, drag (ballistic) coefficient, and other characteristics, such as spacecraft orientation. There are many ways to predict a satellite orbit lifetime, but unfortunately all of the prediction methods must be based on accurate predictions of the long term spacecraft performance and detailed knowledge of the long-term behavior of the Earth's atmosphere. Neither element can be predicted accurately and as a consequence, satellite lifetime predictions are extremely uncertain. The orbit lifetime prediction method developed by Chao and Oltrogge[13] has been recognized by international consensus as the most useful and their generic lifetime predictions in terms of initial orbit inclination, perigee altitude and the characteristic ballistic coefficient of the object is shown in Figure 1.10[12]. This figure illustrates the dependence of natural orbit lifetime with respect to a 25 year guideline.

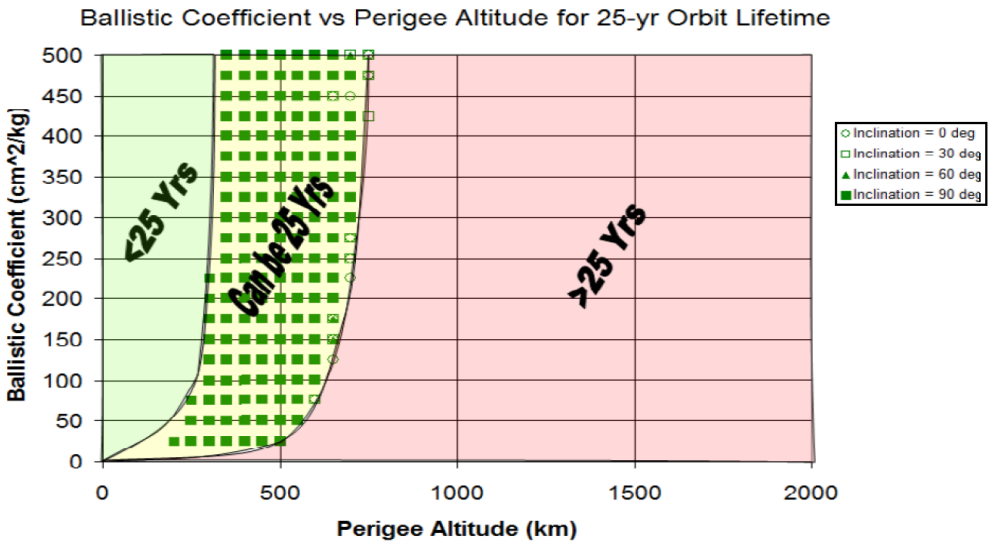

Figure 1.10 Orbit Lifetime Guideline (Chao and Oltrogge[13]).

Their results show that the orbital lifetime is extremely sensitive to orbital altitude. The influence of initial orbit altitude on estimated satellite lifetime is shown in Figure 1.11.

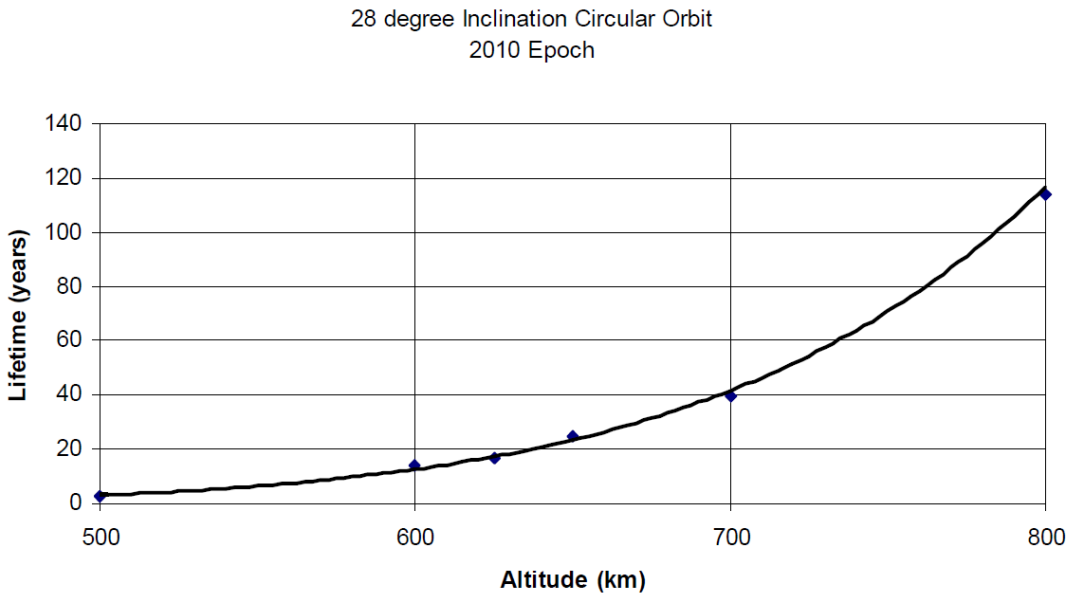

Figure 1.11 Variation of Estimate Satellite Lifetime with Initial Altitude (Chao and Oltrogge[13]).

Orbit altitude is the most significant property for estimating the orbit lifetime. The slope of Figure 1.11 shows the variation of estimated lifetime with the altitude for satellites in 28 degree inclination and is approximately 0.1 years/km[12]. This result suggests that the satellite lifetime could be more than or less than 25 years with an altitude change of just a few kilometers. This is most likely within the uncertainty of being able to maintain an orbit, and becomes worse at higher altitudes, but it does not matter as much from the perspective of the IADC guidelines, since objects in such orbits will require an active means of disposal[12].

The actual solar cycle strongly influences orbital decay. Finkelman and Oltrogge[12] examined solar cycle influences on predicted orbital lifetime. They assumed that the same satellite was inserted initially on the same orbit in one year intervals. The results were significantly different. Predicted satellite lifetimes were halved when launched around 2016, compared with the same satellite launched in the same orbit in 2013 or 2022[12].

They also considered the propellant mass necessary to lower the spacecraft altitude in order to reduce its lifetime to 25 years, at the completion of its mission. It should first be noted that the propellant mass required either to lower or maintain an orbit is relatively small. However, at an 800 km circular altitude, for example, the propellant requirement for orbit lowering in order to comply with the 25 year lifetime is more than ten times the requirement for remaining in the original orbit for another year. In other words, an operator could buy 10 years more orbit lifetime by employing the same propellant mass required to dispose of the satellite within 25 years. Since the major reason for end of mission is propellant depletion, this is a tempting tradeoff[12].

A strong case can be made for refurbishing inoperable communications satellites in Low Earth Orbit, rather than de-orbiting those satellites. However, the risks associated with an unintended collision between an inactive communications satellite and a robotic repair spacecraft must be minimized. A great deal of research has been devoted to minimizing the risks associated with orbital rendezvous and will be summarized in the next section.

1.3.2 Terminal Rendezvous between Two Spacecraft

Orbital rendezvous has been a subject of intense investigation since the beginning of the space age. When astronauts controlled orbital rendezvous, the problem was primarily one of accurate modeling, simulation and training. However, teleoperated or automated rendezvous operations are now feasible. New space technologies and much better knowledge of the space environmental characteristics have improved our ability to safely execute a rendezvous between two spacecraft. In this section two primary studies will be reviewed. One approach is based on cognitive-controlled vision systems for rendezvous management[14], and the other is an examination of an unmanned experimental satellite that became the world's first satellite to use a robot arm to manipulate another satellite [15]. However, the potential for a collision can threaten the continued existence of the two spacecraft and the possible release of debris can threaten other high-value objects as well.

Qureshi, Terzopoulos, and Jasiobedzki[14] demonstrated a robotic arm which was controlled using a vision system that had the ability to capture a free-flying satellite autonomously. They described an embodied, task-oriented vision system which can combine object recognition and tracking with high-level symbolic reasoning. The autonomous system under development can control target satellite approach, maneuver itself to get into the desired docking position, and dock with the target satellite using an on-board controller to estimate the position and track the target satellite. In this *cognitive system*, they demonstrated its ability to estimate the current position and orientation of the target satellite employing captured images, and behavior-based perception and memory units using contextual information to construct a symbolic description of the rendezvous scene. Ultimately, the cognitive module used knowledge of the encoded rendezvous scene dynamics and a type of situation calculus to construct a rendezvous scene interpretation. Finally, the cognitive module formulated a plan to achieve the current goal.

Object recognition and tracking module has the ability to create images from a calibrated video camera-pair mounted on the end-effector of the robotic manipulator and compute subsequently its estimated relative position to the target satellite. Images created by the module during an experiment are shown in Figure 1.12[14]. The left image was taken from a distance of 5 m and the right image was taken from 0.2 m.

Figure 1.12 Recognition and Tracking Module Experiment.

The cognitive vision controller manipulates the image recognition and tracking module. It takes into account several factors such as current task, the current state of the environment, the advice from the symbolic reasoning module and the characteristics of the vision module. The cognitive vision control unit includes two sub-units, perception and memory, in addition to the symbolic reasoning unit. The perception unit receives the most current information from the active vision configuration and computes the estimated target satellite position. The symbolic reasoning unit plans the actions of the active rendezvous element required to accomplish the task. They tested all of the equipment in a simulated virtual environment and in a physical laboratory environment reproducing the illumination conditions of a representative space environment such as a strong light source, very low ambient light and harsh shadows. The demonstration experiment safely captured the simulated target satellite via vision-based sensing, meeting their performance requirements.

Kawano et al.[15] reported on the first autonomous Rendezvous and Docking Vehicle (RDV) of an Engineering Test Satellite-VII (ETS-VII) with an associated uninhabited spacecraft, which is shown schematically in Figure 1.13. The RDV technology demonstrator successfully rendezvoused then coupled two spacecraft. The ETS-VII experiment consisted of two satellites and the experiment was conducted in two steps. First, the chaser satellite released the target satellite. Subsequently, the chaser satellite approached and then docked with the target satellite.

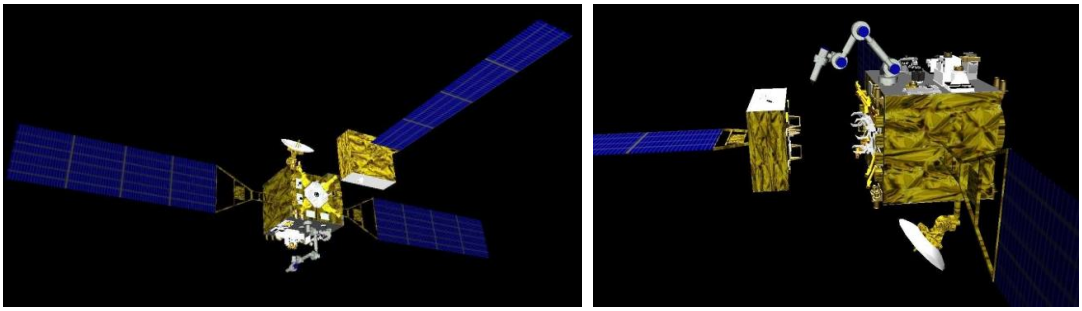

Figure 1.13 ETS-VII Experiment.

The ETS-VII RDV system demonstrated the feasibility of three major autonomous rendezvous functions: 1) autonomous rendezvous and docking by an uninhabited satellite; 2) safe autonomous rendezvous and docking; and 3) low-impact autonomous docking[15].

Uninhabited RDV systems can be categorized either as autonomous RDVs or remotely piloted RDVs. Autonomous RDV was chosen for this demonstrated experiment because of its utility and applicability to a variety of spacecraft types, while enabling them to demonstrate the feasibility of a fully autonomous, highly accurate and reliable rendezvous system that was capable of executing rendezvous and docking even when the spacecraft pair was not in continuous communication with the ground station.

The experiments were initiated when the chaser satellite ejected the target satellite with a departure speed of 1.8 cm/sec. In the first experiment, the chaser satellite started to control its relative attitude and position automatically and separated up to 2 m from the target, which was the holding point. The target and chaser satellites flew in formation for 15 minutes, maintaining the separation distance of 2 m. When the approach command was sent to the chaser satellite, it approached the target satellite with a relative velocity of 1 cm/s, until it captured the target satellite. The first experiment was successfully completed after the chaser satellite automatically docked to the target satellite.

The second experiment (FP-2) was initiated in the same way, but the separation distance was substantially larger (2.5 km rather than 2 m). All of the

command and control processes were the same as in the first experiment, but some of the chaser satellite thrusters did not fire correctly during the first attempt and correcting that fault extended the mission. After modifying the RDV software, the two spacecraft were successfully docked, achieving the milestone of the first successful autonomous rendezvous and docking demonstration.

The ETS-VII experiment successfully demonstrated (1) relative approach, (2) final approach and (3) actual docking[15].

1.3.3 Development of Spacecraft Removal Systems

Spacecraft removal systems are not a new idea. However, some constraints have blocked their development. Challenges related to cost and scheduling resources, operational constraints, liability and political challenges have all presented barriers. These constraints are related to removing objects from an orbit. In addition, it has not yet been widely accepted as being feasible using current technical capabilities. However, the previous and recent major breakup events that occurred in 2009 between a functional satellite (Iridium 33) and a non-functional satellite (Cosmos 2251), depicted in Figure 1.4, and tabulated in Table 1.1, and ongoing space environment modeling efforts have certainly reignited the interest in using spacecraft removal systems to remediate the space environment. In this section, active removal systems and their technical analysis will be reviewed[16], along with an evaluation of propulsive system requirements for de-orbiting a satellite[17].

Karl[16] has analyzed the orbital debris problem and categorized orbital debris by their size. He put forward several ideas for effecting the active removal of orbital debris. Since the orbital debris grows with every launch, satellites must be protected using passive systems such as shielding, or active collision prevention by using small orbital maneuvers to avoid tracked orbital debris.

For orbital debris smaller than 1 cm, a sweeper spacecraft can be considered. If that type of spacecraft was covered with a special material such as foils or fibers[16], possessing material characteristics that provide high strength and low mass, it could collect (sweep) small size orbital debris objects by stopping the high velocity particles without creating new orbital debris. After that type of spacecraft completed its sweep mission, it could be burned up re-entering Earth’s atmosphere.

For orbital debris objects larger than 1 cm, but smaller than 10 cm, a ground-based or satellite-based laser system[16] could be employed to de-orbit the debris. The envisioned laser system would focus the laser on the targeted orbital debris for several minutes, resulting in the ejection of a sublimating material layer. The sublimating material layer can produce a thrust that can alter the orbit and accelerate orbital decay.

Orbital debris larger than 10 cm can be tracked from the ground. For this type of orbital debris, tethers or space tugs[16] were identified as potential debris removal approaches.

Momentum transfer and electrodynamic effects can be used by tether systems. By inducing a swing velocity between the chase vehicle and the target object, by way of a chase vehicle tether, momentum transfer can occur. The tethered system and/or lightweight mechanical tethers[16] can exchange momentum due to the effect of gravity gradients and this momentum change can be sufficient to send the debris on trajectories that either enter the Earth's atmosphere or, at higher orbital altitudes, produce an escape trajectory, in some cases[16].

Space tugs are a logical option for larger objects. A de-orbiter spacecraft can be sent to rendezvous and dock with one or more previously targeted large orbiting objects. After rendezvousing and docking with the object, either its own or a deployed propulsion system can be activated to place the captured object into a trajectory for re-entry into Earth's atmosphere.

Burkhart et al.[17] examined propulsive de-orbiting methods. The primary focus of their study was the identification of the most suitable propulsion systems to de-orbit different classes of spacecraft over the mass range from below 10 kg to more than 2,000 kg. Two satellite types were used as examples for establishing propulsion system options – the Pathfinder and IRS-1C satellites. Pathfinders are a small-sized spacecraft category, while IRS-C1 is medium-sized. Above 615 km, natural satellite lifetimes are longer than 25 years and these satellites require active removal systems. The propulsion systems investigated in the study were chemical and solar-electric propulsion systems. Chemical propulsion systems utilizing cold gas, mono-propellant, bi-propellant, solid propellant, and hybrid propulsion were considered along with electric propulsion utilizing a gas for propulsion. The propulsion systems covered a

range of thrusts and specific impulses (I_{sp}) as shown in Figure 1.14[17]. Figure 1.14a shows the thrust range of all propulsion systems, Figure 1.14b represents the specific impulse range of chemical propulsion systems examined and Figure 1.14c shows the specific impulse range of electrical propulsion systems. Table 1.2 summarizes the advantages and disadvantages of the various propulsion systems[17].

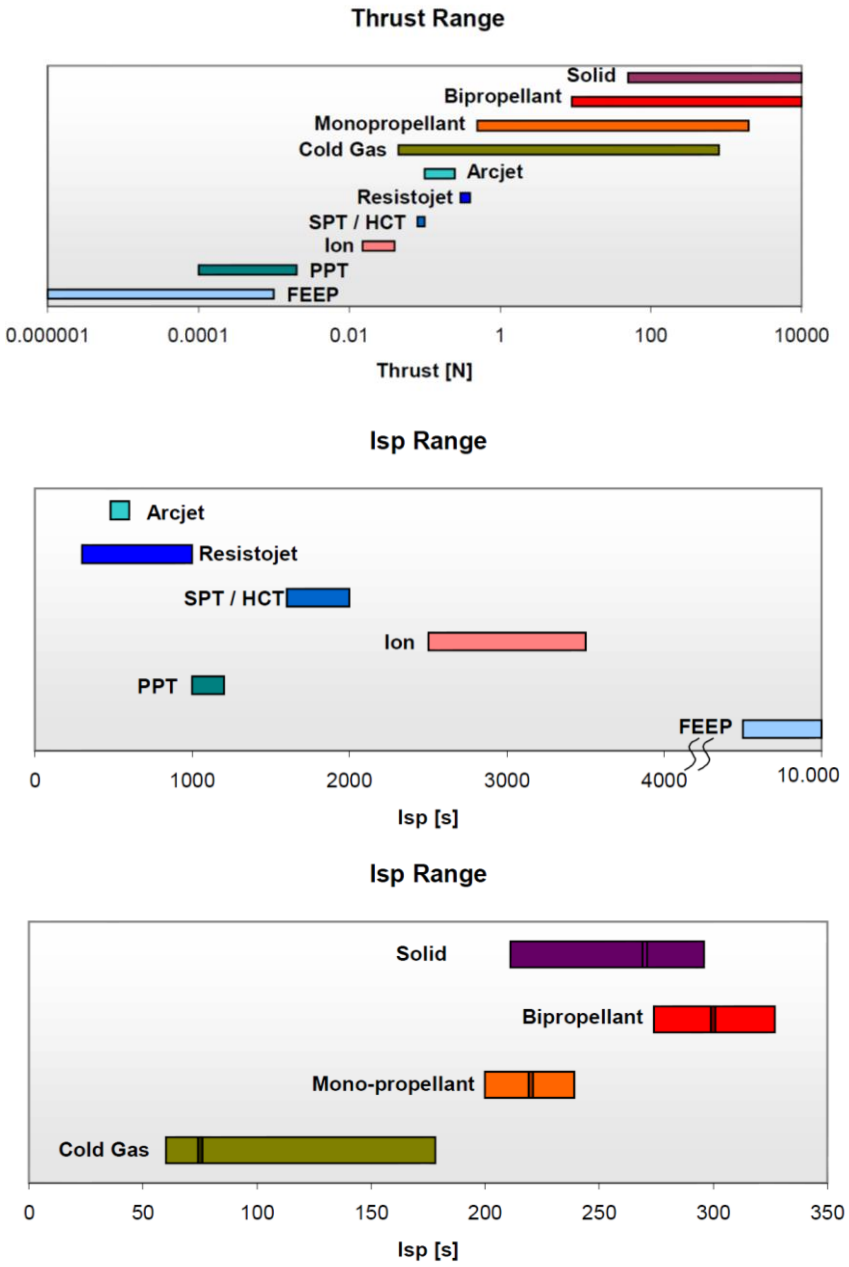

Figure 1.14 Thrust-I_{sp} Range of All Types of Propulsion Systems.

Table 1.2 Advantages and Disadvantages of Propulsion Systems.

Type of Prop.	Advantages	Disadvantages	Type of Prop.	Advantages	Disadvantages
Cold Gas	Simple Low system cost Reliable Safe	Extremely low Isp Moderate impulse capability Low density High pressure	Solid Propulsion	Simple, Reliable Low cost High density Low structural index	One thruster per burn Total Impulse fix Currently not qualified for longterm space
Mono Propellant	Wide thrust range Modulable Proven	Low Isp (mostly) toxic fuels	Hybrid Propulsion	Modulable Simple Reliable Low cost	Not qualified Lack of suitable oxidizer
Bi-Propellant (Storable)	Wide thrust range Modulable Proven	Complex Costly Heavy Toxic	Electrical Propulsion	Very high Isp	Low thrust Complex Long maneuver time Power consumption

Burkhart et al.[17] also discussed specific types of de-orbiting options: 1) uncontrolled de-orbiting, 2) controlled de-orbiting and 3) maneuvering the spacecraft into disposal orbit regions. The uncontrolled de-orbiting process starts with one or more deceleration maneuvers to reduce the object velocity and perigee altitude. This orbital change increases the aerodynamic drag and thus reduces the orbital life time of the object. Controlled de-orbit maneuvers are basically the same as the uncontrolled de-orbiting maneuvers, but they incorporate several propulsive retro-burn and re-entry maneuvers in order to produce a ΔV versus a time profile that follows a trajectory with a predictable ground impact location. Maneuvering spacecraft into disposal orbits (graveyard orbits) is an option but was not discussed in the Burkhart et al.[17] study.

1.4 Description of the GlobalStar Constellation

The Globalstar communication system consists of a space segment, a user segment, a ground segment, and four terrestrial networks, as shown in Figure 1.15.

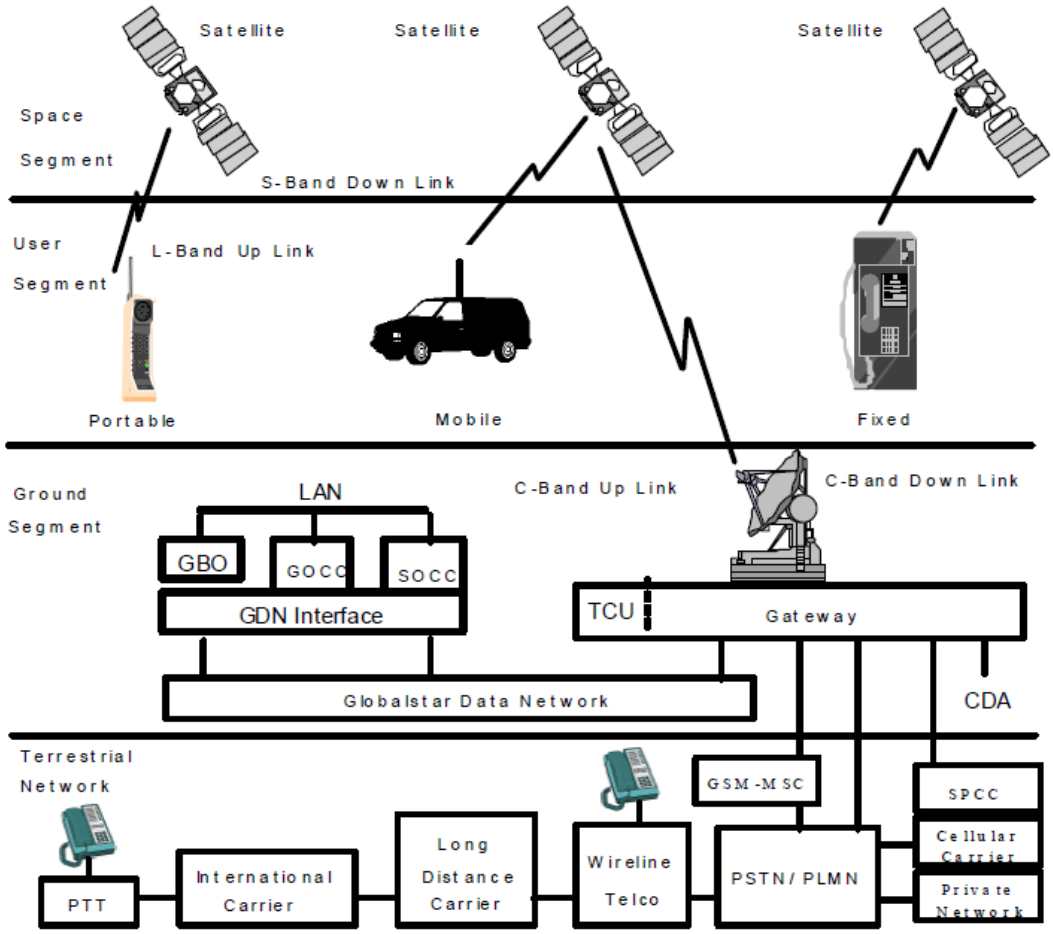

Figure 1.15 Segments of GlobalStar Satellite Constellation.

The space segment of the Globalstar constellation was planned initially to be 52 satellites (48 operational and 4 on-orbit spares). The satellites are in a 48-8-1[18] Walker constellation, in the Space Systems Loral "Big LEO" global mobile communications network, offering global real time voice, data and fax. The Globalstar satellites were launched from the Baikonur Cosmodrome using Soyuz launch vehicles. The satellites are 3-axis stabilized, employing magnetometers on deployable booms, sun sensors, GPS attitude sensors, and carry two deployable solar arrays, capable of delivering 1,100 W. The satellites in the first-generation constellation were designed to operate at full performance for a minimum of 7.5 years. The satellite constellation is depicted in Figure 1.16[18].

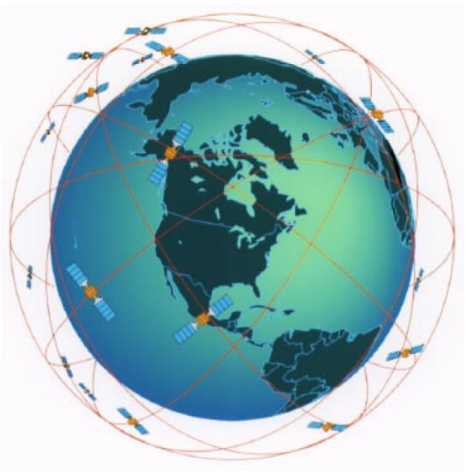

Figure 1.16 GlobalStar Satellite Constellation.

The satellites in the GlobalStar system have been placed into Low Earth Orbits in eight operational planes containing six satellites each, orbiting at nearly constant 1,414 km altitudes, and inclined at 52°. Each satellite has a nominal orbital period of 114 minutes and the overall constellation covers the globe between 67° North and 67° South latitude. The Globalstar system provides communications from any point on the Earth's surface to any other point on the Earth's surface, exclusive of the polar regions. The satellites utilize SS/Loral LS-400 platforms, with a trapezoidal body shape, along with the two deployable solar panels. In that way, multiple satellites can be carried on and be deployed from the same launch vehicle. The satellite propulsion systems employ hydrazine, with a primary function of station keeping. The mass of each satellite is 450 kg, and the dry mass is 350 kg.

The Globalstar satellite is a simple, low-cost satellite designed to minimize both satellite and launch costs. A pictorial sketch of the satellite and some of the major characteristics are summarized in Figure 1.17[18].

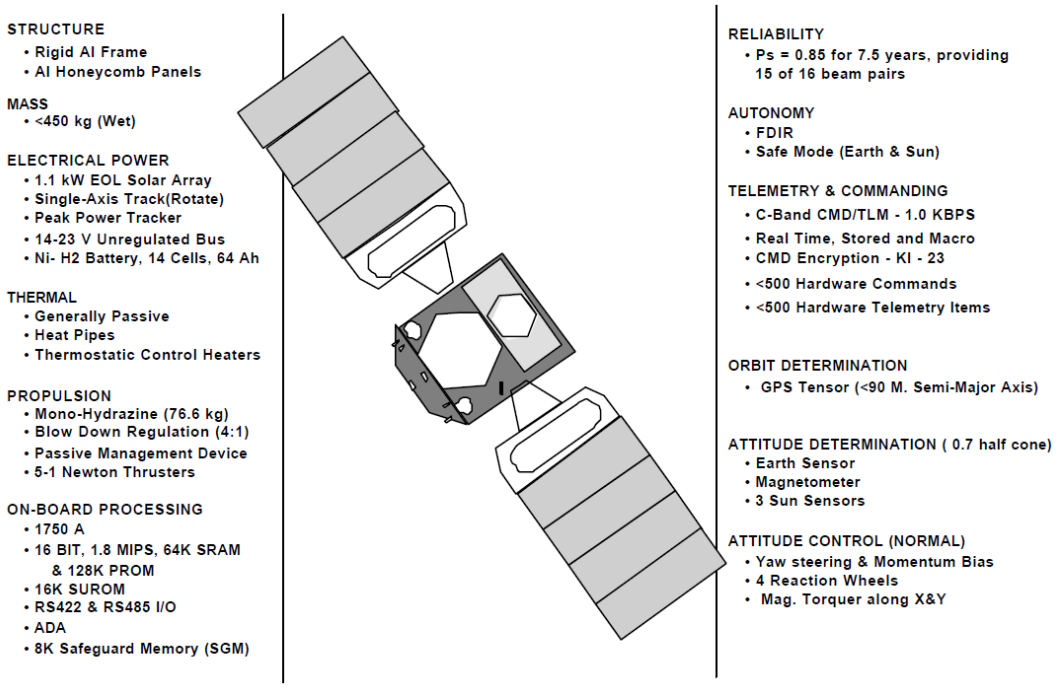

Figure 1.17 GlobalStar Spacecraft Characteristics.

1.5 Thesis Outline

Various governmental agencies and international organizations are beginning to track space debris and research possible mitigation solutions. One such debris mitigation organization is the Inter-Agency Debris Coordinating Committee (IADC) of the United Nations. Guidelines developed by IADC are the current basis for LEO satellite debris mitigation measures[19]. Quoting from that document:

> "A spacecraft or orbital stage should be left in an orbit in which, using an accepted nominal projection for solar activity, atmospheric drag will limit the orbital lifetime after completion of operations. A study on the effect of post mission orbital lifetime limitation on collision rate and debris population growth has been performed by the IADC. This IADC and some other studies and a number of existing national guidelines have found 25 years to be a reasonable and appropriate lifetime limit."

As a result of studies and recommendations made by international organizations, countries with the ability to access space have begun to give attention to the

management of space debris in order to reduce the risks of collision and thus address avoidable manned and unmanned mission failures.

The objective of this thesis is to investigate mitigation of space debris by examining an approach for recovery of a specific population of spent satellites. Decommissioning a spacecraft is the final event associated with any space mission. It has therefore become standard practice to remove non-functional satellites from their original orbits, placing many of them in higher orbits by using the residual propellant in the secondary propulsion system at the end of its useful life. This maneuver is frequently and appropriately called a 'graveyard burn'. It is also becoming the practice in LEO missions to provide controlled re-entry into the Earth's atmosphere. The reason for this controlled re-entry approach is that uncontrolled re-entry can lead to vehicle breakup, providing a hazard on the ground and adding to the problem of space debris hazard.

This study has examined the GlobalStar satellite constellation in order to provide a specific example related to a large population of high-value satellites that occupy a Low Earth Orbit and have the potential of becoming orbital space debris. Since the original GlobalStar satellites were launched in 1999, with planned useful lives of 7.5 years, the first generation of these satellites are now becoming orbital debris. Presently, at least 11 satellites have ceased operation in the GlobalStar constellation orbits, and the GlobalStar Communication Company has begun replacing its original constellation satellites with new second generation GlobalStar satellites. The new second generation of GlobalStar satellites is currently being launched, six-at-a-time starting in October, 2010[20]. As the new second generation satellites have replaced the first generation satellites, GlobalStar has adjusted the orbits of their non-functioning first-generation satellites, placing them in 2,000 km graveyard orbits. The graveyard orbits have reduced the risk associated with non-functioning satellites occupying primary orbits, but those satellites will need to eventually be removed. This thesis has developed a strategy for removing those satellites.

CHAPTER 2

IMPULSIVE ORBIT TRANSFER STRATEGIES

Propulsion systems are employed to effect controlled changes in the orbit of a spacecraft. Orbit transfer maneuvers use directed thrust to accelerate (or decelerate) an orbiting object, changing its inertial velocity (direction and or magnitude) so that at the end of the propulsive maneuver, a different orbit results. These propulsive maneuvers are employed to transfer spacecraft from their launch-vehicle-controlled initial orbits to a different orbit. They are also employed to change the orbital plane, to circularize an orbit or to synchronize the orbit of one spacecraft either with respect to a fixed location on the Earth's surface or with respect to another spacecraft. Most orbital transfer operations utilize chemical propellants in order to better-control orbital adjustments. It is the task of mission planners to determine spacecraft propellant mass allowances required to attain and maintain planned orbital configurations over the lifetime of the spacecraft. Orbital rendezvous with a specified spacecraft is one of the most demanding classes of spacecraft maneuvers and it is necessary to properly estimate the propellant required for these operations.

2.1 Relative Motion in Orbit

A rendezvous maneuver consists of a target vehicle and a chaser vehicle. The target vehicle is the passive, non-maneuvering vehicle, already in a specific orbit. The chaser vehicle is the active vehicle, performing the maneuvers required to achieve an appropriately synchronized target vehicle orbit, and subsequently to overtake and actually rendezvous with the target vehicle. The space shuttle is used regularly as a chase vehicle, rendezvousing with the International Space Station (ISS) which is the target vehicle.

In the geocentric equatorial frame, the position vector of the target vehicle is $\vec{r}$ and the moving or relative frame of reference has its origin located at a specific reference point on the target vehicle, as shown in Figure 2.1. The *x*-axis is directed along $\vec{r}$, the outward radial vector to the target. The *y* axis is perpendicular to $\vec{r}$ and points in the direction of the target satellite's local horizon. The *x* and *y* axes therefore lie in the target's orbital plane, and the *z* axis is normal to that plane[21].

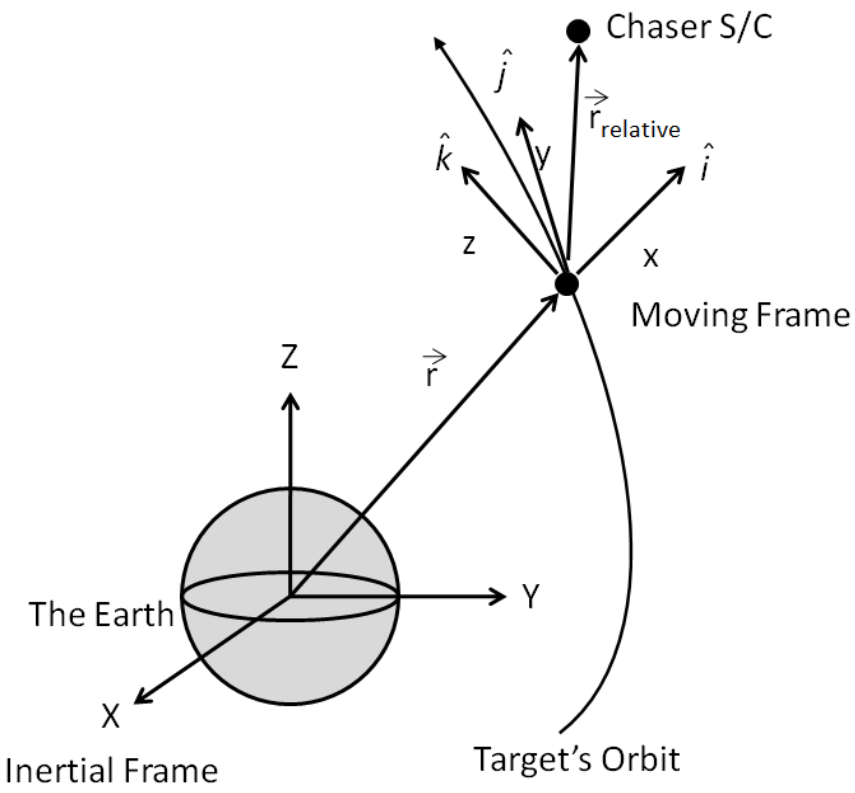

Figure 2.1 Moving Frame Attached to Target S/C from which Chaser S/C Observed.

The angular velocity of the moving frame which contains the *x*,*y z* axes, attached to the target vehicle, is just the angular velocity of the position vector $\vec{r}$, and can be written:

$$\vec{h} = \vec{r} \times \vec{v} = (rv)\hat{k} = (r^2\Omega)\hat{k} = r^2\vec{\Omega}. \tag{2.1}$$

Hence, the angular velocity vector from Equation 2.1 is:

$$\vec{\Omega} = \frac{\vec{r}\times\vec{v}}{r^2} \tag{2.2}$$

The angular acceleration of the coordinate system is achieved by taking the time derivative of Equation 2.2:

$$\frac{d}{dt}\vec{\Omega} = \frac{1}{r^2}\left(\dot{\vec{r}} \times \vec{v} + \vec{r} \times \dot{\vec{v}}\right) - \frac{2}{r^3}\dot{\vec{r}}(\vec{r} \times \vec{v}) \tag{2.3}$$

but

$$\vec{r} \times \vec{v} = \vec{v} \times \vec{v} = 0 \tag{2.4}$$

and the acceleration of the target vehicle is

$$\vec{a} = \dot{\vec{v}} = -\frac{\mu}{r^3}\vec{r}. \tag{2.5}$$

In addition,

$$\vec{r} \times \dot{\vec{v}} = \vec{r} \times \left(-\frac{\mu}{r^3}\vec{r}\right) = -\frac{\mu}{r^3}(\vec{r} \times \vec{r}) = 0 \tag{2.6}$$

Finally, after manipulating Equations 2.2, 2.4, and 2.6, the angular acceleration can be represented as:

$$\frac{d}{dt}\vec{\Omega} = -\frac{2(\vec{r}\times\vec{v})}{r^2}\vec{\Omega} \tag{2.7}$$

At first, it may be hard to visualize the motion of one spacecraft relative to another in orbit. Figure 2.2[21] can simplify that challenge. In Figure 2.2, two orbits are shown and Orbit 1 is a circular orbit while Orbit 2 is elliptical with an eccentricity of 0.125. The two orbits have the same semi-major axes (*a*) and for this reason their orbital periods are the same. A co-moving frame is shown attached to "Observer *A*" in the circular orbit (number 1). At Epoch *I*, Spacecraft *B*, in Elliptical Orbit 2, is directly below the Observer *A* satellite. In other words, *A* must draw an arrow in the negative *x*-direction to point at the position vector locating *B* in the lower orbit. Figure 2.2 shows eight different epochs (*I*, *II*, *III*, . . .), equally spaced around the circular orbit, in order to visualize the relative position of the two spacecraft with respect to each other. Of course, *A*'s observation frame is rotating, because the *x*-axis must always be directed away from the earth. Observer *A* cannot sense this rotation and records the set of observations in their (to them) "fixed" *xy* coordinate system, as shown at the bottom of the Figure 2.2. Coasting at a uniform speed along the circular orbit, *A* sees the other vehicle orbiting them clockwise in a sort of bean-shaped path. The distance between the two spacecraft, in this case, never becomes so great that the Earth intervenes.

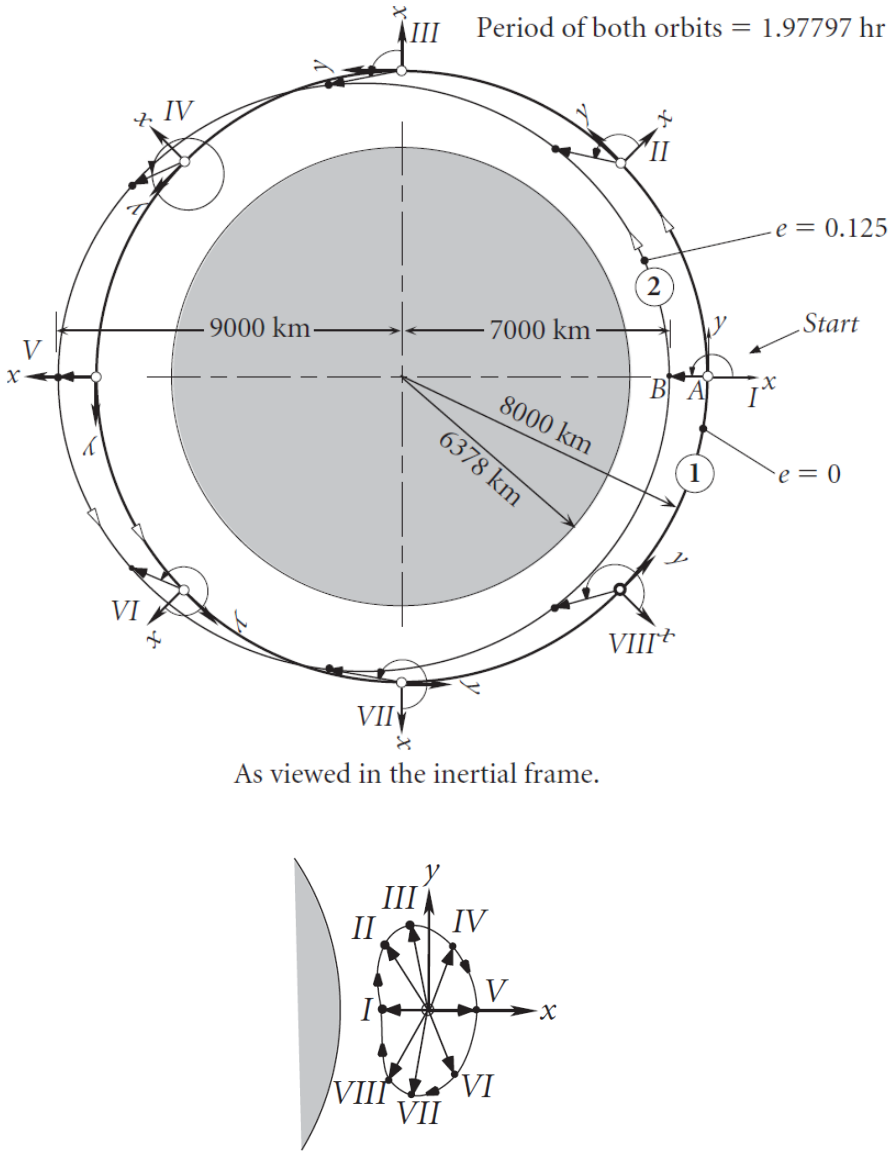

Figure 2.2 Relative Motion of Elliptically Orbiting Spacecraft B and Circularly Orbiting Spacecraft A.

2.2 Linearization of the Equations of Relative Motion in Orbit

Figure 2.3 illustrates two satellites in Earth's orbit trajectories. $\overrightarrow{r_0}$ is the position vector of the target vehicle and $\vec{r}$ is the position vector of the chase vehicle in the inertial coordinate frame.

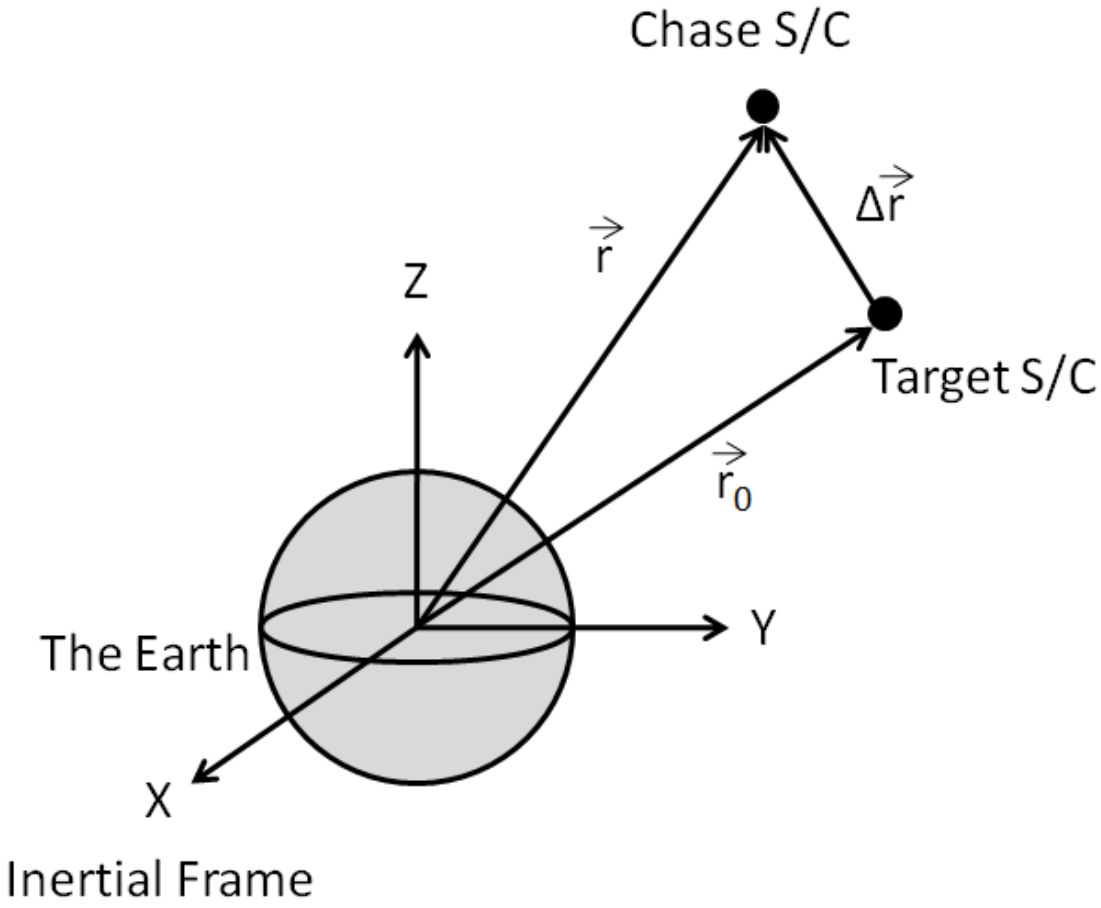

Figure 2.3 Position Vector of Chase Vehicle Relative to Target Vehicle.

We can also define the position vector of the chase vehicle relative to the target vehicle using $\Delta\vec{r}$, given by:

$$\vec{r} = \vec{r_0} + \Delta\vec{r} \tag{2.8}$$

The chase vehicle acceleration can be written:

$$\ddot{\vec{r}} = -\mu \frac{\vec{r}}{r^3} \tag{2.9}$$

where r = $\|\vec{r}\|$. Substituting Equation 2.8 into Equation 2.9 yields the acceleration difference between the chase vehicle and the target vehicle:

$$\Delta\ddot{\vec{r}} = -\ddot{\vec{r}}_0 - \mu \frac{\vec{r}_0 + \Delta\vec{r}}{r^3} \tag{2.10}$$

The symbol Δ is used to represent the relative position vector, and has a magnitude which is very small compared to the magnitude of the other position vectors which are $\overrightarrow{r_0}$ and $\vec{r}$, so that

$$\frac{\Delta r}{r_0} \ll 1, \tag{2.11}$$

where Δr = $\|\Delta\vec{r}\|$ and $r_0 = \|\vec{r}_0\|$.

We can simplify Equation 2.10 by making use of the fact that $\|\Delta\vec{r}\|$ is very small,

$$r^2 = \vec{r}\cdot\vec{r} = (\overrightarrow{r_0} + \Delta\vec{r})\cdot(\overrightarrow{r_0} + \Delta\vec{r}) = \overrightarrow{r_0}\cdot\overrightarrow{r_0} + 2\overrightarrow{r_0}\cdot\Delta\vec{r} + \Delta\vec{r}\cdot\Delta\vec{r}$$

Since $\overrightarrow{r_0}\cdot\overrightarrow{r_0} = {r_0}^2$ and $\Delta\vec{r}\cdot\Delta\vec{r} = \Delta r^2$ yields:

$$r^2 = {r_0}^2\left[1 + \frac{2\overrightarrow{r_0}\cdot\Delta\vec{r}}{{r_0}^2} + \left(\frac{\Delta r}{r_0}\right)^2\right]$$

We can neglect the quadratic term in brackets by virtue of Equation 2.11:

$$r^2 = {r_0}^2\left(1 + \frac{2\overrightarrow{r_0}\cdot\Delta\vec{r}}{{r_0}^2}\right) \tag{2.12}$$

We can neglect all higher order powers of $\Delta r/r_0$. Since $r^{-3} = (r^2)^{3/2}$:

$$r^{-3} = {r_0}^{-3}\left(1 + \frac{2\overrightarrow{r_0}\cdot\Delta\vec{r}}{{r_0}^2}\right)^{-3/2} \tag{2.13}$$

Using the binomial theorem and neglecting higher order terms

$$\left(1 + \frac{2\overrightarrow{r_0}\cdot\Delta\vec{r}}{{r_0}^2}\right)^{-3/2} = 1 + \left(-\frac{3}{2}\right)\left(\frac{2\overrightarrow{r_0}\cdot\Delta\vec{r}}{{r_0}^2}\right)$$

After some manipulation:

$$r^{-3} = {r_0}^{-3}\left(1 - \frac{3}{{r_0}^2}\overrightarrow{r_0}\cdot\Delta\vec{r}\right)^{-3/2}$$

which can be written:

$$\frac{1}{r^3} = \frac{1}{{r_0}^3} - \frac{3}{{r_0}^5}\overrightarrow{r_0} \cdot \Delta\vec{r} \tag{2.14}$$

Substituting Equation 2.14 into the relative acceleration Equation 2.10, we get

$$\Delta\ddot{\vec{r}} = -\ddot{\vec{r}}_0 - \mu\left(\frac{1}{{r_0}^3} - \frac{3}{{r_0}^5}\overrightarrow{r_0} \cdot \Delta\vec{r}\right)(\vec{r}_0 + \Delta\vec{r})$$

$$\Delta\ddot{\vec{r}} = -\ddot{\vec{r}}_0 - \mu\left(\frac{\vec{r}_0 + \Delta\vec{r}}{{r_0}^3} - \frac{3}{{r_0}^5}(\overrightarrow{r_0} \cdot \Delta\vec{r})(\vec{r}_0 + \Delta\vec{r})\right)$$

Again neglecting higher order terms, we get:

$$\Delta\ddot{\vec{r}} = -\ddot{\vec{r}}_0 - \mu\left(\frac{\vec{r}_0}{{r_0}^3} + \frac{\Delta\vec{r}}{{r_0}^3} - \frac{3}{{r_0}^5}(\overrightarrow{r_0} \cdot \Delta\vec{r})\vec{r}_0\right) \tag{2.15}$$

But the acceleration vector for the target vehicle is:

$$\ddot{\vec{r}}_0 = -\mu\frac{\vec{r}_0}{{r_0}^3}$$

Finally we get:

$$\Delta\ddot{\vec{r}} = -\frac{\mu}{{r_0}^3}\left(\Delta\vec{r} - \frac{3}{{r_0}^2}(\overrightarrow{r_0} \cdot \Delta\vec{r})\vec{r}_0\right). \tag{2.16}$$

Equation 2.16 is the linearized version of Equation 2.9, which governs the motion of the chase vehicle with respect to the target vehicle. The expression is linear because $\Delta\vec{r}$ appears only in the numerator and only first order powers of $\frac{\Delta r}{r_o}$ have been included.

2.3 Clohessy-Wiltshire Equations

Figure 2.4 illustrates an attached moving frame of reference *xyz* relative to the target spacecraft. This figure is similar to Figure 2.3, with the difference being that $\Delta\vec{r}$ is restricted by the approximation (Eq. 2.11). The origin of the moving system is located on the target spacecraft. The *x* axes lies along $\overrightarrow{r_0}$ and unit vector $\hat{l}$, can be defined:

$$\hat{\imath} = \frac{\overrightarrow{r_0}}{r_0}. \tag{2.17}$$

From Figure 2.4, the *y* axes is in the direction of the local horizon, and the *z* axes is the normal to the target spacecraft orbital plane described using the right hand rule, where $\hat{k} = \hat{\imath} \times \hat{\jmath}$. The inertial angular velocity of the moving frame of reference is $\vec{\Omega}$, and the inertial angular acceleration is $\dot{\vec{\Omega}}$.

According to the relative acceleration formula, we have:

$$\ddot{\vec{r}} = \ddot{\overrightarrow{r_0}} + \dot{\vec{\Omega}} \times \Delta\vec{r} + \vec{\Omega} \times \left(\vec{\Omega} \times \Delta\vec{r}\right) + 2\vec{\Omega} \times \Delta\vec{v}_{rel} + \Delta\vec{a}_{rel} \tag{2.18}$$

where the relative position, relative velocity and relative acceleration are given by, respectively:

$$\Delta\vec{r}_{rel} = \Delta x\hat{\imath} + \Delta y\hat{\jmath} + \Delta z\hat{k} \tag{2.19a}$$

$$\Delta\vec{v}_{rel} = \Delta\dot{x}\hat{\imath} + \Delta\dot{y}\hat{\jmath} + \Delta\dot{z}\hat{k} \tag{2.19b}$$

$$\Delta\vec{a}_{rel} = \Delta\ddot{x}\hat{\imath} + \Delta\ddot{y}\hat{\jmath} + \Delta\ddot{z}\hat{k} \tag{2.19c}$$

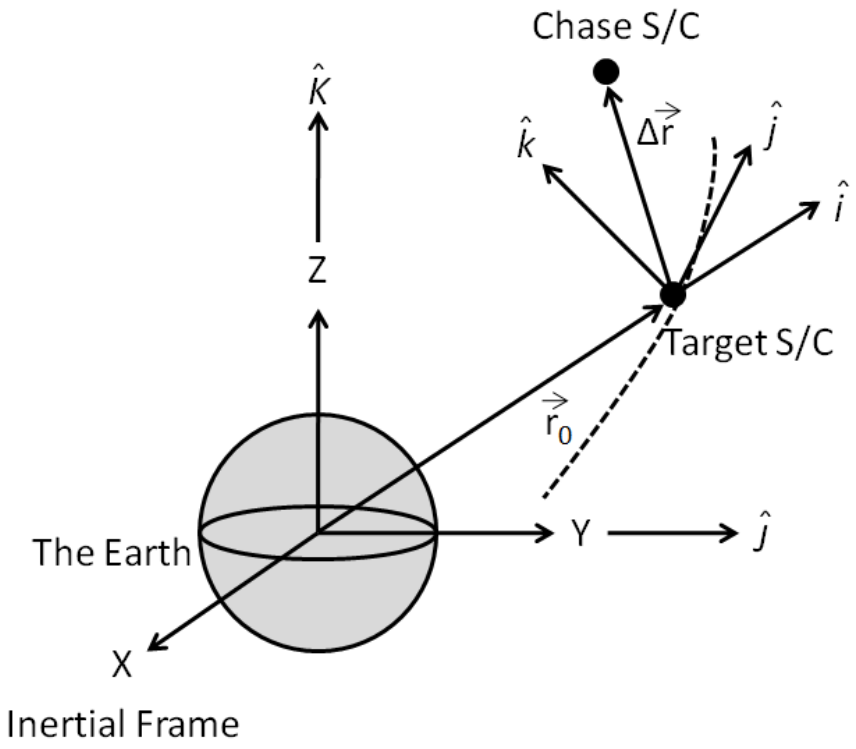

Figure 2.4 Co-moving Clohessy-Wiltshire Frame.

For simplicity, we assume that the orbit of the target spacecraft is circular (e=0) so that the angular acceleration is equal to zero $\left(\vec{\Omega} = 0\right)$. Using this restriction, together with Equation 2.8, and substitution into Equation 2.18 yields:

$$\Delta\ddot{\vec{r}} = \vec{\Omega} \times \left(\vec{\Omega} \times \Delta\vec{r}\right) + 2\vec{\Omega} \times \Delta\vec{v}_{rel} + \Delta\vec{a}_{rel}$$

Applying the vector triple cross product identity rule to the first term on the right hand side of equation, yields:

$$\Delta\ddot{\vec{r}} = \vec{\Omega}\left(\vec{\Omega} \cdot \Delta\vec{r}\right) - \Omega^2\Delta r + 2\vec{\Omega} \times \Delta\vec{v}_{rel} + \Delta\vec{a}_{rel} \qquad (2.20)$$

Since the target spacecraft orbit is circular, we can write the angular velocity of the target spacecraft $\left(\vec{\Omega}\right)$ as:

$$\vec{\Omega} = n\hat{k} \qquad (2.21)$$

where n is the mean motion of target spacecraft, and is constant. Thus:

$$\vec{\Omega} \cdot \Delta\vec{r} = n\hat{k} \cdot \left(\Delta x\hat{\imath} + \Delta y\hat{\jmath} + \Delta z\hat{k}\right) = n\Delta z \tag{2.22}$$

and

$$\vec{\Omega} \cdot \Delta\vec{v}_{rel} = n\hat{k} \times \left(\Delta\dot{x}\hat{\imath} + \Delta\dot{y}\hat{\jmath} + \Delta\dot{z}\hat{k}\right) = -n\Delta\dot{y}\hat{\imath} + n\Delta\dot{x}\hat{\jmath} \tag{2.23}$$

Substituting Equations 2.21, 2.22 and 2.23 along with Equations 2.19, into Equation 2.20 yields:

$$\Delta\ddot{\vec{r}} = n\hat{k}(n\Delta z) - n^2\left(\Delta x\hat{\imath} + \Delta y\hat{\jmath} + \Delta z\hat{k}\right) + 2(-n\Delta\dot{y}\hat{\imath} + n\Delta\dot{x}\hat{\jmath}) + \Delta\ddot{x}\hat{\imath} + \Delta\ddot{y}\hat{\jmath} + \Delta\ddot{z}\hat{k}$$

Finally, collecting terms yields:

$$\Delta\ddot{\vec{r}} = (-n^2\Delta x - 2n\Delta\dot{y} + \Delta\ddot{x})\hat{\imath} + (-n^2\Delta y + 2n\Delta\dot{x} + \Delta\ddot{y})\hat{\jmath} + \Delta\ddot{z}\hat{k} \tag{2.24}$$

This expression gives the components of the chaser's absolute relative acceleration vector in terms of quantities that can be measured in the moving reference frame.

Since the target spacecraft orbit is circular, the mean motion of the target spacecraft is given by:

$$n = \frac{v}{r_0} = \frac{1}{r_0}\sqrt{\frac{\mu}{r_0}} = \sqrt{\frac{\mu}{{r_0}^3}},$$

and therefore:

$$n^2 = \frac{\mu}{{r_0}^3}. \tag{2.25}$$

Recalling Equations 2.17 and 2.19a, we also note that:

$$\vec{r}_0\Delta\vec{r} = (r_0\hat{\imath}) \cdot \left(\Delta x\hat{\imath} + \Delta y\hat{\jmath} + \Delta z\hat{k}\right) = r_0\Delta x \tag{2.26}$$

Substituting Equations 2.19a, 2.25 and 2.26 into the relative acceleration Equation 2.16 yields:

$$\Delta\ddot{\vec{r}} = -n^2\left[\Delta x\hat{\imath} + \Delta y\hat{\jmath} + \Delta z\hat{k} - \frac{3}{{r_0}^3}(r_0\hat{\imath})\right] = 2n^2\Delta x\hat{\imath} - n^2\Delta y\hat{\jmath} - n^2\Delta z\hat{k} \tag{2.27}$$

Combining Equations 2.22 and 2.27, we obtain:

$$(-n^2\Delta x - 2n\Delta\dot{y} + \Delta\ddot{x})\hat{\imath} + (-n^2\Delta y + 2n\Delta\dot{x} + \Delta\ddot{y})\hat{\jmath} + \Delta\ddot{z}\hat{k} = 2n^2\Delta x\hat{\imath} - n^2\Delta y\hat{\jmath} - n^2\Delta z\hat{k}$$

Upon collecting terms on the left-side of the equation, we get:

$$(\Delta\ddot{x} - 3n^2\Delta x - 2n\Delta\dot{y})\hat{\imath} + (\Delta\ddot{y} + 2n\Delta\dot{x})\hat{\jmath} + (\Delta\ddot{z} + n^2\Delta z)\hat{k} = 0$$

That is:

$$\Delta\ddot{x} - 3n^2\Delta x - 2n\Delta\dot{y} = 0 \qquad (2.28a)$$

$$\Delta\ddot{y} + 2n\Delta\dot{x} = 0 \qquad (2.28b)$$

$$\Delta\ddot{z} + n^2\Delta z = 0 \qquad (2.28c)$$

Equations 2.28a, 2.28b and 2.28c are the Clohessy-Wiltshire (CW) equations. When using these equations, we will refer to the moving frame of reference in which they were derived as the Clohessy-Wiltshire frame. The 2.28 equation group is a set of coupled, second order differential equations with constant coefficients. The initial conditions are:

$$\text{At } t = 0, \quad \Delta x = \Delta x_0 \quad \Delta y = \Delta y_0 \quad \Delta z = \Delta z_0$$

$$\Delta\dot{x} = \Delta\dot{x}_0 \quad \Delta\dot{y} = \Delta\dot{y}_0 \quad \Delta\dot{z} = \Delta\dot{z}_0 \qquad (2.29)$$

From Equation 2.28b:

$$\frac{d}{dt}(\Delta\dot{y} + 2n\Delta x) = 0$$

which means:

$$\Delta\dot{y} + 2n\Delta x = constant$$

We find the constant by evaluating the left hand side of the equation at $t = 0$. Therefore:

$$\Delta\dot{y} + 2n\Delta x = \Delta\dot{y}_0 + 2n\Delta x_0$$

so that:

$$\Delta\dot{y} = \Delta\dot{y}_0 + 2n(\Delta x_0 - \Delta x) \tag{2.30}$$

Substituting this result into Equation 2.28a yields:

$$\Delta\ddot{x} - 3n^2\Delta x - 2n[\Delta\dot{y}_0 + 2n(\Delta x_0 - \Delta x)] = 0$$

which, upon rearrangement, becomes:

$$\Delta\ddot{x} + n^2\Delta x = 2n\Delta\dot{y}_0 + 4n^2\Delta x_0 \tag{2.31}$$

The solution of this differential equation is:

$$\Delta x = A\sin nt + B\cos nt + \frac{2}{n}\Delta\dot{y}_0 + 4\Delta x_0 \tag{2.32}$$

Differentiating this equation once with respect to time, we obtain:

$$\Delta\dot{x} = nA\cos nt - nB\sin nt \tag{2.33}$$

Evaluating equation (2.32) at $t = 0$, we find:

$$\Delta x_0 = B + \frac{2}{n}\Delta\dot{y}_0 + 4\Delta x_0 \rightarrow B = -3\Delta x_0 - 2\frac{\Delta\dot{y}_0}{n}$$

Evaluating equation (2.33) at $t = 0$ we find:

$$\Delta\dot{x}_0 = nA \rightarrow A = \frac{\Delta\dot{x}_0}{n}$$

Substituting these values for A and B into Equation 2.32 leads to:

$$\Delta x = \frac{\Delta\dot{x}_0}{n}\sin nt + \left(-3\Delta x_0 - 2\frac{\Delta\dot{y}_0}{n}\right)\cos nt + \frac{2}{n}\Delta\dot{y}_0 + 4\Delta x_0$$

which, upon combining terms, becomes:

$$\Delta x = (4 - 3\cos nt)\Delta x_0 + \frac{\sin nt}{n}\Delta\dot{x}_0 + \frac{2}{n}(1 - \cos nt)\Delta\dot{y}_0 \tag{2.34}$$

Therefore,

$$\Delta\dot{x} = 3n\sin nt\,\Delta x_0 + \cos nt\,\Delta\dot{x}_0 + 2\sin\Delta\dot{y}_0 \tag{2.35}$$

Substituting Equation 2.34 into Equation 2.30 yields:

$$\Delta\dot{y} = \Delta\dot{y}_0 + 2n\left[\delta x_0 - (4 - 3\,cos\,nt)\Delta x_0 + \frac{sin\,nt}{n}\Delta\dot{x}_0 + \frac{2}{n}(1 - cos\,nt)\Delta\dot{y}_0\right]$$

which simplifies to:

$$\Delta\dot{y} = 6n(\cos nt - 1)\Delta x_0 - 2\sin nt\Delta\dot{x}_0 + (4\cos nt - 3)\Delta\dot{y}_0 \qquad (2.36)$$

Integrating this expression with respect to time, we find that:

$$\Delta y = 6n\left(\frac{1}{n}\sin nt - t\right)\Delta x_0 + \frac{2}{n}\cos nt\,\Delta\dot{x}_0 + \left(\frac{4}{n}\sin nt - 3t\right)\Delta\dot{y}_0 + C \qquad (2.37)$$

Evaluating Δy at $t = 0$ yields:

$$\Delta y_0 = \frac{2}{n}\Delta\dot{x}_0 + C \rightarrow C = \Delta y_0 - \frac{2}{n}\Delta\dot{x}_0$$

Substituting this value for *C* into Equation 2.37, we get:

$$\Delta y = 6(\sin nt - nt)\Delta x_0 + \Delta y_0 + \frac{2}{n}(\cos nt - 1)\Delta\dot{x}_0 + \left(\frac{4}{n}\sin nt - 3t\right)\Delta\dot{y}_0 \qquad (2.38)$$

Finally, the solution of Equation 2.28c is:

$$\Delta z = D\cos nt + E\sin nt \qquad (2.39)$$

so that

$$\Delta\dot{z} = -nD\sin nt + nE\cos nt \qquad (2.40)$$

We evaluate the two expressions at $t = 0$ to obtain the constants of integration:

$$\Delta z_0 = D$$

$$\Delta\dot{z}_0 = nE$$

Putting these values for D and E back into Equation 2.38 and Equation 2.40 yields:

$$\Delta z = \cos nt\,\Delta z_0 + \frac{1}{n}\sin nt\,\Delta\dot{z}_0 \qquad (2.41)$$

$$\Delta\dot{z} = -n\sin nt\,\Delta z_0 + \cos nt\,\Delta\dot{z}_0 \qquad (2.42)$$

Now that we have finished solving the Clohessy-Wiltshire equations, we change our notation, denoting the *x*, *y* and *z* components of relative velocity in the moving frame as Δu, Δv and Δw, respectively. That is:

$$\Delta u = \Delta \dot{x} \quad \Delta v = \Delta \dot{y} \quad \Delta w = \Delta \dot{z}$$

The initial conditions for the relative velocity components are then written:

$$\Delta u_0 = \Delta \dot{x}_0 \; \Delta v_0 = \Delta \dot{y}_0 \; \Delta w_0 = \Delta \dot{z}_0$$

Using this notation we write Equations 2.34, 2.35, 2.36, 2.38, 2.41 and 2.42 as

$$\Delta x = (4 - 3\cos nt)\Delta x_0 + \frac{\sin nt}{n}\Delta u_0 + \frac{2}{n}(1 - \cos nt)\Delta v_0 \tag{2.43a}$$

$$\Delta u = 3n \sin nt \, \Delta x_0 + \cos nt \, \Delta u_0 + 2 \sin \Delta v_0 \tag{2.43b}$$

$$\Delta v = 6n(\cos nt - 1)\Delta x_0 - 2 \sin nt \Delta u_0 + (4 \cos nt - 3)\Delta v_0 \tag{2.43c}$$

$$\Delta y = 6(\sin nt - nt)\Delta x_0 + \Delta y_0 + \frac{2}{n}(\cos nt - 1)\Delta u_0 + \left(\frac{4}{n}\sin nt - 3t\right)\Delta v_0 \tag{2.43d}$$

$$\Delta z = \cos nt \, \Delta z_0 + \frac{1}{n}\sin nt \, \Delta w_0 \tag{2.43e}$$

$$\Delta w = -n \sin nt \, \Delta z_0 + \cos nt \, \Delta w_0 \tag{2.43f}$$

Finally, introducing matrix notation to define the relative position and velocity vectors:

$$\{\Delta \vec{r}(t)\} = \begin{Bmatrix} \Delta x(t) \\ \Delta y(t) \\ \Delta z(t) \end{Bmatrix} \qquad \{\Delta \vec{v}(t)\} = \begin{Bmatrix} \Delta u(t) \\ \Delta v(t) \\ \Delta w(t) \end{Bmatrix}$$

and their initial values (at $t = 0$):

$$\{\Delta \vec{r}_0\} = \begin{Bmatrix} \Delta x_0 \\ \Delta y_0 \\ \Delta z_0 \end{Bmatrix} \quad \{\Delta \vec{v}_0\} = \begin{Bmatrix} \Delta u_0 \\ \Delta v_0 \\ \Delta w_0 \end{Bmatrix}.$$

Observe that we have dropped the subscript of relative (rel) introduced in Equation 2.19 because it is non-essential in rendezvous analysis. Equation 2.43 can be represented more compactly in matrix notation as:

$$\{\Delta\vec{r}(t)\} = \left[\vec{\Phi}_{rr}(t)\right]\{\Delta\vec{r}_0\} + \left[\vec{\Phi}_{rv}(t)\right]\{\Delta\vec{v}_0\} \tag{2.44a}$$

$$\{\Delta\vec{v}(t)\} = \left[\vec{\Phi}_{vr}(t)\right]\{\Delta\vec{r}_0\} + \left[\vec{\Phi}_{vv}(t)\right]\{\Delta\vec{v}_0\} \tag{2.44b}$$

where the Clohessy-Wiltshire matrices are:

$$\left[\vec{\Phi}_{rr}(t)\right] = \begin{bmatrix} 4-3\cos nt & 0 & 0 \\ 6(\sin nt - nt) & 1 & 0 \\ 0 & 0 & \cos nt \end{bmatrix} \tag{2.45a}$$

$$\left[\vec{\Phi}_{rv}(t)\right] = \begin{bmatrix} \frac{1}{n}\sin nt & \frac{2}{n}(1-\cos nt) & 0 \\ \frac{2}{n}(\cos nt - 1) & \frac{1}{n}(4\sin nt - 3nt) & 0 \\ 0 & 0 & \frac{1}{n}\sin nt \end{bmatrix} \tag{2.45b}$$

$$\left[\vec{\Phi}_{vr}(t)\right] = \begin{bmatrix} 3n\sin nt & 0 & 0 \\ 6n(\cos nt - 1) & 0 & 0 \\ 0 & 0 & -\mathrm{n}\sin nt \end{bmatrix} \tag{2.45c}$$

$$\left[\vec{\Phi}_{vv}(t) = \begin{bmatrix} \cos nt & 2\sin nt & 0 \\ -2\sin nt & 4\cos nt - 3 & 0 \\ 0 & 0 & \cos nt \end{bmatrix}\right] \tag{2.45d}$$

2.4 Two-Impulse Rendezvous Maneuvers

The typical rendezvous problem is shown in Figure 2.5. At time $t = 0^-$ (the instant preceding *t*=0), the position $\Delta\vec{r}_0$ and $\Delta\vec{v}_0{}^-$ of the chase spacecraft relative to the target is known. At *t*=0 an impulsive maneuver instantaneously changes the relative velocity to $\Delta\vec{v}_0{}^+$ at $t=0^+$ (the instant after *t*=0). The components of $\Delta\vec{v}_0{}^+$ are shown in Figure 2.5.

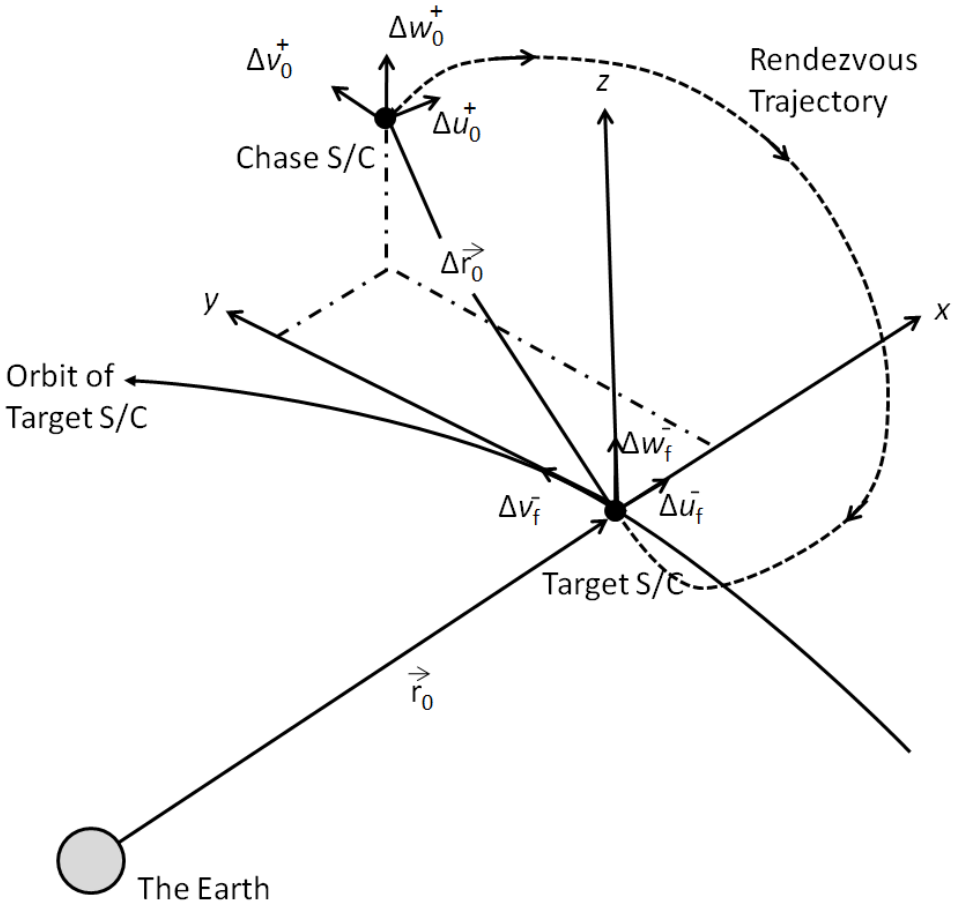

Figure 2.5 Rendezvous Trajectory of a Target Spacecraft in the Neighborhood of Its Chase Spacecraft.

We must determine the values of $\Delta u_0{}^+$, $\Delta v_0{}^+$, $\Delta w_0{}^+$, at the beginning of the rendezvous trajectory, so that the chase spacecraft will arrive at the target in a specified time t_f. The delta-v (ΔV) required to place the chase spacecraft on the rendezvous trajectory is:

$$\{\Delta v_0\} = \{\Delta \vec{v}_0{}^+\} - \{\Delta \vec{v}_0{}^-\} = \begin{Bmatrix} \Delta u_0{}^+ \\ \Delta v_0{}^+ \\ \Delta w_0{}^+ \end{Bmatrix} - \begin{Bmatrix} \Delta u_0{}^- \\ \Delta v_0{}^- \\ \Delta w_0{}^- \end{Bmatrix} \tag{2.46}$$

At time t_f, the chase spacecraft arrives at the target spacecraft (at the origin of the co-moving frame), which means $\{\Delta\vec{r}_f\} = \{\Delta\vec{r}(t_f)\} = \{0\}$. Evaluating Equation 2.44a at t_f, we find:

$$\{0\} = [\vec{\Phi}_{rr}(t_f)]\{\Delta\vec{r}_0\} + [\vec{\Phi}_{rv}(t_f)]\{\Delta\vec{v}_0\} \tag{2.47}$$

Solving this for $\{\Delta\vec{v}_0{}^+\}$ yields:

$$\{\Delta\vec{v}_0{}^+\} = -[\vec{\Phi}_{rv}(t_f)]^{-1}[\vec{\Phi}_{rr}(t_f)]\{\Delta\vec{r}_0\} \tag{2.48}$$

where $[\vec{\Phi}_{rv}(t_f)]^{-1}$ is the matrix inverse of $[\vec{\Phi}_{rv}(t_f)]$. We know the velocity $\Delta\vec{v}_0{}^+$ at the beginning of the rendezvous path; thus substituting equation (2.48) into Equation 2.44b we obtain the velocity $\Delta\vec{v}_f{}^-$ at which point the chase spacecraft arrives at target spacecraft, when $t = t_f{}^-$:

$$\{\Delta\vec{v}_f{}^-\} = [\vec{\Phi}_{vr}(t_f)]\{\Delta\vec{r}_0\} + [\vec{\Phi}_{vv}(t_f)]\{\Delta\vec{v}_0{}^+\}$$

$$\{\Delta\vec{v}_f{}^-\} = [\vec{\Phi}_{vr}(t_f)]\{\Delta\vec{r}_0\} + [\vec{\Phi}_{vv}(t_f)]\left(-[\vec{\Phi}_{rv}(t_f)]^{-1}[\vec{\Phi}_{rr}(t_f)]\{\Delta\vec{r}_0\}\right)$$

Simplifying, we get:

$$\{\Delta\vec{v}_f{}^-\} = \left([\vec{\Phi}_{vr}(t_f)] - [\vec{\Phi}_{vv}(t_f)][\vec{\Phi}_{rv}(t_f)]^{-1}[\vec{\Phi}_{rr}(t_f)]\right)\{\Delta\vec{r}_0\} \tag{2.49}$$

Obviously, an impulsive delta-v (ΔV) maneuver is required at $t = t_f$ to bring the chase spacecraft to rest relative to target spacecraft $(\Delta\vec{v}_f{}^+ = 0)$:

$$\{\Delta\vec{v}_f\} = \{\Delta\vec{v}_f{}^+\} - \{\Delta\vec{v}_f{}^-\} = \{0\} - \{\Delta\vec{v}_f{}^-\} = -\{\Delta\vec{v}_f{}^-\} \tag{2.50}$$

In Equations 2.46 and 2.50 we have employed differences between relative velocities to calculate delta-v (ΔV), which is the difference in absolute velocities. To show that this is valid,

$$\vec{v}^- = \vec{v}_0{}^- + \vec{\Omega}^- \times \vec{r}_{rel}{}^- + \vec{v}_{rel}{}^- \tag{2.51a}$$

$$\vec{v}^+ = \vec{v}_0{}^+ + \vec{\Omega}^+ \times \vec{r}_{rel}{}^+ + \vec{v}_{rel}{}^+ \tag{2.51b}$$

Since the target spacecraft is passive, the impulsive maneuver has no effect on its state of motion, which means $\vec{v}_0{}^{+} = \vec{v}_0{}^{-}$and $\vec{\Omega}^{+} = \vec{\Omega}^{-}$. Furthermore, by assuming impulsive maneuvers, there is no change in the position, $\left(\vec{r}_{rel}{}^{+} = \vec{r}_{rel}{}^{-}\right)$. It follows from Equation 2.51 that:

$$\vec{v}^{+} - \vec{v}^{-} = \vec{v}_{rel}{}^{+} - \vec{v}_{rel}{}^{-} \text{ or } \Delta\vec{v} = \Delta\vec{v}_{rel} \tag{2.52}$$

CHAPTER 3

DEVELOPMENT OF ΔV BUDGETS FOR REPAIRING OR REMOVING GLOBALSTAR SATELLITES

3.1 Problem Formulation

Currently, there are eleven non-functional satellites in the GlobalStar constellation. The orbital tracks of the eleven satellites are depicted in Figure 3.1, where it is noted that all of the non-functional satellites have semi-major axes between 8,132 and 8,521 km and right ascension of ascending nodes (RAAN (Ω)) between 57 and 270 degrees. Their NORAD identifiers and orbital characteristics are summarized in Table 3.1.

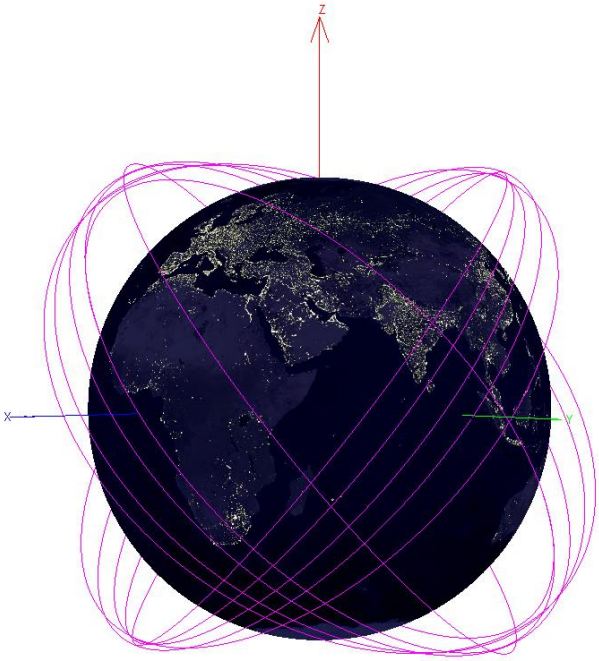

Figure 3.1 Non-functional GlobalStar Satellites Orbits.

Table 3.1 Orbital Characteristics of Non-functional GlobalStar Satellites.

NORAD ID	SEMI-MAJOR AXES (km)	Ω (Degree)
25164U	8232.57	57.942
25964U	8167.01	66.043
25874U	8132.08	75.736
25853U	8334.18	81.121
25306U	8221.30	90.959

NORAD ID	SEMI-MAJOR AXES (km)	Ω (Degree)
25872U	8372.10	172.905
25885U	8343.98	179.299
25771U	8475.23	189.301
25886U	8405.31	195.848
25851U	8521.65	220.276
25308U	8156.13	270.261

The primary goal of this study has been to develop specifications for a set of small dexterous servicing satellites capable of refueling, repairing or de-orbiting GlobalStar satellites. This type of spacecraft has been examined in other studies[22,23]. For the purposes of the present study, the spacecraft will be called Satellite Re-orbiter Spacecraft (SRS) and the performance requirements will be developed for the SRS system in terms of optimal altitude and ephemeras characteristics, assuming that the SRS elements are carried into orbit and deployed from a mothership. In that way, it should be possible to minimize overall SRS system size and operating costs for servicing the 11 non-functional GlobalStar satellite example. In addition, goals of this research include:

1. Determination of SRS maneuvering requirements and acceptable error allowances for autonomous rendezvous and docking with targeted GlobalStar satellites,

2. Capturing (attaching to) a non-functional GlobalStar satellite with SRS's robotic manipulators, and

3. Determination of system requirements needed to propel a non-functional GlobalStar satellite into a predictable de-orbit trajectory.

As shown in Table 3.1, the non-functional GlobalStar satellites can be divided roughly into two separate orbital subsets, based on their right ascension of ascending nodes (RAAN or Ω)—five satellites fall within $57° < \Omega < 91°$, and six satellites are

within 172° < Ω < 271°. Referring to Figure 3.1, it is apparent that the two orbital satellite groups may have evolved from their initial deployments. GlobalStar satellites 25164U, 25964U, 25874U, 25853U and 25306U (Ωs between 57° and 90°) were deployed from one multiple-satellite launch, and GlobalStar satellites 25872U, 25885U, 25771U, 25886U, 25851U and 25308U (Ωs between 172° and 270°) appear to have been deployed from another multiple-satellite launch. A MatLab program was used to represent the NORAD orbits for some aspects of the analysis that follows.

In order to bound this study, it has been assumed that the mothership and its associated SRS fleet have been placed in orbit utilizing the same Soyuz launch vehicle system that has been employed for the multiple-satellite GlobalStar launches. Thus, each SRS element will be a small satellite, deployed from the orbiting mothership with overall mass and dimensional constraints derived from existing GlobalStar launch specifications. On that basis, an optimum number of SRS elements can be established in terms of affecting the largest number of rendezvous and repair/de-orbit sorties with a minimum number of Earth launches. Obviously, the propellant requirements, both for orbital rendezvous and de-orbit, when necessary, represents the most important design driver. Since it is not possible to differentiate repairable GlobalStars from recoverable GlobalStars *a priori*, this study has assumed that none of the non-functioning GlobalStars can be repaired as a "worst case" baseline. As a consequence, a main purpose of this study has been to determine optimal propellant allowances to de-orbit the non-functional GlobalStar satellites. On that basis, it was necessary to estimate the velocity increments required for the entire sequence of operations, starting from deployment from the mothership, then proceeding through orbital rendezvous, satellite capture and subsequently de-orbiting non-repairable GlobalStar satellites.

3.2 ΔV Calculations for Rendezvous and De-orbiting Maneuvers

3.2.1 ΔV Rendezvous Maneuvers of SRS with Non-functional GlobalStar Satellite

Assuming that there are two distinct groups of non-functional GlobalStar satellites, rendezvous calculations have been made assuming that the mothership was placed in an orbit that facilitated a minimum ΔV propulsive requirement for one SRS

unit in each satellite subset. By being launched into an optimal circular orbit relative to the desired rendezvous orbit for the selected GlobalStar satellite, a minimum propellant rendezvous can be executed. In order to develop an optimal strategy, the analysis has considered each of the non-functional GlobalStar satellites in each subset to be the initial rendezvous candidate. In that way the optimum mothership orbit can be selected on the basis of minimizing the total ΔV requirements for all of the remaining GlobalStar satellites in that suite (subset).

All of the GlobalStar satellite orbits are nearly circular. Furthermore, when the mothership is placed in its initial orbit, it is desirable to place the mothership in a slightly different orbit than the initial target GlobalStar in order to minimize risk. By placing the mothership in a circular orbit sharing the orbital plane containing the target satellite, a low-ΔV rendezvous can occur—provided that the mothership's orbit is synchronized with the target satellite orbit. Furthermore, by deploying the remaining SRS vehicles from a circular mothership orbit rather than the slightly elliptic GlobalStar orbits, synchronization of the other SRS spacecraft with the remaining GlobalStar satellites for rendezvous can be controlled more easily. The semi-major axes of the subsequent SRS deployments can be controlled using the ΔV burn, and by waiting an appropriate number of (mothership and target GlobalStar) orbits and determining the time when the propulsive kick is to be completed, it is possible to place the SRSs in the desired rendezvous orbits with the desired separation distances for initiating rendezvous.

Since all of the remaining SRS vehicles were to be deployed from the same mothership orbit, it was only necessary to determine the ΔV requirements for each of the remaining SRS vehicles, starting from the selected mothership orbit. The ΔV sets were computed in the calculation order, shown in Figures 3.2 and 3.3.

Figure 3.2 Sequence of ΔV Requirement Calculations for the Five GlobalStar Suite.

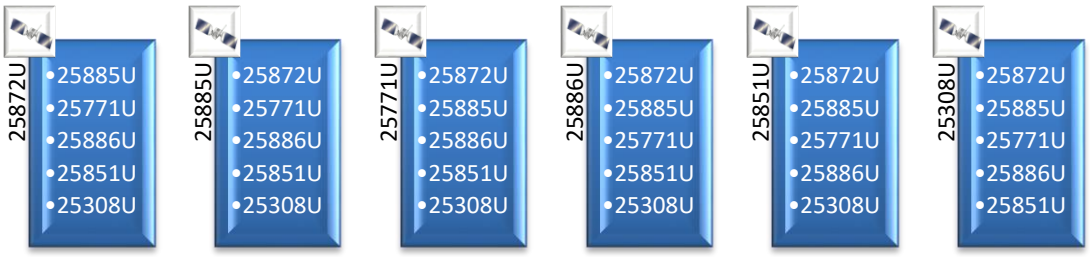

Figure 3.3 Sequence of ΔV Requirement Calculations for the Six GlobalStar Suite.

Non-functional GlobalStar satellite positions and classical orbital elements [semi-major axes (a), eccentricity (e), inclination angle (i), right ascension of ascending nodes (Ω), argument of periapsis (w) and true anomaly (θ)] are known from their NORAD data. The NORAD data for each non-functional GlobalStar satellite are shown in Table 3.2. In an actual multiple satellite recovery and/or deorbit mission, after the mothership carrying the SRS set was placed into its optimal orbit and the first rendezvous and repair operation was completed, the orbital data for the remaining GlobalStar targets would be updated in order to set up the second SRS rendezvous and repair operation, and so on. In that way, the sequence of operations can be adjusted to accommodate the various inspection, repair and/or deorbit operations, minimizing ground station manpower and operational costs, while recognizing that the restricted two-body approach incorporated in this optimization process cannot predict actual orbits over extended periods of time. The actual optimization process can only be simulated in this study example by using NORAD orbital data spread over a period of time characterizing a complete SRS sequence. That approach allows realistic actual adjustments in orbits to occur.

When this research topic was selected, the public was unaware of GlobalStar's decision to place their non-functioning satellites in parking orbits where they represented a minimum risk to their other functioning satellites. As mentioned in Chapter 1, every orbiting object in the space environment can be hazardous to functional satellites. These non-functional satellites could trigger a nearly continuous chain reaction collision event in near-Earth orbital space. This effect is known as the *Kessler Syndrome*, or effect, as proposed by NASA scientist Donald J. Kessler in 1978. It is a scenario in which the density of objects in Low Earth Orbit (LEO) is high enough that collisions between objects could cause a cascade – each collision generating debris which increases the likelihood of further collisions[24]. However, in support of the present active removal research topic, it was announced recently that Canadian Robotics was exploring a rendezvous and repair partnership that would enable a commercial satellite operator to extend functional satellite lifetimes using an approach similar to the type proposed here[25]. A robotic servicer satellite is being designed to add in-orbit refueling and simple repairs to existing commercial satellite fleets. The robotic servicer satellite could add years of life to valuable spacecraft that would otherwise be decommissioned for lack of fuel. The servicer also will be able to perform some repairs, possibly including releasing snagged solar arrays.

As a result, this thesis should be considered as developing an appropriate methodology for recovering or removing specific sets of non-functioning satellites utilizing a minimum risk and minimum cost (based on launch mass requirements) methodology.

Examination of the NORAD two-line ephemerus element datasets showed that all 11 of the non-functional satellites had been maneuvered out of their regular communications network orbits. This presented a problem, since the methodology developed in this thesis is based on using efficient, low-overhead orbital rendezvous synchronization timing schemes. The simple synchronization timing schemes based on the restricted two-body model developed in Appendix A, are of limited accuracy since they do not include orbital perturbations resulting from gravity variations, aerodynamic drag, third-body perturbations, and solar pressure. However, as more sophisticated simulations have shown (AGI's STK software package has been used in this thesis), inclusion of all of the modeled orbital perturbation effects does not

replicate precisely the actual NORAD data for long (several days or weeks) periods of time. The low-overhead approach is most useful if the current NORAD data were used in the actual SRS orbit change and rendezvous calculations. However, this thesis can only simulate that process by using historical NORAD data to model the GlobalStar servicing and removal operations. Since the 11th non-functional satellite in the dataset contained in Table 3.1 was maneuvered into its present orbit in February, 2011, historical data can only go back to that date in order to model the overall approach. On that basis, it has been assumed that the mothership was launched into its initial orbit on February 11, 2011. The reference NORAD dataset for 11 February 2011, is contained in Table 3.4.

NORAD data for all non-functional GlobalStar satellites between 11 February 2011 and 11 April of 2011, have been used to represent the overall approach. Eccentricity (e), inclination angle (i), right ascension of ascending nodes (Ω) and argument of periapsis (w) can be read directly from the two-line ephemerus NORAD data, but semi-major axes (a) and true anomaly (θ) were needed in the rendezvous calculations, and a MatLab program was written to utilize the NORAD data to determine all of the classical orbital elements*.

* Also, the NORAD data contain the date and time when the data for each GlobalStar satellite was recorded. Table 3.4 represents the February 11th, 2011 data. The repeating "11042" digital entries in the first row of data for each satellite indicate that the NORAD data were taken on the 42th day of 2011. The 42th day of 2011 is 11th February of 2011.

Table 3.2 Orbital Characteristics of 11 Non-functional GlobalStar Satellites[26].

NORAD ID	TWO LINE ELEMENT SET
25164U	1 25164U 98008C 11042.27601744 -.00000071 00000-0 10000-3 0 7296 2 25164 052.0023 057.3745 0000149 321.9325 038.1480 11.61427210575277
25306U	1 25306U 98023A 11042.09193041 -.00000072 00000-0 10000-3 0 7276 2 25306 051.9853 090.8838 0002023 116.3436 243.7593 11.65378538580223
25308U	1 25308U 98023C 11042.12384752 -.00000075 00000-0 10000-3 0 5634 2 25308 051.9886 270.0730 0002339 107.8269 252.2814 11.79671745590136
25771U	1 25771U 99031B 11042.56731775 -.00000062 00000-0 10000-3 0 5071 2 25771 051.9853 188.1960 0002651 092.8436 267.2664 11.12082454534490
25851U	1 25851U 99037A 11042.90107616 -.00000061 +00000-0 +10000-3 0 09214 2 25851 051.9987 218.4390 0014989 130.6948 229.5152 11.04483496517358
25853U	1 25853U 99037C 11042.57093445 -.00000068 +00000-0 +10000-3 0 04237 2 25853 051.9808 079.8836 0001553 041.9023 318.1907 11.42106505533702
25872U	1 25872U 99041A 11042.82911121 -.00000066 +00000-0 +10000-3 0 04385 2 25872 051.9400 171.1145 0001056 117.6764 242.4149 11.33739573530588
25874U	1 25874U 99041C 11042.56386101 -.00000075 00000-0 10000-3 0 4494 2 25874 051.9817 074.3992 0000554 357.9397 002.1440 11.83302850532798
25885U	1 25885U 99043C 11042.47178723 -.00000067 00000-0 10000-3 0 3992 2 25885 052.0122 178.3449 0005661 086.1141 274.0314 11.39135958522237
25886U	1 25886U 99043D 11042.88984758 -.00000065 +00000-0 +10000-3 0 04440 2 25886 051.9971 193.9635 0002805 148.7290 211.3681 11.27553664528541
25964U	1 25964U 99062D 11042.43323594 -.00000074 00000-0 10000-3 0 3960 2 25964 051.9800 065.0615 0006216 188.6931 171.3790 11.76690374504624

Assuming that the mothership is inserted into an appropriate rendezvous position (on 11 February 2011) for deploying the initial SRS for the final rendezvous phase with its designated satellite, every satellite in each suite was considered to be the initial target. It was assumed that at least one day should be allowed for engaging the initial SRS with its target GlobalStar. Subsequently, the remaining target GlobalStars were considered to be the next rendezvous target (four GlobalStars for the $57° < \Omega < 91°$ case and five GlobalStars for the $172° < \Omega < 271°$ case). It was assumed that each of the remaining SRS vehicles would only be released from the mothership when its orbital position was optimal in terms of enabling that SRS to change its orbit plane, completing its ΔV plane-change maneuver so that it was set up to proceed immediately in a close-proximity rendezvous. The time delay and orbital maneuvering ΔV requirements for optimally changing the SRS inclination and right ascension of ascending nodes were estimated for all of the remaining satellites in each GlobalStar suite. Using this “optimal wait time for rendezvous” approach, it was only necessary to estimate the orbital plane change ΔV requirements for maneuvering the remaining SRS spacecraft from the mothership’s orbit into their GlobalStar satellite

target orbits. The optimal mothership orbit for each of the two GlobalStar satellite suites could then be identified on the basis of the total orbital plane change ΔV requirements for that suite.

Non-coplanar transfer calculations to change the SRS orbit inclinations and associated right ascension of ascending nodes for the five GlobalStar satellite suite in Figure 3.2 were calculated using:

$$\Delta V_{MG} = 2V_{\oplus,\mathrm{MSCOn}} \sin\frac{\vartheta_{MG}}{2} \tag{3.1}$$

where $$\vartheta_{MG} = \cos^{-1}[\cos i_M \cos i_G + \sin i_M \sin i_G \cos(\Omega_G - \Omega_M)] \tag{3.2}$$

Here, subscript *G* represents the target GlobalStar and subscript *M* represents the mothership orbit, while $V_{\oplus,MSCOn}$ is the circular orbital velocity of the mothership when it is located in the circular orbit associated with the *n*th GlobalStar satellite.

Table 3.3 contains the orbital information for the five-GlobalStar satellite suite. For the purposes of demonstrating this method, the perigee velocity has been used as the target circular velocity for the mothership when it is placed initially in the orbital plane of the specified GlobalStar.

Table 3.3 Orbital Characteristics of Five Non-functional GlobalStar Satellites.

Satellite Name	(i)	(Ω)	(e)	(T)	($V_{perigee}$)
GlobalStar 25164U	52.045°	57.942°	0.001048	7433.85 sec.	6.9656 km/sec
GlobalStar 25964U	52.043°	66.043°	0.000651	7345.24 sec.	6.9901 km/sec
GlobalStar 25874U	52.034°	75.736°	0.000641	7298.17 sec.	7.0056 km/sec
GlobalStar 25853U	52.057°	81.121°	0.001027	7571.92 sec.	6.9228 km/sec
GlobalStar 25306U	52.058°	90.959°	0.000617	7418.60 sec.	6.9673 km/sec

Using these circular velocities given by:

$$V_{circular} = \sqrt{\frac{\mu}{a}}, \tag{3.3}$$

and the GlobalStar orbital data, it was possible to prescribe the mothership circular orbit candidates, as given in Table 3.4. In addition, the plane change angular maneuver requirements, using equation (3.2), for the various combinations of GlobalStar reference orbits are summarized in Table 3.5.

Table 3.4 Orbital Inclination Angular Plane-Change Requirements between the Different Combinations of Mothership and Non-functional GlobalStar Satellite Orbits.

MSCO	GS(1)	GS(2)	GS(3)	GS(4)	GS(5)
MSCO-1	--	6.3855	14.0080	18.2304	25.8971
MSCO-2	6.3855	--	7.6387	11.8767	19.5884
MSCO-3	14.0080	7.6387	--	4.2455	11.9900
MSCO-4	18.2304	11.8767	4.2455	--	7.7549
MSCO-5	25.8971	19.5884	11.9900	7.7549	--

Table 3.5 Circular Velocities for Every Option of Mothership Orbit with respect to the Five Non-functional GlobalStar Satellite Subset.

	Semi-major Axes (a)	Circular velocity ($V_{circular}$)
GS-25164U - MSCO1	8232.57 km	6.9583 km/sec
GS-25964U - MSCO2	8167.01 km	6.9861 km/sec
GS-25874U - MSCO3	8132.08 km	7.0011 km/sec
GS-25853U - MSCO4	8334.18 km	6.9157 km/sec
GS-25306U - MSCO5	8221.30 km	6.9630 km/sec

Using Equation 3.1, the overall orbital plane change velocity increments can be calculated for every combination of the five non-functional GlobalStar satellite orbits. The individual SRS velocity increments and overall total velocity increments required from each candidate mothership orbit are summarized in Table 3.6.

Table 3.6 Velocity Increments to Change Inclination and Right Ascension of Ascending Nodes for Each Starting Point of Mothership.

MSCO	GS(1) 25164U	GS(2) 25964U	GS(3) 25874U	GS(4) 25853U	GS(5) 25306U	Total ΔV (km/sec)
MSCO-1	--	0.7751	1.6970	2.2047	3.1184	7.7952
MSCO-2	0.7782	--	0.9307	1.4455	2.3768	5.5312
MSCO-3	1.7074	0.9327	--	0.5187	1.4624	4.6212
MSCO-4	2.1912	1.4310	0.5123	--	0.9353	5.0698
MSCO-5	3.1205	2.3690	1.4545	0.9417	--	7.8857

As shown in Table 3.6, a mothership circular orbit set up for the initial SRS spacecraft to rendezvous with MSCO-3 (Non-functional GlobalStar satellite 25874U) has significant advantages over the other mothership orbit candidates. That circular orbit minimizes the total ΔV requirements for SRS orbital plane change maneuvers and can be used as the starting point for setting up the subsequent sequence of SRS deployments based on the wait time required for optimal orbital plane change maneuvers.

In order to proceed, it is necessary to utilize universal time to locate the mothership in its orbit and all of the GlobalStars in the target suite, to start the rendezvous for the first stack of non-functional GlobalStar satellites. Also, we are able to use spherical trigonometry as shown in Figure 3.4[27], to develop expressions for ϑ and i whenever a ΔV applies at the intersection of the target spacecraft and chase spacecraft orbits. We determine the location of the burn by using the cosine law and it enables us to avoid quadrant checks. Hence, for the impulse argument of latitude on the initial orbit, which is called $u_{initial}$, is calculated from:

$$u_{initial} = \cos^{-1}\left(\frac{\sin(i_{final})\cos(\Delta\Omega) - \cos(\vartheta)\sin(i_{initial})}{\sin(\vartheta)\cos(i_{initial})}\right) \qquad (3.4)$$

and the impulsive argument of latitude on the final orbit, which is called u_{final}, is calculated from:

$$u_{final} = \cos^{-1}\left(\frac{\cos(i_{initial})\sin(i_{final}) - \sin(i_{initial})\cos(i_{final})\cos(\Delta\Omega)}{\sin(\vartheta)}\right) \qquad (3.5)$$

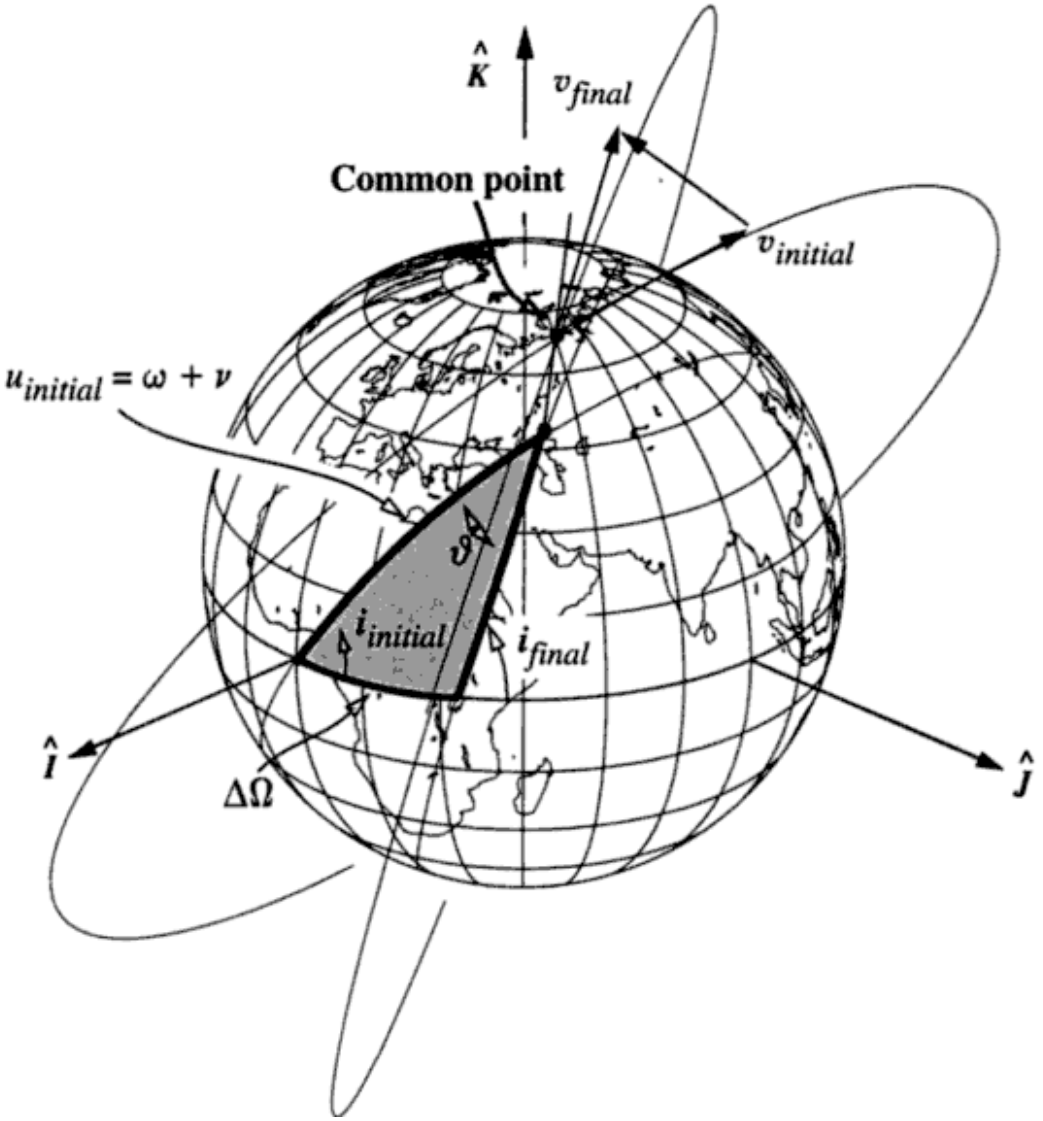

Figure 3.4 Geometry for Changes to Inclination and Right Ascension of Ascending Node.

Calculated locations of impulsive burn completions are shown in Table 3.7.

Table 3.7 Location of Burn to Change Inclination and Right Ascension of Ascending Node.

		MSCO-3
GS(1) 25164U	u_i	95.4556°
	u_f	84.4553°
GS(2) 25964U	u_i	94.5846°
	u_f	85.1877°
GS(3) 25874U	u_i	-
	u_f	-
GS(4) 25853U	u_i	91.3466°
	u_f	88.0331°
GS(5) 25306U	u_i	92.9183°
	u_f	86.9470°

The same calculation and process can be employed for the other six non-functional GlobalStar satellites whose orbital parameters are summarized in Table 3.8, while the calculated values for ϑ_{if}, mothership circular velocities and velocity increments required for the orbital plane changes are provided in Tables 3.9, 3.10 and 3.11.

Table 3.8 Orbital Characteristics of Five Non-functional GlobalStar Satellites.

Satellite Name	(i)	(Ω)	(e)	(T)	($V_{perigee}$)
GlobalStar 25872U	51.952°	172.905°	0.000533	7623.65 sec.	6.9037 km/sec
GlobalStar 25885U	52.013°	179.299°	0.001089	7585.27 sec.	6.9192 km/sec
GlobalStar 25771U	51.966°	189.30°	0.001190	7764.94 sec.	6.8661 km/sec
GlobalStar 25886U	51.991°	195.848°	0.000689	7669.06 sec.	6.8911 km/sec
GlobalStar 25851U	51.969°	220.276°	0.002141	7828.83 sec.	6.8539 km/sec
GlobalStar 25308U	51.937°	270.261°	0.000913	7330.57 sec.	6.9972 km/sec

Table 3.9 ϑ_{if} for Non-functional Six GlobalStar Satellites.

MSCO	GS(1) 25872U	GS(2) 25885U	GS(3) 25771U	GS(4) 25886U	GS(5) 25851U	GS(6) 25308U
MSCO-1	--	5.0367	12.8962	18.0261	36.889	72.5066
MSCO-2	5.0367	--	7.8769	13.0239	32.0176	68.3434
MSCO-3	12.8962	7.8769	--	5.1566	24.2831	61.4908
MSCO-4	18.0261	13.0239	5.1566	--	19.1884	56.8839
MSCO-5	36.889	32.0176	24.8231	19.1884	--	38.868
MSCO-6	72.5066	68.3434	61.4908	56.8839	38.868	--

Table 3.10 Circular Velocities for every Option of MotherShip Orbit with respect to the Six Non-functional GlobalStar Satellite Subset.

	Semi-major Axes (a)	Circular velocity ($V_{circular}$)
GS-25872U - MSCO1	8372.10 km	6.90 km/sec
GS-25885U - MSCO2	8343.98 km	6.9117 km/sec
GS-25771U - MSCO3	8475.23 km	6.8579 km/sec
GS-25886U - MSCO4	8405.31 km	6.8864 km/sec
GS-25851U - MSCO5	8521.65 km	6.8392 km/sec
GS-25308U - MSCO6	8156.13 km	6.9908 km/sec

As can be seen in Table 3.11, MSCO-3 (Non-functional GlobalStar satellite 25771U) is the logical orbit for minimizing the overall ΔV requirements for the second subset of non-functional GlobalStar satellites.

Table 3.11 Summary of Velocity Increments for Plane Change and Right Ascension of the Ascending Node Adjustments for SRS Units Departing from the Different Candidate MotherShip Orbits.

MSCO	GS(1) 25872U	GS(2) 25885U	GS(3) 25771U	GS(4) 25886U	GS(5) 25851U	GS(6) 25308U	Total ΔV (km/sec)
MSCO-1	--	0.6063	1.5498	2.1619	4.3661	8.1608	16.8449
MSCO-2	0.6073	--	0.9494	1.5677	3.8123	7.7642	14.7009
MSCO-3	1.5403	0.9420	--	0.617	2.8848	7.0119	12.996
MSCO-4	2.1576	1.562	0.6195	--	2.2955	6.5595	13.1941
MSCO-5	4.3277	3.7723	2.9399	2.2798	--	4.5511	17.8708
MSCO-6	8.2681	7.8531	7.1477	6.659	4.652	--	34.5799

The six satellite subset demonstrates the challenge of rendezvous and de-orbit strategies when an ‘outlier’ satellite is present. From Figure 3.1, it can be seen that non-functional GlobalStar satellite 25308U is not in an orbit that is completely similar to the other five GlobalStars in the subset. That observation is more apparent in Table 3.11, where the required ΔVs for the necessary plane-change maneuvers to depart from one of the first five GlobalStar mothership orbit candidates, setting up for rendezvous with outlier MSCO-6, ranges between 4.55 and 8.16 km/s. Furthermore, the velocity increments required to maneuver the other five SRS units from the MSCO-6 orbit to set up for rendezvous with the other GlobalStar orbits in this set range from 4.65 to 8.26 km/s. Those velocity increments are comparable to the velocity increment required to launch the mothership into its initial orbit. Consequently, it is not feasible to achieve the desired launch mass and cost savings for rendezvous with and de-orbiting this six-satellite set.

Possible efficiencies can be achieved with the second set of non-functional GlobalStar satellites only if the five satellites with compatible orbits are considered. By eliminating non-functional GlobalStar satellite 25308U, the velocity increments required for the plane change maneuvers for the remaining four satellites are tabulated in Table 3.12. As in the original five-satellite example, it can be seen here that by launching the mothership into the rendezvous orbit for GlobalStar 25771U (MSCO-3), substantial propellant savings are possible.

Table 3.12 demonstrates the similarity between this second satellite set and the example set already presented. It is not necessary to repeat the mass estimation steps for this set, since they are so similar to the example already discussed.

Table 3.12 Velocity Increments to Change Inclination and Right Ascension of Ascending Nodes for Each Starting Point of Mothership after Eliminating GS(6)

MSCO	GS(1) 25872U	GS(2) 25885U	GS(3) 25771U	GS(4) 25886U	GS(5) 25851U	Total ΔV (km/sec)
MSCO-1	--	0.6063	1.5498	2.1619	4.3661	8.6841
MSCO-2	0.6073	--	0.9494	1.5677	3.8123	6.9367
MSCO-3	1.5403	0.9420	--	0.617	2.8848	5.9841
MSCO-4	2.1576	1.562	0.6195	--	2.2955	6.6346
MSCO-5	4.3277	3.7723	2.9399	2.2798	--	13.3197

In this analysis, the perturbing forces such as Earth's gravitational field, atmospheric drag, solar radiation pressure, and other planetary gravitational forces have been neglected. All orbit calculations were made using the restricted two-body model, along with NORAD data. As mentioned in Chapter Two, this analysis has used two-impulse rendezvous, Clohessy–Wiltshire equations and Hohmann transfer orbits in the calculations. MatLab-based programs have been employed for the calculations and plots. In the calculations, the goal has been to minimize overall ΔV requirements for changing trajectories. Furthermore, it has been assumed that operational costs are sufficiently low that rendezvous time intervals needed for optimal ΔVs can be quite long. Since orbit perturbations must be considered in identifying minimum energy orbital maneuver opportunities over periods of weeks or months, it was decided to restrict minimum energy maneuver opportunities to the 24 hour period following a simulated rendezvous. In that way, actual orbit variations should be small and the restricted two-body modeling approach can be employed. Hence, minimum required ΔV options were found by choosing the best time, between 0 hour and 24 hours, to achieve the rendezvous between the next assigned SRS and its non-functional GlobalStar satellite target. A required ΔV vs. maneuver completion time graph, as shown in Figure 3.5, was developed in order to find the best time for each rendezvous.

The first SRS will be inserted to a circular orbit nearly 1.5 km in front of the mothership and the orbital elements for the first rendezvous case (with satellite 25874U) is shown in Table 3.13.

Table 3.13 Classical Orbital Elements of First Rendezvous.

	25874U	SRS-3
a (km)	8132.08	8132.08
e	0.000641	0
i (deg)	52.034	52.034
Ω (deg)	75.736	75.736
w (deg)	65.071	0
θ (deg)	140.746	205

The two satellites are so close to each other after the SRS-3 orbit insertion maneuver that a minimal ΔV burn is required. The assumed orbital separation distances during the coarse and fine rendezvous stages were based on the ETS-VII autonomous rendezvous experiment[15]. In the ETS-VII study, autonomous rendezvous was divided into three elements based on separation distance: *approach phase* (from 10 km to 500 m), final *approach phase* (500 m to 2 m) and *docking phase* (within 2 m). These distances were found to be appropriate in staging the orbital rendezvous experiment.

After completing the initial rendezvous and de-orbit operations on GlobalStar satellite 25874U, the mothership could dispense the next SRS vehicle. In that way, potential collisions between the mothership and a prematurely-deployed “next” SRS vehicle with GlobalStar satellite 25874U could be avoided.

First rendezvous parameters and plots:

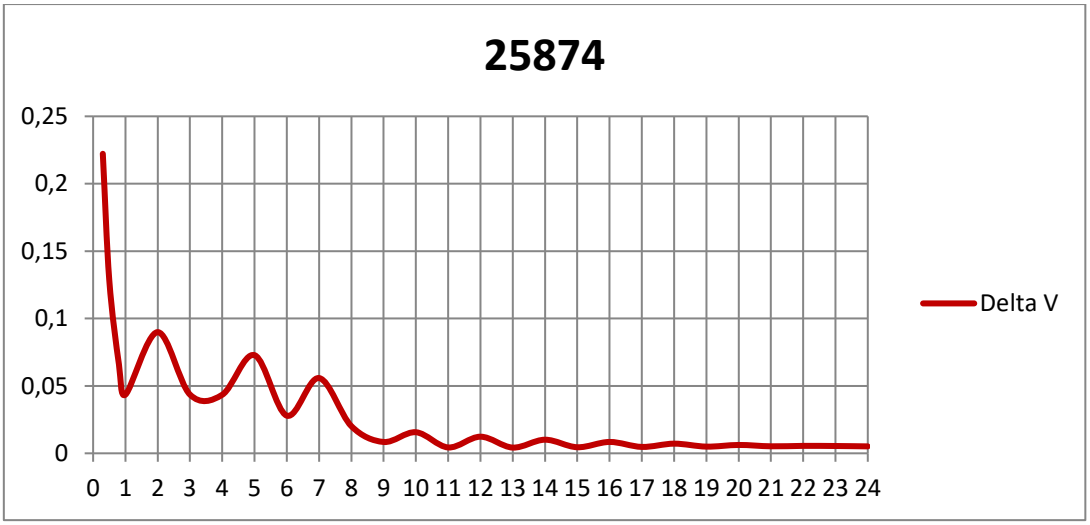

Figure 3.5 ΔV Requirements for Rendezvous between Non-functional GlobalStar Satellite 25874U and SRS-3 in 24 Hours.

As seen in Figure 3.5, the time-sequenced ΔV requirement is “damped” to a nearly constant minimum value, after 16 hours. Both minimum ΔV requirement and time delay were investigated. The Clohessy–Wiltshire equations consider time to find the best ΔV requirements. When the number of orbits prior to rendezvous is increased, the flight time for rendezvous is changed. In that way, the required velocity increment can be reduced by waiting.

Table 3.14 Timeline for First Rendezvous.

DATE	TIME	ACTION
11 Feb 2011	00:00:00.000	Start of Mission
11 Feb 2011	00:15:00.000	SRS-3 Release from Mothership
11 Feb 2011	00:30:00.000	First Rendezvous Initial Location
11 Feb 2011	13:30:00.000	End of First Rendezvous

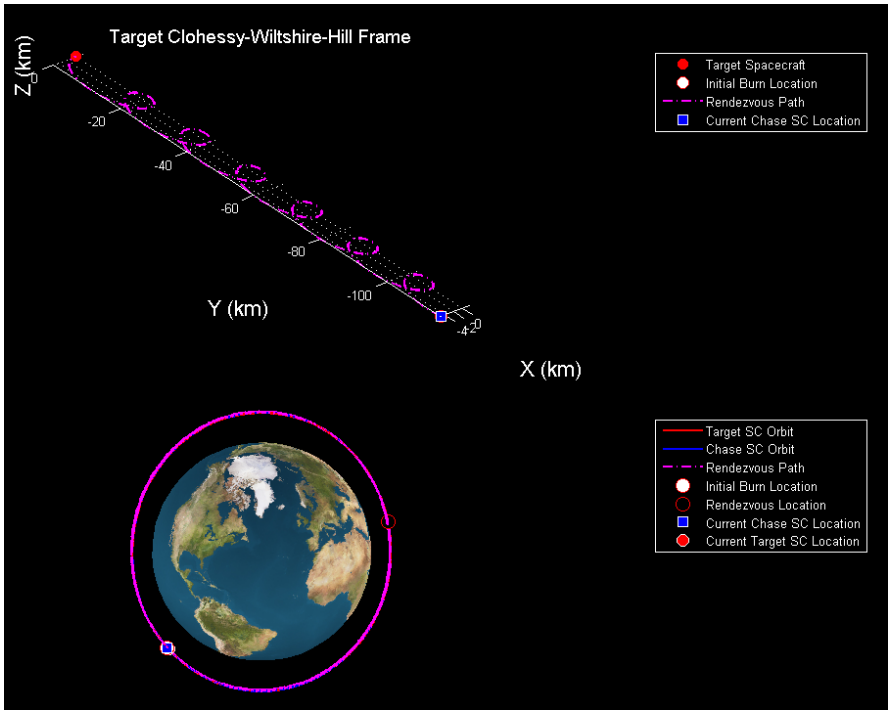

Figure 3.6 Rendezvous of SRS with GlobalStar 25874U.

The best time to achieve rendezvous between the deployed SRS vehicle and GlobalStar 25874U was 13 hours for minimum ΔV. The required ΔV was 0.0042 km/sec.

After completion of the initial SRS deployment and servicing or removal of 25874U, the second rendezvous is initiated. In order to minimize ΔV requirements, each successive SRS deployment has attempted to exploit multiple orbit encounter maneuvers, thereby using time delays rather than larger ΔVs. Satellites in different orbits have different periods and simple Keplerian orbital mechanics can be employed to estimate optimal delay times. One day was allowed for placing the mothership in its desired orbit and accomplishing the first rendezvous and de-orbit operation. While that is an aggressive assumption, the process being described for multiple servicing deployments can be adjusted somewhat arbitrarily after the first satellite has been serviced or removed. For this representative case, GlobalStar satellite 25164U was the second satellite and the second rendezvous was initiated with an SRS plane change maneuver after its release. After SRS release, it was necessary to calculate the time required to complete the plane change maneuver, placing the second SRS in its

approach phase position. Using that maneuver time and the universal time when the SRS was to arrive at its rendezvous station, it was possible to estimate the time when the SRS orbit maneuver should be initiated. The desired orbital characteristics for the second rendezvous (with 25164U) are summarized in Table 3.15, followed by the graph showing the required orbital maneuver delta V as a function of arrival time.

Table 3.15 Classical Orbital Elements of Second Rendezvous.

	25164U	SRS-1
a (km)	8232.57	8132.08
e	0.001048	0
i (deg)	52.045	52.045
Ω (deg)	57.942	57.942
w (deg)	100.522	0
θ (deg)	66.5132	165.1816

Second rendezvous parameters and plot:

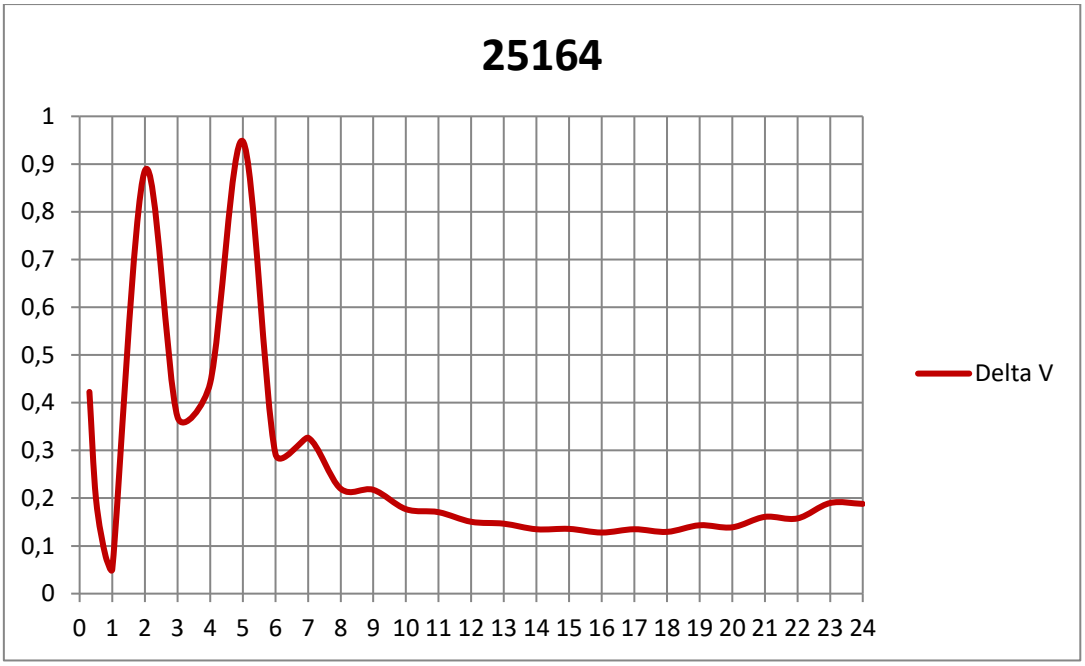

Figure 3.7 ΔV Requirements for Rendezvous between Non-functional GlobalStar Satellite 25164U and SRS-1 in 24 Hours.

Table 3.16 Timeline for Second Rendezvous.

DATE	TIME	ACTION
11 Feb 2011	13:45:00.000	SRS-1 Release from Mothership
11 Feb 2011	14:04:26.400	Initial Location after the Plane Change for SRS-1
13 Feb 2011	07:04:26.400	Second Rendezvous Initial Location
13 Feb 2011	08:04:26.400	End of Second Rendezvous

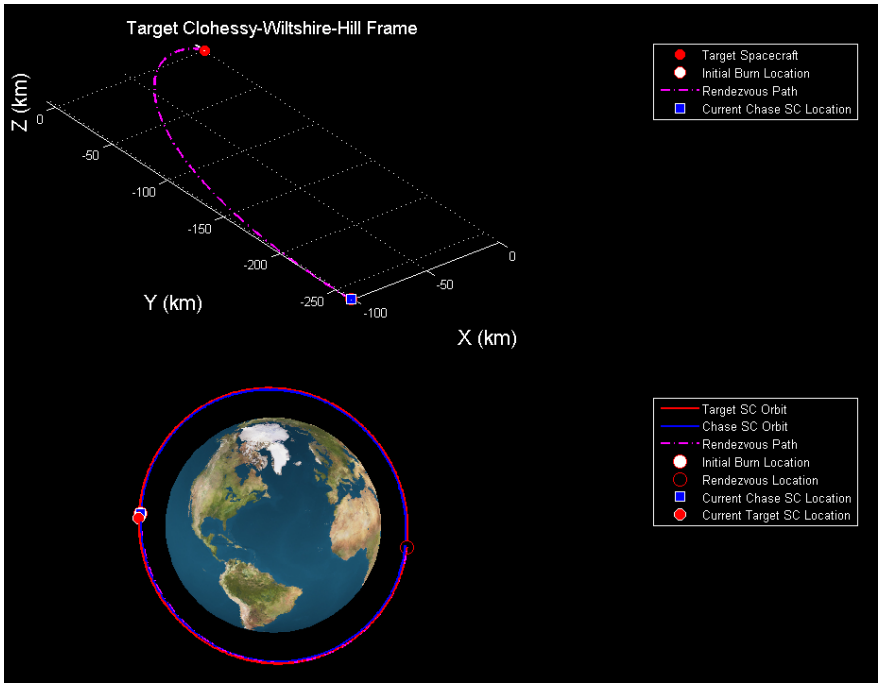

Figure 3.8 Rendezvous of SRS with GlobalStar 25164U.

The best time for the second rendezvous between the second SRS and its GlobalStar satellite target (25164U), is 1 hour after completion of the first GlobalStar intercept and recovery operation. At that time, the required rendezvous velocity increment was 0.0513 km/sec. Since that is such a short time interval and since the actual completion time for a real GlobalStar intercept and recovery operation could be very different from the assumed conditions, it is important to note from Figure 3.7, that low velocity increment rendezvous insertion opportunities also occur approximately 16 hours after the rendezvous opportunity window has been opened.

After completion of the second rendezvous, the mothership dispenses its third SRS. The third rendezvous (with GlobalStar satellite 25853U) orbital parameters are summarized in Table 3.17, and the ΔV requirements vs. on-station arrival time are displayed in Figure 3.9.

Table 3.17 Classical Orbital Elements of Third Rendezvous.

	25853U	SRS-4
a (km)	8334.18	8132.08
e	0.001027	0
i (deg)	52.057	52.057
Ω (deg)	81.121	81.121
w (deg)	113.359	0
θ (deg)	346.4246	97.0742

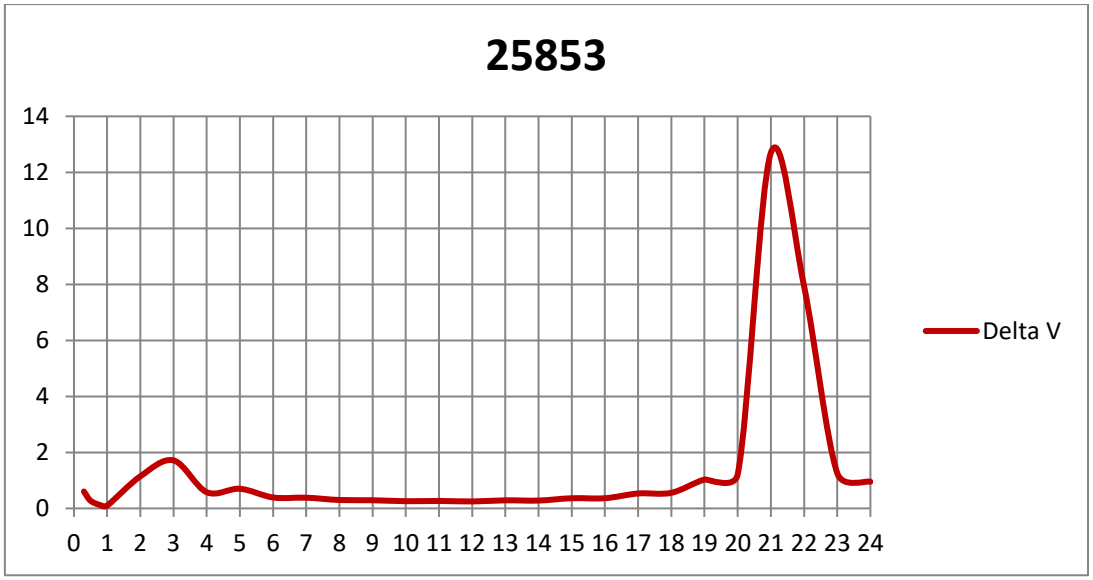

Figure 3.9 ΔV Requirements for Rendezvous between Non-functional GlobalStar Satellite 25853U and SRS-4 in 24 Hours.

Table 3.18 Timeline for Third Rendezvous.

DATE	TIME	ACTION
13 Feb 2011	08:29:26.400	SRS-4 Release from Mothership
13 Feb 2011	08:37:22.800	Initial Location after the Plane Change for SRS-4
13 Feb 2011	16:46:58.800	Third Rendezvous Initial Location
13 Feb 2011	17:46:58.800	End of Third Rendezvous

Third rendezvous parameters and plot:

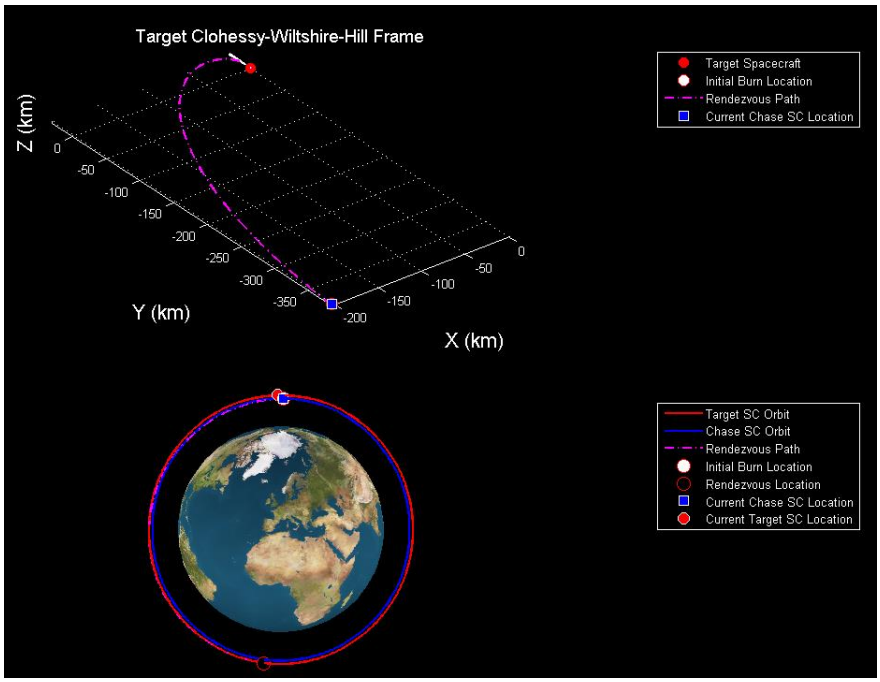

Figure 3.10 Rendezvous of SRS with GlobalStar 25853U.

SRS with GlobalStar satellite 25853U, rendezvous time is 1 hour and needed rendezvous velocity is 0.0999 km/s. After completing the third rendezvous, the mothership will release the fourth SRS from the its orbit. The fourth rendezvous will be with GlobalStar satellite 25306U and the orbit parameters for the fourth rendezvous (25306U) are shown in Table 3.19.

Table 3.19 Classical Orbital Elements of Fourth Rendezvous.

	25306U	SRS-2
a (km)	8221.30	8132.08
e	0.000617	0
i (deg)	52.058	52.058
Ω (deg)	90.959	90.959
w (deg)	72.992	0
θ (deg)	273.5079	345.102

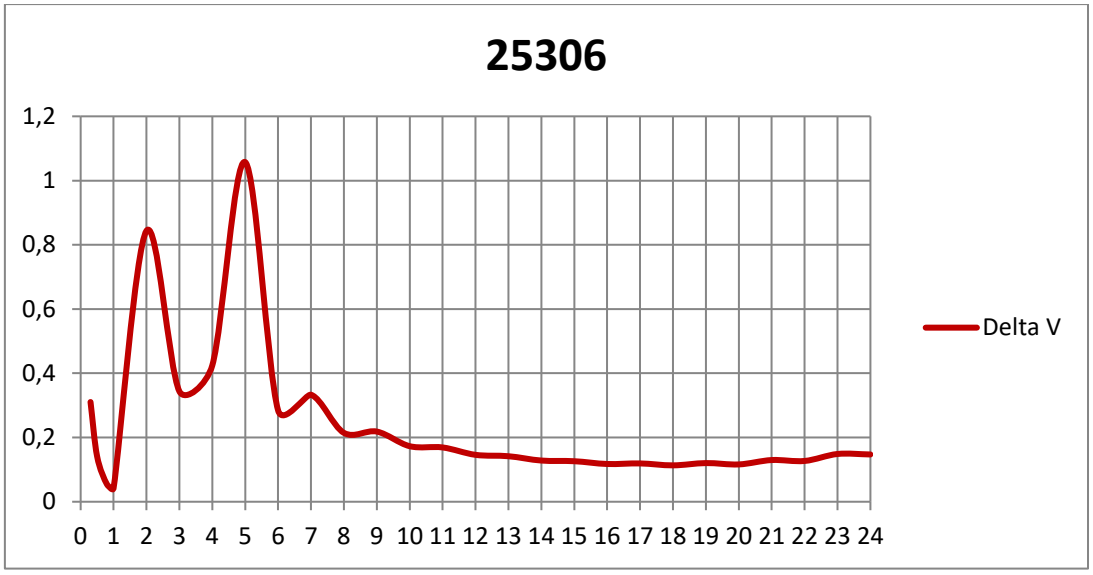

Figure 3.11 ΔV Requirements for Rendezvous between Non-functional GlobalStar Satellite 25306U and SRS-2 in 24 Hours.

Table 3.20 Timeline for Fourth Rendezvous.

DATE	TIME	ACTION
13 Feb 2011	18:00:00.000	SRS-2 Release from Mothership
13 Feb 2011	18:46:40.800	Initial Location after the Plane Change for SRS-4
14 Feb 2011	06:22:40.800	Fourth Rendezvous Initial Location
14 Feb 2011	07:22:40.800	End of Fourth Rendezvous

Fourth rendezvous parameters and plot:

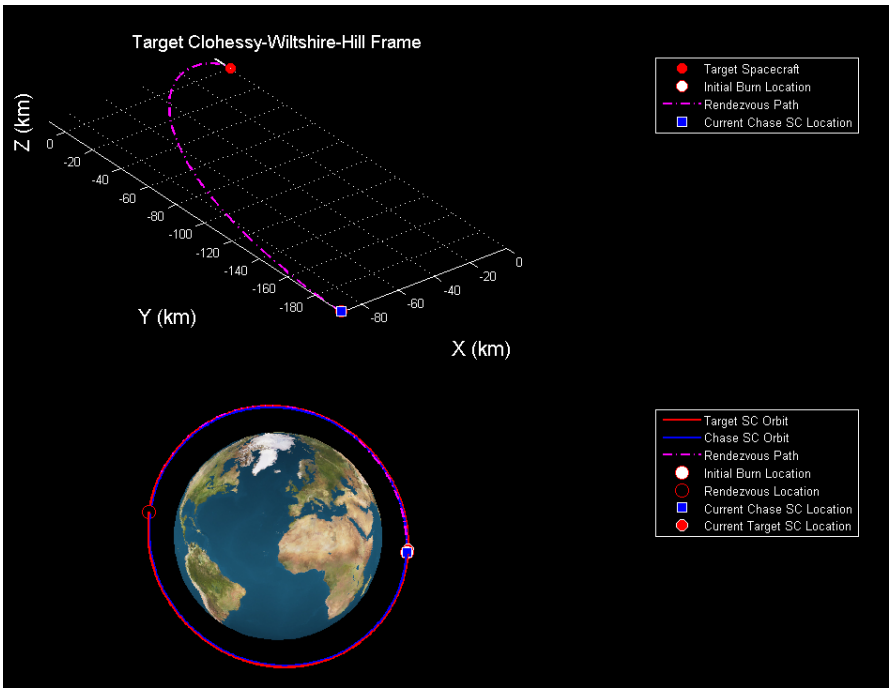

Figure 3.12 Rendezvous of SRS with GlobalStar 25306U.

The optimal SRS time for rendezvous with GlobalStar satellite 25306, is 1 hour and the required rendezvous velocity is 0.0418 km/s. After completing the fourth rendezvous, the mothership will release the fifth SRS for deployment into the GlobalStar 25964U orbit. The fifth rendezvous will be GlobalStar satellite 25964U and orbit and values for the fifth rendezvous (25964U) are given in Table 3.21.

Table 3.21 Classical Orbital Elements of Fifth Rendezvous.

	25964U	SRS-5
a (km)	8167.01	8132.08
e	0.000651	0
i (deg)	52.043	52.043
Ω (deg)	66.043	66.043
w (deg)	148.004	0
θ (deg)	43.4082	190.3018

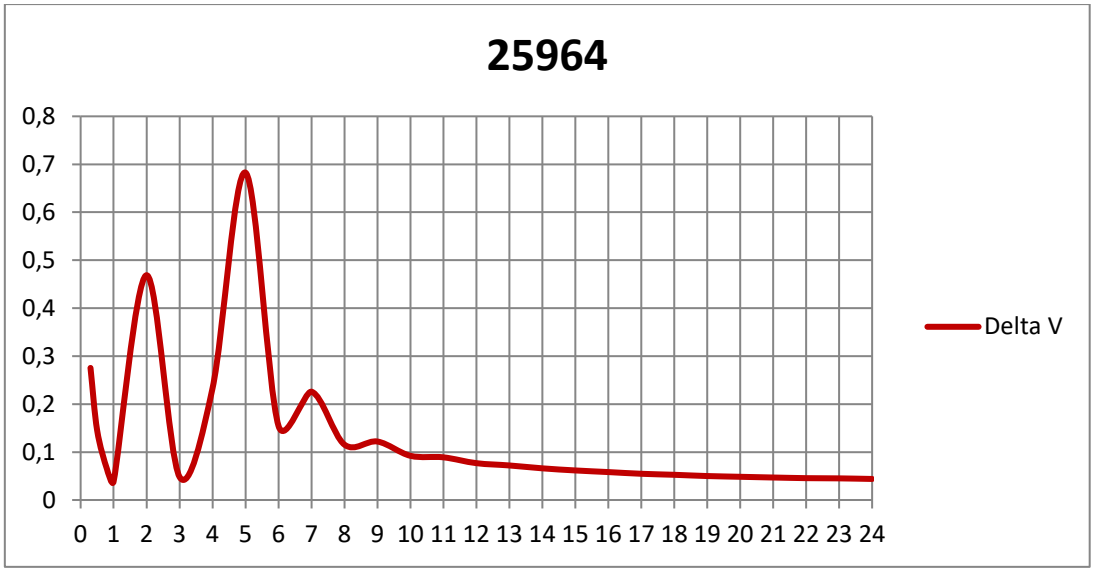

Figure 3.13 ΔV Requirements for Rendezvous between Non-functional GlobalStar Satellite 25964U and SRS-5 in 24 Hours.

Table 3.22 Timeline for Fifth Rendezvous.

DATE	TIME	ACTION
14 Feb 2011	08:00:00.000	SRS-5 Release from Mothership
14 Feb 2011	08:57:36.000	Initial Location after the Plane Change for SRS-5
18 Feb 2011	18:57:36.000	Fifth Rendezvous Initial Location
18 Feb 2011	19:57:36.000	End of Fifth Rendezvous

Fifth rendezvous parameters and plot:

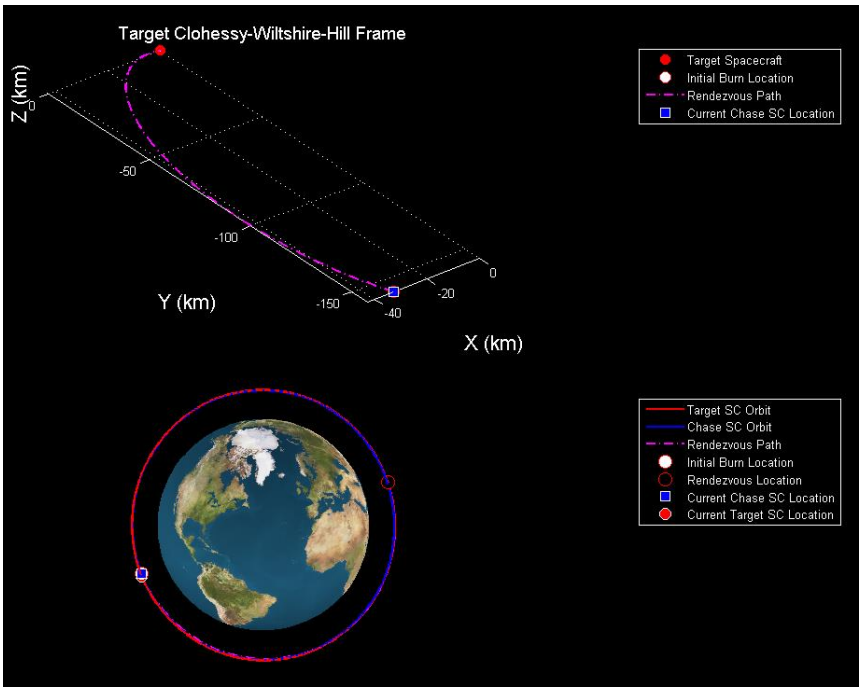

Figure 3.14 Rendezvous of SRS with GlobalStar 25964U.

Again, the optimal delay time for SRS rendezvous with GlobalStar 25964, is 1 hour and the needed rendezvous velocity increment is 0.0386 km/s.

In the methodology development, the second subset of non-functional GlobalStar satellites' will not be investigated using the same detailed rendezvous and de-orbiting process just discussed, because it is the same process and calculations as the first subset. Other than the outlier problem discussed previously, the subset analysis just presented can be considered representative of the second subset.

3.2.2 ΔV Calculation for SRS and Non-functional GlobalStar Satellite's De-orbiting Maneuver

This analysis has assumed that the initial velocity increments were applied instantaneously at the apogee of the grabbed non-functional GlobalStar satellite with SRS orbit. The assumed Earth reference radius was 6,378 km, and the Earth's

gravitational parameter was 398,600 km^3s^{-2}. In addition, a re-entry (perigee) altitude of 150 km has been used. The de-orbiting sketch is shown in Figure 3.15.

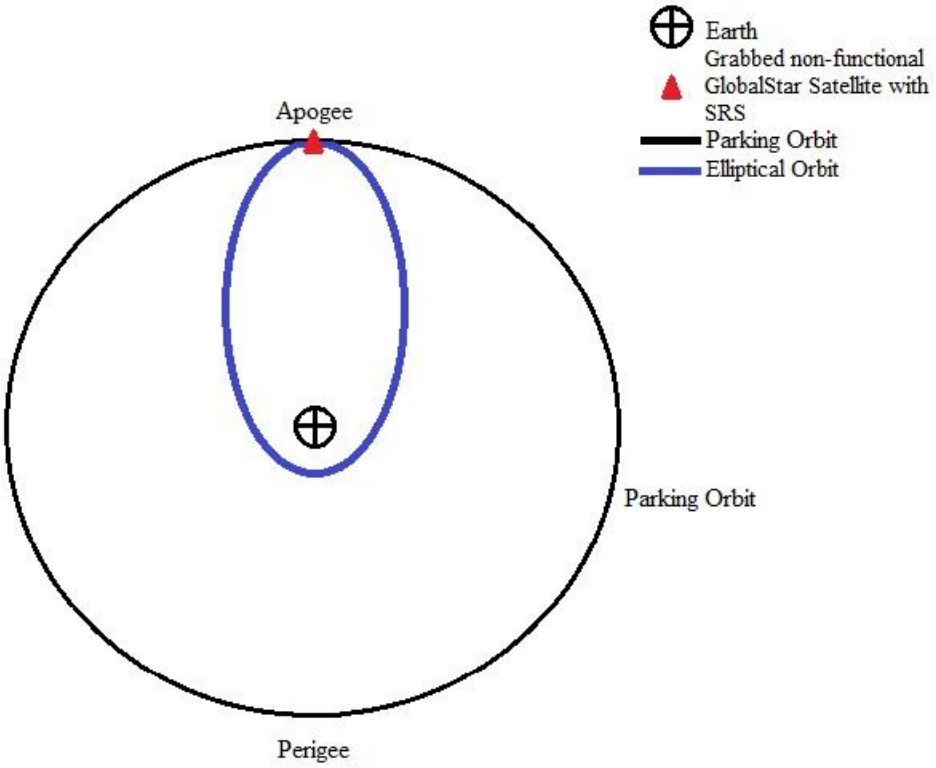

Figure 3.15 De-orbit Maneuver.

The ΔV calculations proceeded as follows:

1. Use NORAD two-line ephemeras data to characterize a specific GlobalStar target,

2. Calculate the GlobalStar orbit period in seconds,

$$T = \frac{Earth's\ Rotational\ Speed}{Reverse\ per\ day\ of\ satellite} = \frac{24*60*60}{Reverse\ per\ day\ of\ satellite} \tag{3.6}$$

3. Use the orbit period to calculate the semi-major axis:

$$a = \sqrt[3]{\left(\frac{T}{2*\pi}\right)^2 * \mu} \tag{3.7}$$

4. Using the tabulated eccentricity, determine:

$$r_{apogee} = a * (1 + e) \tag{3.8a}$$

$$r_{perigee} = a * (1 - e) \tag{3.8b}$$

5. Calculate the apogee and perigee velocities:

$$E = -\frac{\mu}{2*a} \tag{3.9}$$

$$V_{apogee} = \sqrt{2 * \left(E + \frac{\mu}{r_{apogee}}\right)} \tag{3.10a}$$

$$V_{perigee} = \sqrt{2 * \left(E + \frac{\mu}{r_{perigee}}\right)} \tag{3.10b}$$

6. Determine the SRS transfer orbit specifications where:

$$r_{apogee(transfer)} = r_a \tag{3.11a}$$

$$r_{perigee(transfer)} = R_{Earth} + 150 = 6378 + 150 \tag{3.11b}$$

$$a_{transfer} = \frac{r_{apogee(transfer)} + r_{perigee(transfer)}}{2} \tag{3.11c}$$

7. Determine the required transfer velocity:

$$E_{transfer} = -\frac{\mu}{2*a_{transfer}} \tag{3.12}$$

$$V_{apogee(transfer)} = \sqrt{2 * \left(E_{transfer} + \frac{\mu}{r_{apogee(transfer)}}\right)} \tag{3.13}$$

8. Calculate the transfer ΔV;

$$\Delta V = V_{apogee(transfer)} - V_{apogee} \tag{3.14}$$

The required initial transfer velocity increments for each spent GlobalStar satellite set is summarized in Table 3.22.

Table 3.23 Required Initial Velocities to Get into De-orbiting Trajectory.

NORAD ID	REQUIRED ΔV
25164U	0.4148
25964U	0.3996
25874U	0.3945
25853U	0.4326
25306U	0.4108

All calculations were made sequentially. The mothership released its SRS' along its orbit, to enable the SRS to set up for the specific rendezvous. As already described, the various SRS rendezvous operations were sequenced for minimum ΔV and, allowing time for actual rendezvous and latch-up, combined SRS-GlobalStar satellite elements resulted. If a GlobalStar could be repaired, the SRS unit would disconnect from it and the SRS propulsion system would be used to propel the SRS onto an appropriate re-entry trajectory. The worst case is when the GlobalStar cannot be repaired and the combined SRS-GlobalStar "satellite" needs to be removed from orbit. SRS and non-functional GlobalStar satellite pairs got into de-orbiting trajectory. Also a 10% ΔV allowance was added for all rendezvous maneuvers. The calculated required ΔV values are shown in Figure 3.24.

Table 3.24 Required ΔV to Achieve Rendezvous.

	REQUIRED ΔV				
	SRS PLANE CHANGE ΔV (km/sec)	SRS RENDEZVOUS ΔV (km/sec)	ΔV ALLOWANCE (km/sec)	DE-ORBIT ΔV (km/sec)	TOTAL ΔV (km/sec)
25164U	1.7074	0.0513	0.005	0.4148	2.1785
25964U	0.9327	0.0386	0.004	0.3996	1.4109
25874U	0	0.0042	0.0005	0.3945	0.3992
25853U	0.5187	0.0999	0.009	0.4326	1.0602
25306U	1.4624	0.0418	0.005	0.4108	1.9200

All rendezvous were calculated by using a restricted two-body problem analysis and frozen time. In real calculations, the NORAD data must be updated as close to the actual rendezvous time as possible.

3.2.3 Propellant mass and burn time calculations for SRS and Non-functional GlobalStar satellite de-orbit operations

Except for the close proximity maneuvers, orbital rendezvous propellant mass and maneuver time allowances are required. The rocket equation can be employed to estimate the propellant required for each distinct orbital maneuver tabulated in Tables 3.6 and 3.11. That is,

$$\Delta V = U_{eq}(10^{-3}) \ln\left(\frac{m_{unburned}+m_{propellant}}{m_{unburned}}\right) \quad (3.15a)$$

where $$U_{eq} = I_{sp}(9.80665) \quad (3.15b)$$

and the assumed specific impulse is $I_{sp} = 220$ seconds[28] (3.15c)

The specific ΔV requirements for the three primary SRS-GlobalStar rendezvous and servicing maneuvers are summarized in Table 3.25. The propulsive maneuvers must be analyzed in reverse in order to determine the estimated initial mass of each SRS unit, and the associated maneuver initiation times. The de-orbit ΔV-based propellant mass requirement has been labeled Prop 1; the propellant mass required for insertion of the SRS into the rendezvous orbit has been labeled Prop 2; and the initial orbital plane change maneuver (from the mothership orbit) propellant requirement has been labeled Prop 3.

Table 3.25 Required ΔV and Needed Propellant for Missions.

		REQUIRED ΔV (m/sec)	TOTAL MASS (kg)					
MISSION 1 — 25164U	De-orbit GS1	414.8	SRS 1	GS 1	Descent Prop	Prop 1		
			150	450	10	129		
	Two-impulsive Rendezvous	56.3	SRS 1			Prop 1	Prop 2	
			150			129	8	
	Plane Change	1707.4	SRS 1			Prop 1	Prop 2	Prop 3
			150			129	8	358
	Initial SRS 1	-	SRS 1			Total Prop		
			150			495		
		REQUIRED ΔV (m/sec)	TOTAL MASS (kg)					
MISSION 2 — 25964U	De-orbit GS2	399.6	SRS 2	GS 2	Descent Prop	Prop 1		
			150	450	10	124		
	Two-impulsive Rendezvous	42.6	SRS 2			Prop 1	Prop 2	
			150			124	6	
	Plane Change	932.7	SRS 2			Prop 1	Prop 2	Prop 3
			150			124	6	157
	Initial SRS 2	-	SRS 2			Total Prop		
			150			287		
		REQUIRED ΔV (m/sec)	TOTAL MASS (kg)					
MISSION 3 — 25874U	De-orbit GS3	394.5	SRS 3	GS 3	Descent Prop	Prop 1		
			150	450	10	122		
	Plane Change	5	SRS 3			Prop 1	Prop 2	
			150			122	1	
	Initial SRS 3	-	SRS 3			Total Prop		
			150			123		
		REQUIRED ΔV (m/sec)	TOTAL MASS (kg)					
MISSION 4 — 25853U	De-orbit GS4	432.6	SRS 4	GS 4	Descent Prop	Prop 1		
			150	450	10	135		
	Two-impulsive Rendezvous	108.9	SRS 4			Prop 1	Prop 2	
			150			135	16	
	Plane Change	518.7	SRS 4			Prop 1	Prop 2	Prop 3
			150			135	16	83
	Initial SRS 4	-	SRS 4			Total Prop		
			150			234		
		REQUIRED ΔV (m/sec)	TOTAL MASS (kg)					
MISSION 5 — 25306U	De-orbit GS5	410.8	SRS 5	GS 5	Descent Prop	Prop 1		
			150	450	10	128		
	Two-impulsive Rendezvous	46.8	SRS 5			Prop 1	Prop 2	
			150			128	7	
	Plane Change	1462.4	SRS 5			Prop 1	Prop 2	Prop 3
			150			128	7	287
	Initial SRS 5	-	SRS 5			Total Prop		
			150			422		

In order to translate these incremental propellant requirements into maneuver burn times, it is necessary to specify both the propellant and the thrusters. Since the

GlobalStar satellites employ hydrazine propellant, it will be the assumed propellant for the SRS propulsion systems. EADS' subsidiary Astrium has a long history of providing reliable space-qualified hydrazine thrusters for all types of spacecraft. Commercially available off-the-shelf (COTS) hydrazine propulsion units can be obtained with thrust levels of 1N, 2N, 5N, 10N, 20N and 400N[29]. In order to properly size the SRS vehicles, it is necessary to select thrusters that are capable of performing the various ΔV maneuvers in time intervals that are compatible with the GlobalStar orbital periods.

Burn times can be calculated for specific thrusters by using the equation that defines specific impulse to determine the mass flow rate for the specified thruster and its stated specific impulse. That is, using:

$$\frac{Thrust}{\dot{m}_{Thrust}} = I_{sp}(9.80665)\ , \tag{3.16}$$

the mass flow rates for the various Astrium thruster sizes can be calculated and are summarized in Table 3.25.

Table 3.26 Propellant Mass Flow Rates for Various Astrium COTS Thrusters.

	1N	2N	5N	10N	20N	400N
$\dot{m}_{Thrust}$ (kg/sec)	$4.635x10^{-4}$	$9.270x10^{-4}$	$2.317x10^{-3}$	$4.635x10^{-3}$	$9.270x10^{-3}$	0.185

Employing the five SRS mission scenarios from Table 3.24, 1N, 10N and 400N thrusters were considered as SRS propulsion unit candidates. The associated burn times required for the different thruster and mission combinations are given in Table 3.27 where:

$$Burn\ Time = \frac{m_{prop}}{\dot{m}_{Thrust}} \tag{3.17}$$

Table 3.27 Burn Times for the Mission for Different Thrust Levels.

	BURN TIME for Prop 1 (sec)			BURN TIME for Prop 2 (sec)			BURN TIME for Prop 3 (sec)		
	1N	10N	400N	1N	10N	400N	1N	10N	400N
Mission 1	278,964	27,896	697	16,504	1,650	41	773,031	77,303	1932
Mission 2	267,788	26,778	669	12,211	1,221	30	338,101	33,810	845
Mission 3	263,214	26,321	659	1,402	140	4	-	-	-
Mission 4	292,125	29,212	730	33,009	3,300	83	178,640	17,864	446
Mission 5	886,299	88,629	2215	13,613	1,361	34	618,381	61,838	1545

Table 3.27 demonstrates that the 400N hydrazine thruster can be employed to yield reasonable burn times. Table 3.28 is an estimated total mission payload for the complete five-satellite subset mission, demonstrating that the total mass is within the capabilities of the Soyuz launch system.

Table 3.28 Total Mission Payload Mass of Five Non-functional GlobalStar Set

	MASS (kg)	DESCENT PROPELLANT (kg)	PROPELLANT (kg)	TOTAL (kg)
Mother Ship	750	20	250	1020
SRS-1	150	10	495	655
SRS-2	150	10	287	447
SRS-3	150	10	123	283
SRS-4	150	10	234	394
SRS-5	150	10	422	582
TOTAL	1500	70	1811	3381

The Globalstar satellites were launched from the Baikonur Cosmodrome using Soyuz launch vehicles[18], with launch payload masses of about 3,000 kg for their six satellite clusters. The estimated mission payload summarized in Table 3.28 can be launched using a Soyuz launch vehicle.

CHAPTER 4

CONCLUSIONS AND RECOMMENDATIONS FOR FUTURE WORK

Analytical Graphics, Inc., STK software and MatLab-based simulations were employed to develop a methodology for systematically removing non-functioning (GlobalStar) satellites from a large constellation. The methodology can be employed for other constellations which have non-functional satellites or for a specific group of non-functional satellites that threatens other functional satellites. The proposed methodology employed a mothership to carry a small set of servicing and repair satellites (SRSs) into an optimal orbit from which they can be released and guided to specific target satellites. The mini-satellites were assumed to be capable of autonomous rendezvous with their target satellites, incorporating manipulators to grab the target satellite, after the autonomous rendezvous phase. After linking with the target satellite, the SRS spacecraft could either repair the non-functioning satellite and de-orbit itself or place the linked SRS-GlobalStar pair in a de-orbit trajectory whose perigee altitude was 150 km, in order to quickly re-enter the atmosphere and be destroyed.

The ΔV velocity increment requirements for an overall mission were estimated, considering each of the non-functioning satellite orbits to be candidate mothership orbits, in a step-by-step process in order to identify the minimum total ΔV requirement and thus the best opportunity to execute a minimum-cost rendezvous and de-orbiting mission. This analysis showed that it was possible to employ a mothership-SRS payload design with a nominal total mass similar to the total mass associated with second-generation, six-satellite GlobalStar satellite launch payloads. In the five-GlobalStar example, an optimal mothership orbit was identified and overall system estimates appeared to be reasonable.

For the remaining six non-functioning GlobalStar satellites, this analysis showed that one of the satellites was an “outlier” in the sense that its orbital parameters were not compatible with the other five satellites in the set. As a result, the estimated ΔV requirements for removing all six GlobalStars using SRS vehicles from

a single mothership was shown to be impractical because the ΔV requirements for many of the required rendezvous maneuvers were nearly the same as the ΔV requirements for launching the SRS vehicles from Earth. On the other hand, when the outlier GlobalStar was excluded, the mothership approach demonstrated potential mass and associated cost savings that were similar to the detailed five GlobalStar example.

A more detailed study of this approach is warranted. Since the non-functioning GlobalStar satellites have been placed in graveyard orbits, a different satellite constellation could be considered. The appropriate constellation should utilize satellites that have sufficient design data to enable a more accurate characterization of the actual rendezvous and docking maneuvers, as well as permitting the development of an SRS tool kit and spare parts set that could be incorporated in the SRS design to repair solar arrays and other satellite components. Furthermore, a study should be conducted to determine the feasibility of refueling constellation satellites with minimum risk of collisions or explosions. The mothership methodology satisfies an acceptable risk threshold by using different parking orbit than the target satellites' orbits, but the methodology needs more accurate assessment of the risk associated with each SRS rendezvous. Orbit change maneuvers need more propellant than executing a rendezvous maneuver. A more careful passive method strategy such as drifting in right ascension of the ascending node, small changes in orbit that would cause the SRS vehicles to drift differently than the target satellite and low-thrust propulsion for the orbit change can be used to make the orbital plane change should also be investigated.

REFERENCES

1. Rodriguez H.M., Liou J.C., “Orbital Debris: Past, Present, and Future.”, *Proceedings of American Institute of Aeronautics and Astronautics (AIAA)*, Annual Technical Symposium, 9 May 2008, Houston (TX), Webster (TX). Available at http://www.aiaa-houston.org/uploads/Documents/pres041.ppt.
2. United States Strategic Command (STRATCOM), Space Control and Space Surveillance Factsheet. Available at http://www.au.af.mil/au/awc/awcgate/usspc-fs/space.htm.
3. National Research Council, “Orbital Debris: A Technical Assessment”, *National Academy Press*, 1995, Washington, D.C.. Available at http://books.nap.edu/books/0309051258/html/index.html.
4. A Computer-Generated Image Comparison of Man-Made Objects. Available at http://orbitaldebris.jsc.nasa.gov/photogallery/photogallery.html.
5. *NASA Orbital Debris Quarterly News*, Volume 15, Issue 1, January 2011.
6. Wright D., “Colliding Satellites: Consequences and Implications”, *Union of Concerned Scientists*, 26 February 2009. Available at http://www.ucsusa.org/assets/documents/nwgs/SatelliteCollision-2-12-09.pdf.
7. Rossi A., “Population Models of Space Debris”, *International Astronomical Union*, 2005, doi: 10.1017/S1743921304008956.
8. Press release, “Gokturk Reconnaissance and Surveillance Satellite Project.” Contract Signature Under Secretariat of the Defense Industries, July 2009, Ankara/TURKEY. Available at http://www.finmeccanica.it/EN/Common/files/Holding/Corporate/Sala_stampa/Comunicati_stampa/Anno_2009/SSM_Gokturk_16_07_09_inglese.pdf .
9. Turkish Air Force Official Website about Future Projects. Available at http://www.hvkk.tsk.tr/PageSub/Calismalarimiz/Projeler/GokturkProjesi.aspx.
10. Petro A.J., “Techniques for Orbital Debris Control.”, *Journal Of Spacecraft and Rockets*, Vol. 29, No. 2, pp. 260, March-April 1992.
11. Spencer D.B., Luu K.K., Campbell W.S., Sorge M.E., Jenkin A.B., “Orbital Debris Hazard Assessment Methodologies for Satellite Constellations”, *Journal of Spacecraft and Rockets*, Vol. 38, No. 1, pp. 120-125, January–February 2001.

12. Finkleman D., Oltrogge D., “Twenty-five Years, More or Less?”, *AIAA/AAS Astrodynamics Specialist Conference*, 2-5 August 2010, Toronto, Ontario Canada, Reference Number: AIAA 2010-7822.
13. Space Systems - Determining Orbit Lifetime, Doc.No.: ISO DIS 27852, *International Organization for Standardization*, 2009, Geneva, Switzerland. Available at http://aiaa.kavi.com/apps/group_public/download.php/1009/ISO_CDC_27852_(E) %20(2).pdf.
14. Qureshi F.Z., Terzopoulos D., Jasiobedzki P., “Cognitive Vision for Autonomous Satellite Rendezvous and Docking”, *9th IAPR Conference on Machine Vision Applications*, May 2005, Tsukuba Science City, Japan. Available at www.cs.ucla.edu/~dt/papers/mva05/mva05.pdf.
15. Kawano I., Mokuno M., Kasai T., Suzuki T., “Results of Autonomous Rendezvous Docking Experiment of Engineering Test Satellite-VII”, *Acta Astronautica* Vol:53, Issue 1, pp. 1-8, July 2003. Available at http://www.sciencedirect.com/science/article/pii/S0094576502001959.
16. Karl A., “Active Removal of Space Debris – Discussing Technical and Economical Issues”, IAC-06-B6.4.04.
17. Burkhardt H., Sippel M., Krulle G., Janovsky R., Kassebom M., Lubberstedt H., Romberg O., Fristsche B., “Evaluation of Propulsion Systems for Satellite End-of-Life De-orbiting.”, *38th AIAA/ASME/SAE/ASEE Joint Propulsion Conference & Exhibit*, 7-10 July 2010, Indianapolis, Indiana. Reference Number: AIAA 2002-4208.
18. Description of the GlobalStar System Handbook, GS-TR-94-0001 Revision E, 27 December 2000. Available at http://gsproductsupport.files.wordpress.com /2009/04/description-of-the-globalstar-system-gs-tr-94-0001-rev-e-2000-12-07.pdf.
19. IADC Space Debris Mitigation Guidelines, *Inter-Agency Debris Coordination Committee*, IAD-02-01, Rev. 1, September 2007.
20. Press Release for Launch of Second Generation GlobalStar Satellites, http://www.globalstar.com/en/index.php?cid=7010&pressId=633, 20 October 2010, Covington, L.A.
21. Curtis H., “Orbital Mechanics for Engineering Students”, *Elsevier Aerospace Engineering Series*, 2005, ISBN: 0 7506 6169 0.

22. Nishida S., Kawamoto S., Okawa Y., Terui F., Kitamura S., “Space Debris Removal System Using a Small Satellite”, *Acta Astronautica* Vol. 65, pp. 95-102, 2009.
23. Robinson E.Y., “Spacecraft for Removal of Space Orbital Debris”, Patent number: US 6,655,637 B1, Date of Patent: 2 December 2003.
24. Kessler D.J., Cour-Palais B.G., “Collision Frequency of Artificial Satellites: The Creation of a Debris Belt”, *Journal of Geophysical Research*, Vol. 83, No. A6, 1 June 1978.
25. Morring F., “Changing the Game”, *Aviation Week and Space Technology*, pp. 23-25, 21 March 2011.
26. Two Line Element Set Data (TLE) for Non-functional GlobalStar Satellites. Available at http://www.space-track.org/perl/id_query.pl.
27. Vallado D.A., “Fundamentals of Astrodynamics and Applications”, *Space Technology Library*, ISBN:0-7923-6903-3, Microcosm, Inc., 21 May 2001.
28. Properties of Hydrazine Thrusters. Available at http://cs.astrium.eads.net/sp/brochures/hydrazine-thrusters.
29. COTS Hydrazine Propulsion Units. Available at http://www.astrium.eads.net/en/who-is-astrium.
30. Prussing J.E., Conway B.A., “Orbital Mechanics”, *Oxford University Press* 1993, New York, ISBN: 0-19-507834-9.
31. Types of Conic Sections. Available at http://en.wikipedia.org/wiki/Conic_section.
32. Seifert H., “Space Technology”, John *Wiley and Sons Inc.*, 1959, New York.

APPENDIX A

BASIC ORBITAL MECHANICS FOR SATELLITE REMOVAL

The basis of the analytical description of the motion of bodies in space is a combination of two of Newton's Law: the Second Law of Motion and the Law of Gravitation.

Newton's Second Law of Motion can be expressed as:

$$\vec{F} = \frac{\mathrm{d}}{\mathrm{dt}} (\mathrm{m}\vec{\mathrm{v}}) \tag{A.1}$$

That is, the external force applied to a body is equal to the time rate of change of the linear momentum of the body.

Newton's Law of Gravitation may be expressed as:

$$\vec{F} = \frac{\mathrm{G}\mathrm{m}_1\mathrm{m}_2}{\mathrm{r}^2} \left(\frac{\vec{\mathrm{r}}}{\mathrm{r}}\right) \tag{A.2}$$

stating that the force on body 1 is due to the attraction of body 2, varying directly with the product of their masses, and inversely with the square of the separation distance r, where the direction of the unit vector is given by $\vec{r}/_r$, and $\vec{\mathrm{r}}$ locates m_2 in terms of m_1 G is the Universal constant which has the value 6.67259 x 10^{-11} m^3 kg^{-1} s^{-2}.

A.1 Equations of Motion for the n-Body Problem

In space, all celestial objects interact with each other. Astronomers and mathematicians want to solve a problem: find the positions and velocities of the bodies at any other time from given initial positions and velocities. It is clearly a very practical problem to solve for the attractional force of the Sun, all the planets and moons in the solar system acting on each other, and also including orbiting spacecraft. If $\overrightarrow{R_i}$ represents the position of a body, whose mass is m_i, with respect to the origin *O* of an inertial reference frame, as shown in Figure A.1[30], the position of the j^{th} mass with respect to the i^{th} mass can be designated $\vec{r}_{ij}$, where;

$$\vec{r}_{ij} = \vec{R}_j - \vec{R}_i, \;\; i, j = 1,2,3,\ldots,\mathrm{n} \tag{A.3}$$

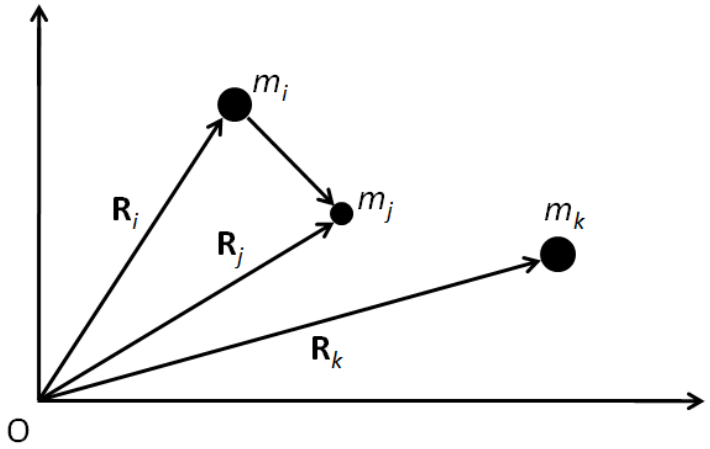

Figure A.1 Relative Position in an Inertial Frame.

The attraction of the i^{th} body is determined by the attraction of the n-1 other bodies acting on it. Using Equation A.1 and A.2 and summing over the system of masses yields:

$$m_i\vec{\ddot{R}}_i = \vec{F}_i = G\sum_{j=1}^{n}\frac{m_i m_j}{{r_{ij}}^3}\vec{r}_{ij} \quad j \neq i \tag{A.4}$$

Now, since $\vec{r}_{ij} = -\vec{r}_{ij}$, Equation A.4 can be summed over all of the bodies in the system to yield:

$$\sum_{i=1}^{n} m_i\vec{\ddot{R}}_i = 0 \tag{A.5}$$

which can be summed over all of the bodies to yield:

$$\sum_{i=1}^{n} m_i\vec{\ddot{R}}_i = \vec{C}_1, \text{ a constant vector,} \tag{A.6}$$

then integrated to yield:

$$\sum_{i=1}^{n} m_i \dot{\vec{R}}_i = \vec{C}_1\, t + \vec{C}_2 \tag{A.7}$$

Defining the center of mass,

$$\vec{R}_{cm} = \sum m_i \vec{R}_i \Big/ \sum m_i, \tag{A.8}$$

Equation A.7 determines the motion of the system center of mass, which is rectilinear and from Equation A.6 at constant velocity[30]. The linear momentum of the system is thus conserved, which is expected since the system of bodies is subject to no net external force.

A.2 The Two-Body Problem

While the general formulation would be the best approach, it is known that systems consisting of three objects or more do not yield closed-form solutions. Hence, it is necessary to, from Equation A.4,

$$\ddot{\vec{R}}_2 - \ddot{\vec{R}}_1 = \ddot{\vec{r}}_{12} = \frac{Gm_1}{{r_{12}}^3}\vec{r}_{21} - \frac{Gm_2}{{r_{12}}^3}\vec{r}_{12} \tag{A.9}$$

or:

$$\ddot{\vec{r}}_{12} + \frac{G(m_1+m_2)}{{r_{12}}^3}\vec{r}_{21} = 0 \tag{A.10}$$

or:

$$\ddot{\vec{r}} + \frac{\mu}{r^3}\vec{r} = 0 \tag{A.11}$$

where, $\mu \equiv G(m_1+m_2)$ is the gravitational constant for the particular two-body problem and the subscript notation is dropped because it is no longer necessary.

Since μ completely characterizes the system, solutions can be developed to these two-body problems in terms of μ. In many applications the mass of the central body is much larger than the "orbiting mass" ($m_1 \gg m_2$), and in this case μ can be approximated as Gm_1. Thus each large celestial body has its own cataloged value of μ.

Equation A.11, governing the position $\vec{r}$ of m_2 relative to m_1 is nonlinear, but several constant constraints on the motion exist. For example, taking the vector product:

$$\vec{r} \times \ddot{\vec{r}} + \vec{r} \times \frac{\mu}{r^3}\vec{r} = 0, \tag{A.12}$$

which can be integrated to give,

$$\vec{r} \times \dot{\vec{r}} = \vec{h} \text{ , a constant vector.} \tag{A.13}$$

The vector $\vec{r}$ is then normal to the constant vector $\vec{h}$. This implies that the relative motion lies in a fixed plane in space called the orbit plane, with $\vec{h}$ as its characteristic normal vector. Figure A.2 illustrates the position vector ($\vec{r}$) and the velocity vector (v) are in the same plane and their cross product is perpendicular to that plane[30].

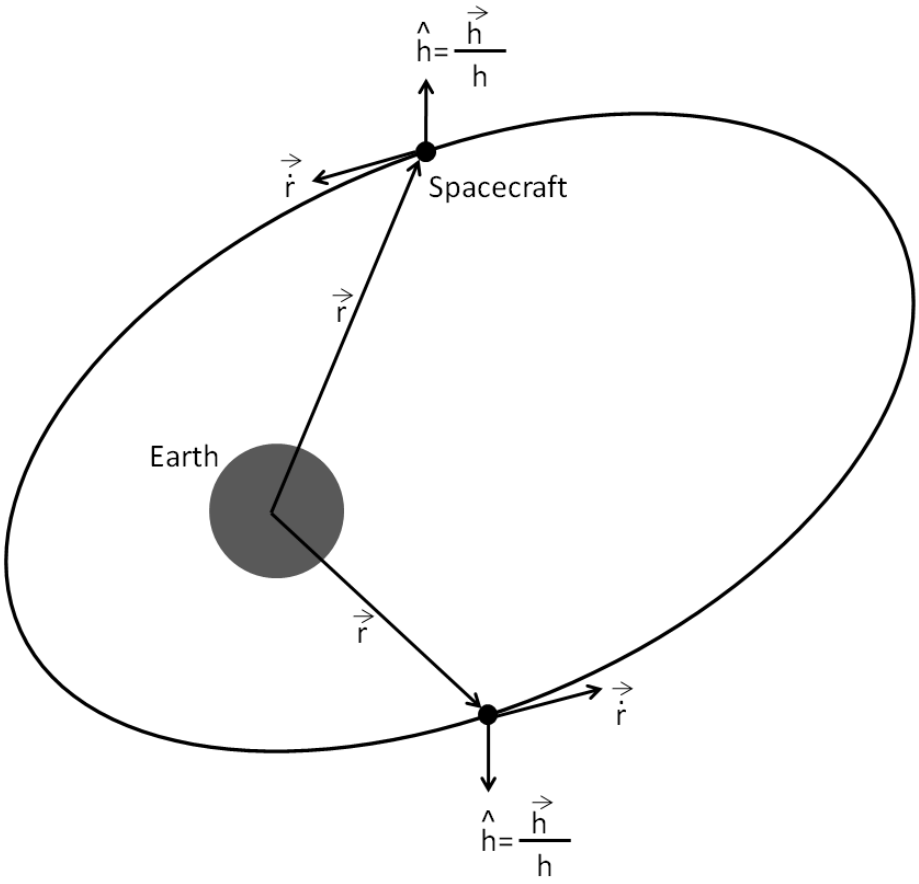

Figure A.2 Spacecraft Path around the Earth in Orbital Plane.

Now, to solve Equation A.11, take the cross product with the constant vector $\vec{h}$;

$$\ddot{\vec{r}} \times \vec{h} = \frac{-\mu}{r^3}\left(\vec{r} \times \vec{h}\right) = \frac{-\mu}{r^3}\vec{r} \times \left(\vec{r} \times \dot{\vec{r}}\right)$$

$$= \frac{\mu}{r^3}\left[\dot{\vec{r}}(\vec{r} \cdot \vec{r}) - \vec{r}\left(\vec{r} \cdot \dot{\vec{r}}\right)\right] \quad \text{(A.14)}$$

or, $$\ddot{\vec{r}} \times \vec{h} = \mu\left(\frac{\dot{\vec{r}}}{r} - \frac{\vec{r} * \dot{r}}{r^2}\right) \quad \text{(A.15)}$$

As shown in Figure A.3, the components of the velocity vector are $\dot{\vec{r}}_r = \dot{r}_r * \hat{\varepsilon}_r$ and $\dot{\vec{r}}_\theta = \dot{r}_\theta * \hat{\varepsilon}_\theta$, where $\hat{\varepsilon}_r$ and $\hat{\varepsilon}_\theta$ are the radial and tangential unit vectors respectively, and θ is the angular position of the radius vector. Substituting the components of the velocity vector into Equation A.13 yields:

$$\vec{r} \times \dot{\vec{r}} = \vec{h} = (\vec{r}\hat{\varepsilon}_r) \times (\dot{r}_r\hat{\varepsilon}_r + \dot{r}_\theta\hat{\varepsilon}_\theta) = r\dot{r}\hat{h} \quad \text{(A.16)}$$

As we know $\hat{h} = \frac{\vec{h}}{h}$ and from Equation A.16 the magnitude of the specific angular momentum h can be written as;

$$h = r\dot{r}_\theta = r^2\frac{d\theta}{dt} \quad \text{(A.17)}$$

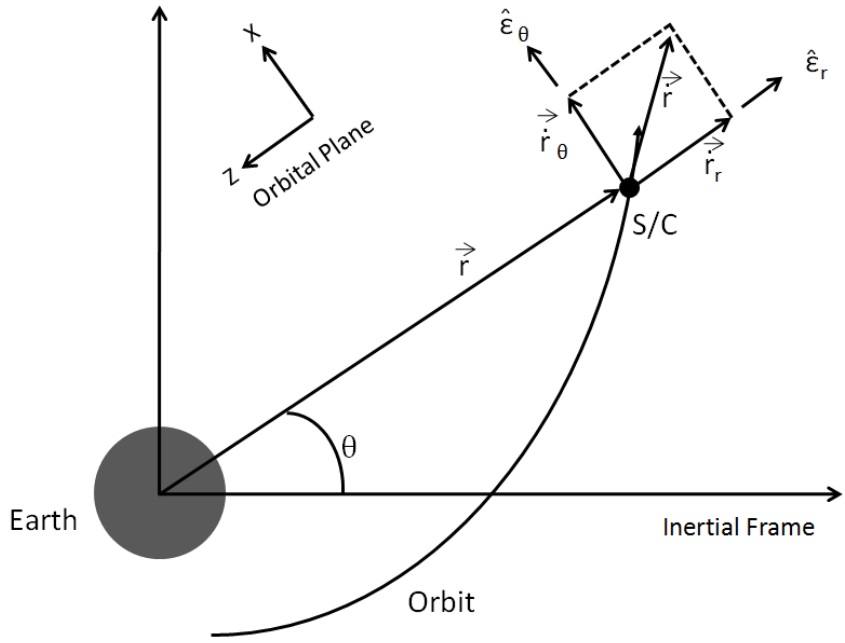

Figure A.3 Spacecraft Velocity Components in Orbital Plane.

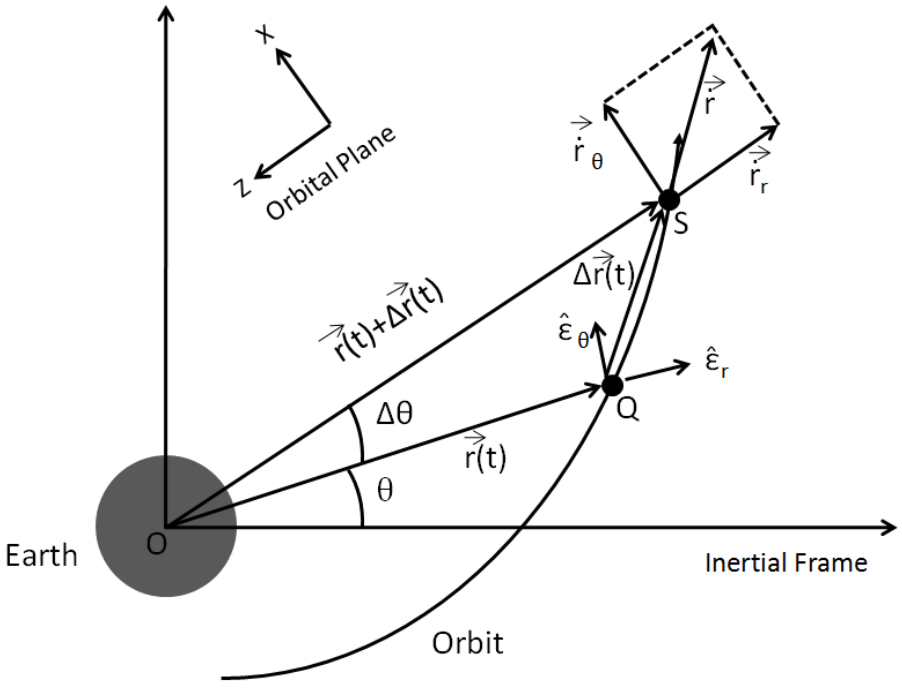

Figure A.4 Area Swept by Position Vector during Time Interval Δt.

Figure A.4 represents the area swept out by the position vector during an infinitesimal time interval. The area of triangle OQS can be expressed as ΔA and it can be written as;

$$\Delta A = \frac{1}{2}(r + \Delta r) r \sin \Delta\theta = \frac{1}{2}(r + \Delta r)\, r \Delta\theta \frac{\sin \Delta\theta}{\Delta\theta} \tag{A.18}$$

Taking the limit of Equation A.18 and substituting Equation A.17, the rate at which area is swept is given by:

$$\frac{dA}{dt} = \frac{1}{2} r^2 \frac{d\theta}{dt} = \frac{h}{2} \tag{A.19}$$

A vectoral approach was used to integrate Equation A.11 in order to obtain the orbit trajectory formula. Recall that $\hat{\varepsilon}_r = \frac{\vec{R}}{R}$, and taking the time derivative of the unit vector yields:

$$\frac{d\hat{\varepsilon}_r}{dt} = \frac{\dot{\vec{r}}}{r} - \frac{\dot{r}\vec{r}}{r^2} = \frac{r^2\dot{\vec{r}} - r\dot{r}\vec{r}}{r^3} = \frac{(\vec{r}\cdot\vec{r})\dot{\vec{r}} - (\vec{r}\cdot\dot{\vec{r}})\vec{r}}{r^3} \tag{A.20}$$

Now note that:

$$\frac{d}{dt}\left(\frac{\vec{r}}{r}\right) = \frac{r\dot{\vec{r}} - \vec{r}\dot{r}}{r^2} \tag{A.21}$$

Therefore, Equation 2.15 becomes;

$$\dot{\vec{r}} \times \vec{h} = \mu \frac{d}{dt}\left(\frac{\vec{r}}{r}\right) \tag{A.22}$$

which may be integrated directly to yield;

$$\dot{\vec{r}} \times \vec{h} = \mu \left(\frac{\vec{r}}{r} + \vec{e}\right) \tag{A.23}$$

where $\vec{e}$ is a dimensionless vector constant of integration. Because $\vec{e}$ is normal to $\vec{h}$, $\vec{e}$ must lie in the orbit plane. Taking the dot product of $\vec{r}$ with Equation A.23 yields a scalar equation:

$$\vec{r} \cdot \left(\vec{r} \times \vec{h}\right) = \vec{r} \cdot \left\{\mu \left(\frac{\vec{r}}{r} + \vec{e}\right)\right\} \tag{A.24}$$

or;

$$\left(\vec{r} \times \vec{r}\right) \cdot \vec{h} = h^2 = \mu\left(r + \left(\vec{r} \cdot e\right)\right) = \mu(r + re\cos\theta) \tag{A.25}$$

where the angle θ is defined as the angle between $\vec{r}$ and $\vec{e}$. Solving for r yields;

$$r = \frac{{}^{h^2}/_{\mu}}{1+e\cos\theta} \tag{A.26}$$

which is the equation of a conic section in polar coordinates with the origin of the coordinate frame at the focus of the conic section. From Equation A.26 we see that r will have its minimum value when θ=0, that is, the vector $\vec{e}$ represents the direction of minimum separation distance.

Equation A.26 represents a conic section because it is exactly the same equation which results from the formal definition of a conic section and types of conic sections is shown on Figure A.5[31].

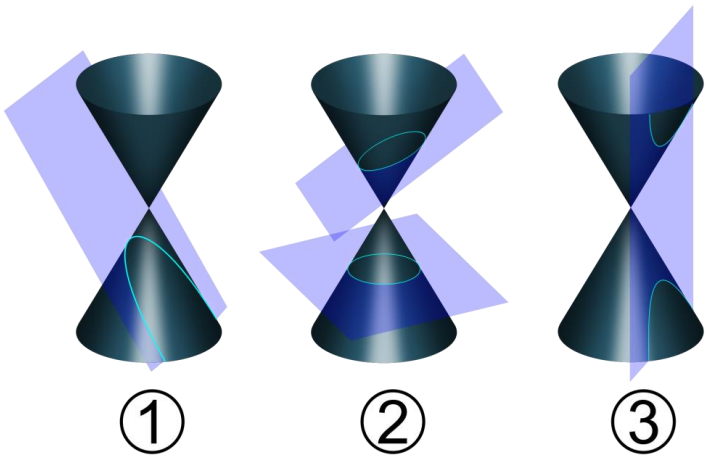

Figure A.5 Types of Conic Sections: (1) Parabola (2) Circle – Ellipse (3) Hyperbola.

In mathematics, a conic section (or just a conic) is a curve obtained by intersecting a cone (more precisely, a right circular conical surface) with a plane. In analytic geometry, a conic may be defined as a plane algebraic curve of degree two. It can be defined as the locus of points whose distances are in a fixed ratio to some point, called a *focus*, and some line, called a *directrix*.

Note that we have succeeded in obtaining a closed-form solution to the nonlinear equation of motion (A.11). However, the independent variable in the solution is not time, but the polar angle θ, which is called true anomaly. Fortunately, we now have a geometrical description of the orbit; one can calculate r for all values of θ if the constants μ, h and e (also called eccentricity) are given. However, we have lost track of where the orbiting mass is at a specified time. The missing time information is also evident in the fact that, although the solution to equation (A.11) requires six integration constants, our two vector constants $\vec{h}$ and $\vec{e}$ provide only five independent constants due to the fact that $\vec{h} \cdot \vec{e} = 0$.

A.3 Elliptical Orbits

In celestial mechanics an elliptic orbit is a Kepler orbit when the eccentricity is greater than 0 and less than 1 (thus excluding the circular orbit). In a wider sense elliptic orbit is a Kepler orbit with negative energy. The equation governing the conic section described using Equation A.26 is:

$$r = \frac{h^2/\mu}{1+e*\cos\theta} \tag{A.27}$$

where r represents the magnitude of $\vec{r}$, e represents eccentricity and θ represents the true anomaly, as shown in Figure A.6. Also shown in the figure is the semi-major axis *a*, the semi-minor axes *b* represents , the semi-latus rectum *p* and the distance between the two foci $2*c$.

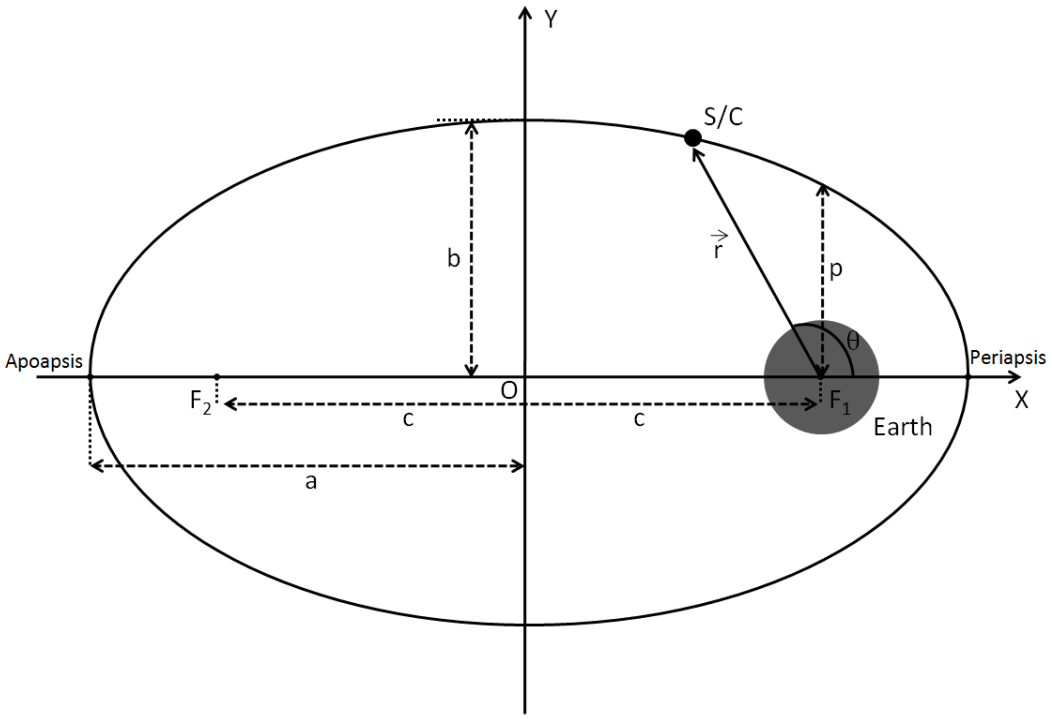

Figure A.6 Elliptical Orbit around the Earth.

Smallest $\vec{r}$ vector and so smallest magnitude of $\vec{r}$ vector have to at the periapsis point. At periapsis point true anomaly (θ) is equal to 0° so Equation A.27 yields:

$$r_p = \frac{h^2/\mu}{1+e\cos 0} = \frac{h^2/\mu}{1+e} \tag{A.28}$$

The largest $\vec{r}$ vector and thus the largest magnitude of $\vec{r}$ vector have to at the apoapsis point of the elliptical orbit around the Earth. At apoapsis point true anomaly (θ) is equal to 180° so Equation A.27 yields:

$$r_a = \frac{h^2/\mu}{1+e\cos 180} = \frac{h^2/\mu}{1-e} \tag{A.29}$$

We can calculate eccentricity by dividing Equation A.28 and Equation A.29;

$$\frac{r_p}{r_a} = \frac{\frac{h^2/\mu}{1+e}}{\frac{h^2/\mu}{1-e}} = \frac{1-e}{1+e}$$

$$r_p(1+e) = r_a(1-e)$$

$$e = \frac{r_a - r_p}{r_a + r_p} \tag{A.30}$$

Obviously we can see at Figure A.6, adding length of periapsis and apoapsis to each other, we have twice times of semi-major axes (2a). If we add Equation A.28 to Equation A.29 and divided by 2, we can calculate semi-major axes;

$$r_p + r_a = 2a = \frac{h^2/\mu}{1+e} + \frac{h^2/\mu}{1-e}$$

$$a = \frac{h^2}{\mu}\frac{1}{1-e^2} \tag{A.31}$$

An alternative form of Equation A.27 can be written by using the semi-major axis definition.

$$r = a\frac{1-e^2}{1+e\cos\theta} \tag{A.32}$$

Comparing Equation A.27 and Equation A.32 yields the specific angular momentum, *h*, as a function of the masses and orbit geometry;

$$h = \sqrt{[\mu a(1-e^2)]} \tag{A.33}$$

When true anomaly (θ) equals to 90°, Equation A.32 yields;

$$r = a(1-e^2) = p \tag{A.34}$$

and as shown and defined at Figure A.6, this distance is referred to as the semi-latus rectum (*p*). And from Equation A.32,

$$r = \frac{p}{1+e\cos\theta} \tag{A.35}$$

comparing Equation A.27 and Equation A.35; the specific angular momentum (*h*)

and the semi-latus rectum (*p*) are related by:

$$p = \frac{h^2}{\mu} \tag{A.36}$$

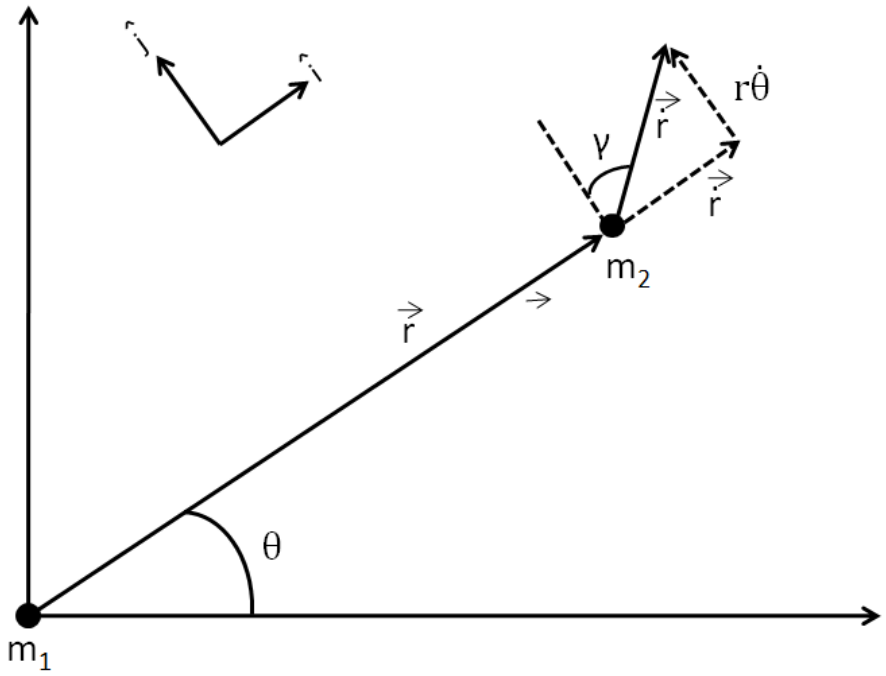

Figure A.7 Unit Vector Definitions.

With reference to Figure A.7, which illustrates the motion of m_2 and as seen an observer on m_1, we see that

$$\vec{r} = \dot{r}\hat{\imath} + r\dot{\theta}\hat{\jmath} \tag{A.37}$$

where the unit vectors rotate with the radius vector. Then, from Equation A.27 we have

$$\vec{h} = \vec{r} \times \dot{\vec{r}} = (r\hat{\imath}) \times \left(\dot{r}\hat{\imath} + r\dot{\theta}\hat{\jmath}\right) = r^2\dot{\theta}\hat{k} \tag{A.38}$$

However, that the differential element of area swept out by the radius vector as it rotates through an angle of $d\theta$ is, $dA=(1/2)r^2 d\theta$. Therefore, this implies that;

$$\frac{dA}{dt} = \frac{1}{2} r^2 \frac{d\theta}{dt} = \frac{h}{2} = \text{constant} \tag{A.39}$$

That is, the rate at which the radius vector sweeps out area is a constant, and orbital angular momentum is conserved. This verifies Kepler's Second Law. Besides, the time required for one complete orbit, the orbital period T is;

$$\mathrm{T} = \frac{\text{enclosed area of the ellipse}}{\mathrm{dA/dt}} \tag{A.40}$$

or;

$$T = \frac{\pi ab}{\dot{A}} = \frac{2\pi ab}{h} = \frac{2\pi a a\sqrt{(1-e^2)}}{(\sqrt{\mu a})\sqrt{(1-e^2)}}$$

$$T = 2\pi\sqrt{\frac{a^3}{\mu}} \tag{A.41}$$

A.4 The Orbit in Space

Six constants are required to completely specify the orbit of a particular satellite with respect to the attracting center. In the most elementary form the six components of the state vectors $\vec{r}$ and $\vec{v}$ at a specified time will serve this purpose. Unfortunately, $\vec{r}$ and $\vec{v}$ do not directly yield much information about orbit. For example, they do not explicity tell us what type of conic the orbit present. So another set of six constants, *the orbital elements*, is much more descriptive of the orbit.

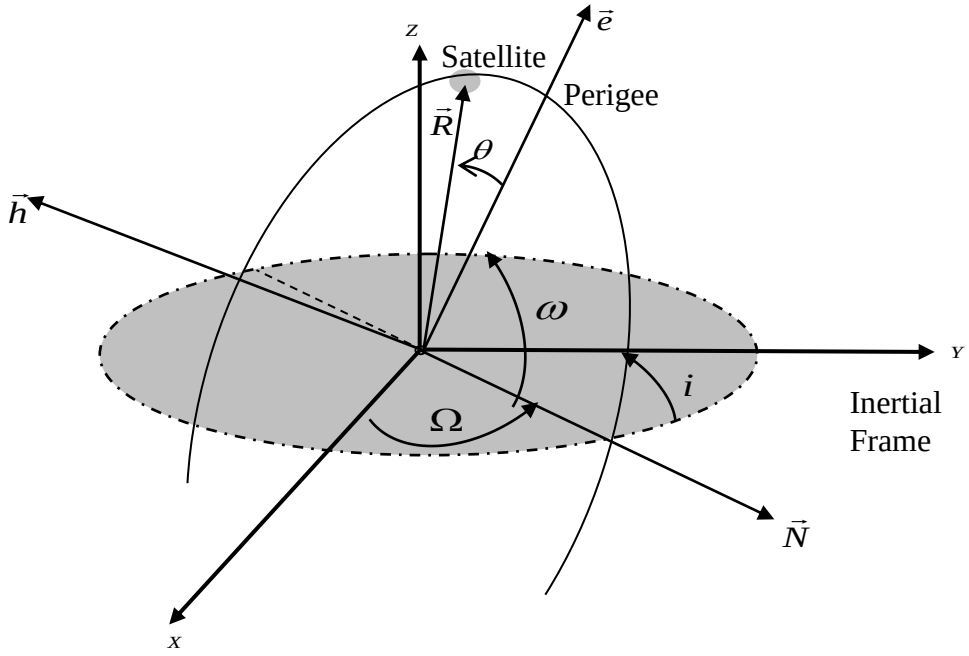

Figure A.8 Earth Centered Inertial Frame and Orbital Elements.

In Figure A.8, orbital elements are shown which have not yet been defined. Inertial frame, that is commonly used, can be defined in terms of X, Y and Z. The X and Y axes lie in the Earth's equatorial plane and the Earth spins around the Z axis. The X axis defined in a direction from the Earth to the Sun at the Vernal Equinox (21 March). This direction points to the constellation of Aries, it is called Aries direction. The Z axis is in the northerly direction and along the Earth's spin axes. It is at the angle of 23°27'8'' to the normal of the ecliptic plane. The Y axes makes up a right handed orthogonal set with X and Z axes.

Inclination (i) is the angle between the $\vec{K}$ unit vector (Z axes) and the angular momentum vector ($\vec{h}$).

Longitude of the ascending node (Ω) is the angle, in the fundamental plane, between the $\vec{I}$ unit vector (X axes) and the point where the satellite crosses through the fundamental plane in northerly direction measured counterclockwise when viewed from the north side of the fundamental plane.

Argument of periapsis (ω) is the angle, in the plane of satellite's orbit, between the ascending node and the periapsis point, measured in the direction of the satellite's motion.

A.5 Position in an Elliptical Orbit as a Function of Time

We can calculate time of flight on the elliptical orbit with an auxiliary circle which is radius is equals to elliptical orbit's semi-major axes (a) which is shown in Figure A.9[32]. We can use geometric approaches and after some manipulations, we have a relation between true anomaly (θ) and eccentric anomaly (E);

$$\tan\frac{\theta}{2} = \sqrt{\frac{1+e}{1-e}}\tan\frac{E}{2} \tag{A.42}$$

and

$$\tan\frac{E}{2} = \sqrt{\frac{1-e}{1+e}}\tan\frac{\theta}{2} \tag{A.43}$$

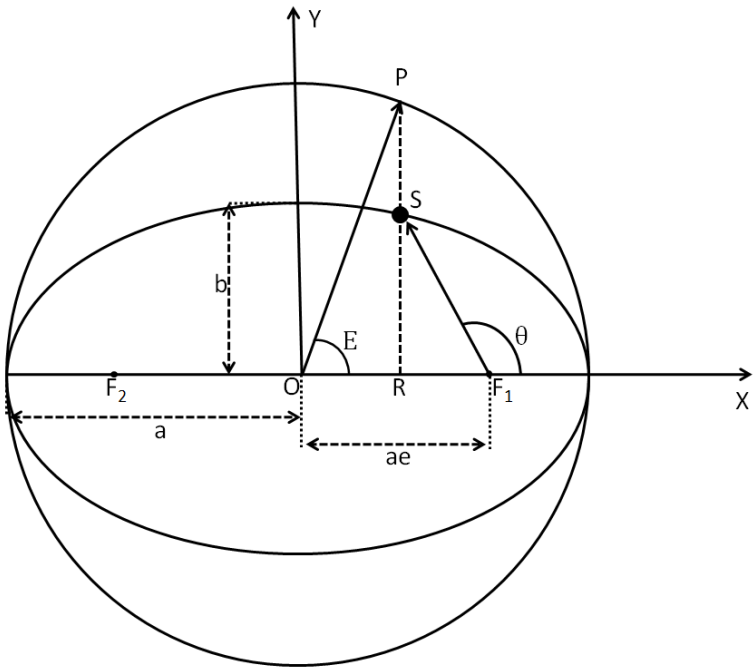

Figure A.9 Definition of Eccentric Anomaly.

The mean angular rate of the satellite, symbolized by *n*, and also called mean motion is:

$$n = \frac{2\pi}{T} = \sqrt{\frac{\mu}{a^3}} \tag{A.44}$$

With the help of eccentric anomaly, time of flight of the satellite between two points can be defined as:

$$t = \sqrt{\frac{a^3}{\mu}}(E - e\sin E) \tag{A.45}$$

Therefore, we may define an auxiliary angle $M=n*t$, called mean anomaly, which represents physically the angular displacement of a fictitious satellite that travels at the mean angular rate *n* as opposed to the rate $\dot{\theta}$. In terms of mean anomaly can be written as:

$$M = nt = \sqrt{\frac{\mu}{a^3}}\left(\sqrt{\frac{a^3}{\mu}}(E - e\sin E)\right) = E - e\sin E \tag{A.46}$$

VITA

GOKSEL GURGENBURAN

DEGREES

- ***Bachelor of Science : Electronic Engineering***

  Turkish Air Force Academy, Yesilkoy/Istanbul, August 2005

PROFESSIONAL CHRONOLOGY

- Air Technical School Commands, Gaziemir/Izmir, Human Resources Officer Course, September 2006 - March 2007

- 3rd Air Maintenance and Supply Center, Etimesgut/Ankara, Human Resources Officer, May 2007-August 2009.

- Turkish Air Force Academy, Yesilkoy/Istanbul - Aerospace Engineering Department, Old Dominion University, Norfolk, Virginia, M.S. Student, September 2009-August 2011.